Water Availability and Use Science Program

Prepared in cooperation with the Gulf Coastal Plains and Ozarks Landscape Conservation Cooperative and the Department of the Interior Southeast Climate Adaptation Science Center

Simulation of Water Availability in the Southeastern United States for Historical and Potential Future Climate and Land-Cover Conditions

Scientific Investigations Report 2019–5039

U.S. Department of the Interior
U.S. Geological Survey

Cover photograph: Middle Creek Falls, Middle Creek Gulf, Signal Mountain, Hamilton County, Tennessee. Photograph by Alan Cressler, U.S. Geological Survey.

Water Availability and Use Science Program

Simulation of Water Availability in the Southeastern United States for Historical and Potential Future Climate and Land-Cover Conditions

By Jacob H. LaFontaine, Rheannon M. Hart, Lauren E. Hay, William H. Farmer, Andrew R. Bock, Roland J. Viger, Steven L. Markstrom, R. Steve Regan, and Jessica M. Driscoll

Prepared in cooperation with the Gulf Coastal Plains and Ozarks Landscape Conservation Cooperative and the Department of the Interior Southeast Climate Adaptation Science Center

Scientific Investigations Report 2019–5039

U.S. Department of the Interior
U.S. Geological Survey

U.S. Department of the Interior
DAVID BERNHARDT, Secretary

U.S. Geological Survey
James F. Reilly II, Director

U.S. Geological Survey, Reston, Virginia: 2019

For more information on the USGS—the Federal source for science about the Earth, its natural and living resources, natural hazards, and the environment—visit https://www.usgs.gov or call 1–888–ASK–USGS.

For an overview of USGS information products, including maps, imagery, and publications, visit https://store.usgs.gov.

Suggested citation:
LaFontaine, J.H., Hart, R.M., Hay, L.E., Farmer, W.H., Bock, A.R., Viger, R.J., Markstrom, S.L., Regan, R.S., and Driscoll, J.M., 2019, Simulation of water availability in the Southeastern United States for historical and potential future climate and land-cover conditions: U.S. Geological Survey Scientific Investigations Report 2019–5039, 83 p., https://doi.org/10.3133/sir20195039.

ISSN 2328-0328 (online)

Acknowledgments

The authors acknowledge the Gulf Coastal Plains and Ozarks Landscape Conservation Cooperative (GCPO LCC), the Department of the Interior Southeast Climate Adaptation Science Center, and the U.S. Geological Survey (USGS) Water Availability and Use Science Program for the financial support to complete this work. Additionally, the authors acknowledge the GCPO LCC Technical Advisory Team for their guidance and suggestions throughout the project. Finally, the authors would like to acknowledge the technical reviewers David Bjerklie (USGS New England Water Science Center), John Faustini (U.S. Fish and Wildlife Service), Yvonne Allen (U.S. Fish and Wildlife Service), and Derek Rosendahl (Department of the Interior South Central Climate Adaptation Science Center) whose input greatly enhanced the final report.

Contents

Figures

Tables

Conversion Factors

U.S. customary units to International System of Units

Multiply	By	To obtain
	Length	
mile (mi)	1.609	kilometer (km)
	Area	
square mile (mi^2)	2.590	square kilometer (km^2)
	Flow rate	
cubic foot per second (ft^3/s)	0.02832	cubic meter per second (m^3/s)
cubic foot per second per square mile ($[ft^3/s]/mi^2$)	0.01093	cubic meter per second per square kilometer ($[m^3/s]/km^2$)

Temperature in degrees Fahrenheit (°F) may be converted to degrees Celsius (°C) as

$$°C = (°F - 32) / 1.8.$$

Datum

Vertical coordinate information is referenced to the North American Vertical Datum of 1988 (NAVD 88).

Horizontal coordinate information is referenced to the North American Datum of 1983 (NAD 83).

Altitude, as used in this report, refers to distance above the vertical datum.

Abbreviations

AET	actual evapotranspiration
BCCA	Bias Correction Constructed Analog
CMIP5	Coupled Model Intercomparison Project Phase 5
CONUS	conterminous United States
DAYMET	Daily Surface Weather and Climatological Summaries
DEM	digital elevation model
EFC	environmental flow components
EROS	U.S. Geological Survey Earth Resources Observation and Science Center

FAST	Fourier Amplitude Sensitivity Test
GCM	general circulation model
GCPO LCC	Gulf Coastal Plains and Ozarks Landscape Conservation Cooperative
GCPO-PRMS	application of the Precipitation-Runoff Modeling System in the Southeastern United States
GDP	U.S. Geological Survey GeoData Portal
GIS	geographic information system
HIT	hydrologic index tool
HRU	hydrologic response unit
KS test	Kolmogorov-Smirnov statistical test
MWBM	Monthly Water Balance Model
NAWQA	National Water Quality Assessment
NHDPlus	National Hydrography Dataset version 1
NHM	U.S. Geological Survey National Hydrologic Model
NHM-MWBM	National Hydrologic Model application of the Monthly Water Balance Model
NHM-PRMS	National Hydrologic Model application of the Precipitation-Runoff Modeling System
NLCD2001	National Land Cover Database 2001
NRMSE	normalized root mean square error
NSE	Nash-Sutcliffe model efficiency index
OF	objective function
PET	potential evapotranspiration
P_{bias}	percent bias
PRMS	Precipitation-Runoff Modeling System
RCP	representative concentration pathway
SCE	Shuffled Complex Evolution
SNODAS	Snow Data Assimilation System
SPARROW	SPAtially Referenced Regressions On Watershed attributes
STATSGO	Soils Data for the Conterminous United States
SWE	snow water equivalent
USGS	U.S. Geological Survey

Simulation of Water Availability in the Southeastern United States for Historical and Potential Future Climate and Land-Cover Conditions

By Jacob H. LaFontaine, Rheannon M. Hart, Lauren E. Hay, William H. Farmer, Andrew R. Bock, Roland J. Viger, Steven L. Markstrom, R. Steve Regan, and Jessica M. Driscoll

Abstract

A study was conducted by the U.S. Geological Survey (USGS), in cooperation with the Gulf Coastal Plains and Ozarks Landscape Conservation Cooperative (GCPO LCC) and the Department of the Interior Southeast Climate Adaptation Science Center, to evaluate the hydrologic response of a daily time step hydrologic model to historical observations and projections of potential climate and land-cover change for the period 1952–2099. The model simulations were used to compute the potential changes in hydrologic response and streamflow statistics across the Southeastern United States, using historical observations of climate and streamflow. Thirteen downscaled general circulation models with four representative concentration pathways were used to represent a range of potential future changes in climate (a total of 45 future simulations) from the Coupled Model Intercomparison Project Phase 5. The streamflow statistics were selected to describe streamflow conditions that may be most useful in defining the suitability for each river or stream to support sustaining populations of priority aquatic species across the GCPO LCC. An application of the Precipitation-Runoff Modeling System (included as part of the USGS National Hydrologic Model) was used to develop the hydrologic simulations. The results showed increases in air temperature across the study area, with the highest increases occurring in the northern part of the study area during July to September. The results showed a mix of increases and decreases in precipitation accumulation across the study area and across seasons, with decreases in precipitation accumulation across all seasons for the southwestern part of the study area. Actual evapotranspiration decreased for the southeastern part of the study area and increased for the northwestern part of the study area. The results showed general decreases in runoff across the study area, with increases in runoff in areas surrounding large metropolitan regions where potential future increases in impervious area occur. Results from a statistical analysis (Kolmogorov-Smirnov test) showed that the downscaled general circulation models generally have more skill in producing historical streamflow statistics in the duration and magnitude categories and less skill in producing historical streamflow statistics in the frequency, rate of change, and timing categories for this study area. The potential changes in the streamflow statistics and the results of the Kolmogorov-Smirnov test are available through the GCPO LCC Conservation Planning Atlas, an online science-based mapping platform built specifically for land managers and planners.

Introduction

The U.S. Geological Survey (USGS), in cooperation with the Gulf Coastal Plains and Ozarks Landscape Conservation Cooperative (GCPO LCC) and the Southeast Climate Adaptation Science Center, has developed methods to quantify water availability and hydrologic behavior for historical and potential future conditions in the Southeastern United States in response to climate and landscape dynamics (fig. 1). Estimates of water availability and hydrologic behavior provide resource managers with information that can be used to determine the allocation and allowable use of natural resources, as well as information about potential effects of climate and land use on those resources. Using guidance provided in the GCPO LCC Integrated Science Agenda (John Tirpak, U.S. Fish and Wildlife Service, written commun., 2014), specifically the GCPO LCC Strategic Habitat Conservation Framework, estimates of hydrologic response were developed to support defining desired environmental conditions for priority habitat types in terms of three primary landscape attributes: (1) amount, (2) configuration, and (3) condition. For aquatic systems, a subset of these landscape attributes can be quantified by streamflow characteristics such as duration, frequency, magnitude, rate of change, and timing (Richter and others, 1996). The duration characteristics describe the magnitude of streamflows for various lengths of time (for example, 1-day, 3-day, 7-day, 30-day, 90-day duration) that may coincide with a natural or anthropogenic process.

The frequency characteristics describe the number of times that streamflow rises above or falls below some predefined threshold. The magnitude characteristics describe the average daily streamflow volume for each month. The rate of change characteristics describe the rate at which streamflows increase or decrease for a given time series, or how many times streamflow changes from increasing to decreasing for a given time series. The timing characteristics describe the date of occurrence for the annual or seasonal extreme high or low streamflow. All five categories of streamflow characteristics can be used to inform how aquatic habitats may respond to temporal changes in those characteristics (Richter and others, 1996). Assessing both the historical and potential future change in these characteristics is a priority for the GCPO LCC region. This study also supports the goals and objectives listed in the USGS Water Science Strategy, most directly (1) providing society the information it needs regarding the amount and quality of water in all components of the water cycle at high temporal and spatial resolution, nationwide, and (2) predicting changes in the quantity and quality of water resources in response to changing climate, population, land use, and management scenarios (U.S. Geological Survey, 2007; Evenson and others, 2013).

Managers today are often required to prioritize decisions based on quantitative analyses of aquatic resources, with increasing attention placed on the need for water availability and dynamics information at ungaged locations (Blöschl, 2006). Understanding the changes in the distribution and quantity of, and demand for, water resources in response to climate variability and change is essential to planning for, and adapting to, future climatic conditions (Lins and others, 2010). Measured streamflow data are available at a limited number of locations across the conterminous United States (CONUS), with only a fraction of those streamgages providing reference-quality (relatively free of anthropogenic effects) streamflow information (Kiang and others, 2013). To plan for future conditions and challenges, it is important that land-, water-, and cultural-resource managers understand the limitations and uncertainties associated with the characterization of these changes when making management decisions. The existing streamgage network is a mix of basins with substantial anthropogenic effects (for example, dams, water use, urbanization) and those with little to no anthropogenic effects. To assess how affected a gaged basin may be, or to determine a baseline condition in an ungaged basin, a streamflow time series representing a “naturalized” state may be of use. Numerous methods have been proposed to predict streamflow in ungaged watersheds; however, no one method has been universally accepted or demonstrated to work in all environments (Blöschl and others, 2013, tables A7–A10). All watersheds have unique configurations of geologic, topographic, climatic, hydrologic, ecologic, and land-use characteristics that affect how much water is available, the sources and quality of water, and how water is routed. To determine and predict water availability in an individual watershed, resource managers will need to utilize the findings of techniques that take these many factors into account.

The assumption of stationarity in water resources planning may no longer be valid (Milly and others, 2008). Using past hydrologic behavior as a guide for future expectations of water availability could lead to incomplete or erroneous conclusions for managing the balance between societal and environmental needs. The use of process-based modeling applications that can incorporate landscape and climatic changes to simulate potential hydrologic response to such perturbations is one option to make stationarity less of a central assumption. This study incorporates multiple modeling methods with multiple types of ancillary information to move away from single model simulations toward a more robust synthesis of hydrologic response for historical and potential future conditions.

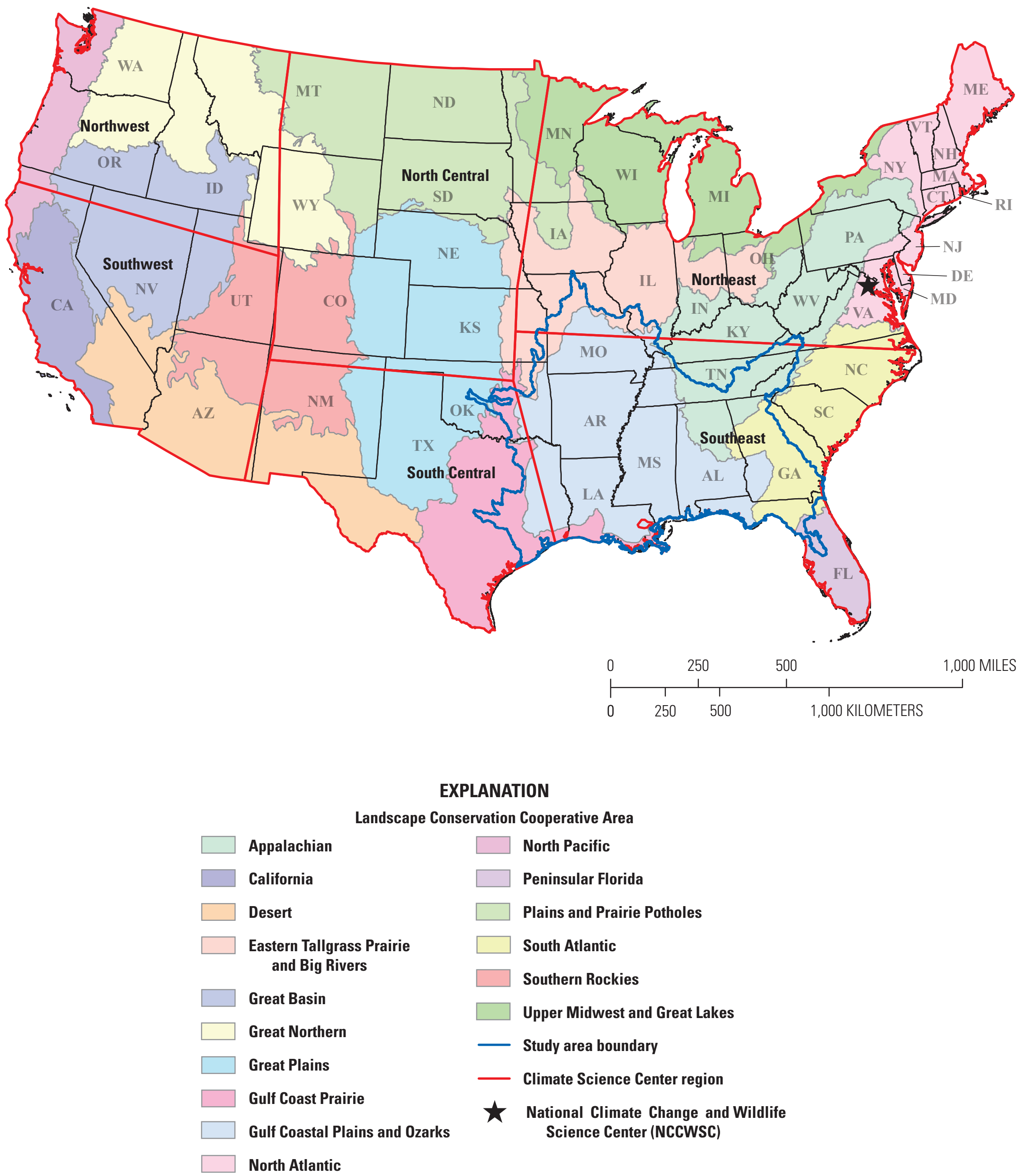

Figure 1. Map showing the locations of the study area, the National Climate Change and Wildlife Science Center, the Department of the Interior Climate Science Center (CSC) regions, and the Landscape Conservation Cooperative areas.

Purpose and Scope

This report documents the construction, calibration, evaluation, and use of a hydrologic model to simulate the effects of historical and potential future climate and land-cover conditions on water availability and streamflow dynamics in an approximately 446,600-square-mile (mi^2) region of the Southeastern United States. The hydrologic model was developed using the USGS Precipitation-Runoff Modeling System (PRMS; Leavesley and others, 1983; Markstrom and others, 2015), a deterministic, distributed-parameter, process-based model used to simulate the effects of precipitation, air temperature, and land use on basin hydrology. The PRMS model was used to provide hydrologic simulations for the period 1952–2099. PRMS parameters describing vegetation and impervious area were derived from annual estimates of land cover from 1952 to 2099 to incorporate land-cover dynamics in the hydrologic simulations. Daily maximum and minimum air temperature and precipitation data, preprocessed and interpolated from measured data to an approximately 12-kilometer (km) grid for 1949–2010, were used as historical climatic forcings for the PRMS model. The PRMS model was calibrated for the period 1980–2010, using measured streamflow, output from a Monthly Water Balance Model (MWBM), output from statistical streamflow models, and datasets of actual evapotranspiration (AET) and snow water equivalent (SWE). Statistically downscaled projections of climatic forcings from 13 general circulation models (GCMs) included as part of the Coupled Model Intercomparison Project Phase 5 (CMIP5) were used to assess potential future hydrologic response for the period 2045–2075. The GCMs were downscaled by the Bureau of Reclamation (2013) using the Daily Bias Correction Constructed Analogs (BCCA) method. Fifty-two statistics describing the duration, frequency, magnitude, rate of change, and timing of streamflows are presented for the periods 1952–2010 (historical baseline) and 2045–2075 (future evaluation period). These 52 metrics were selected to describe streamflow conditions that may be most useful in defining the suitability for each river or stream to support sustaining populations of priority aquatic species across the GCPO LCC.

Previous Investigations

This study combines large-scale hydrologic modeling, potential future climate inputs, dynamic land-cover inputs, and characterization of streamflow using various streamflow statistics. Many studies have focused on describing hydrological, water-quality, and ecological conditions for various parts of the Southeastern United States. Past hydrologic assessments for historical and potential future conditions in the Southeast document changes across the region (Mulholland and others, 1997; Cruise and others, 1999; Wood and others, 2002; Bosch and others, 2006; Sun and others, 2008; O’Driscoll and others, 2010; Sun, 2013; Barros and others, 2014; Marion and others, 2014; LaFontaine and others, 2015; Bock and others, 2016a. The USGS National Water Quality Assessment (NAWQA) Project has provided basin-, regional-, and national-scale assessments of water-quality status and trends in U.S. streams and rivers (https://water.usgs.gov/nawqa/studies/mrb/pubs.html, accessed September 23, 2017). The USGS has developed regional-scale nutrient assessments using the SPAtially Referenced Regressions On Watershed attributes (SPARROW) model (Booth and others, 2011; Garcia and others, 2011; Hoos and others, 2013). Estimates of potential future hydrologic conditions in the Southeastern United States have been developed for parts of the study area or as part of a larger study (Wood and others, 2002; Bock and others, 2016a). Bock and others (2016a, b) developed an application of the Monthly Water Balance Model (McCabe and Markstrom, 2007) for the CONUS that simulated potential future hydrologic response using 235 downscaled GCMs. Wood and others (2002) developed a gridded application of the Variable Infiltration Capacity (Liang and others 1994, 1996, 1999) model for the Eastern United States with grid cells approximately 150 square kilometers in area. Mulholland and others (1997) evaluated the effects of climate change on freshwater ecosystems in the Southeastern United States and found a general increase in net primary production, a decrease in habitat for cool water species, a reduction in summer base flows, and shorter periods of riparian wetland inundation.

Land-cover change and its associated stressors (for example, population growth and water use) can have a substantial effect on hydrologic response (Paul and Meyer, 2001; Barros and others, 2014). The Southeastern United States has gone through several phases of land-cover change; from forest to agriculture during the colonial period through the early 20th century; reforestation in many areas during the middle part of the 20th century; and more recently substantial urban, suburban, and agricultural development (Scott, 2006). Each of these phases of land-cover change across the Southeastern United States has affected the hydrologic response in the region. LaFontaine and others (2015) simulated the hydrologic response of the Apalachicola-Chattahoochee-Flint River Basin to potential changes in climate and land cover and found that potential land-cover change (urbanization in particular) had a substantial effect on the partitioning of runoff sources. Sun and others (2008) evaluated water-supply stress for the Southeastern United States and found that population increases led to water-supply stresses in urban areas. A review by O’Driscoll and others (2010) found that urbanization can affect many instream processes such as channel geomorphology, sediment transport, water quality, ecosystem processes, and biological communities due to changes in the duration and frequency of high and low flows, as well as water-quality changes from increased urban runoff. The effects of land-cover change may be scale dependent, with more effects at the local scale, and would therefore need to be included in analyses of potential future hydrologic response.

Hydrologic indices, including climate, landscape, and streamflow characteristics, are useful tools to group streams by similar behavior and provide predictive capacity to ecological models (McManamay and Frimpong, 2015; Leasure and others, 2016). Hydrologic indices have been used to assess ecological flow requirements and fish population dynamics in the Southeastern United States (Freeman and others, 2013; Knight and others, 2012; Murphy and others, 2013; Knight and others, 2014). Using ecologically relevant hydrologic characteristics, Poff (1996) was able to classify a set of 420 relatively unregulated streams into 10 distinctive stream types. Hundreds of hydrologic indices have been developed in the past to characterize streamflow regimes and behavior. Examples of hydrologic index suites are the Indicators of Hydrologic Alteration developed by Richter and others (1996) and the USGS hydrologic index tool (HIT; Henriksen and others, 2006). These indices generally focus on describing the duration, frequency, magnitude, rate of change, and timing of streamflow for a given watershed and provide a mechanism to compare hydrologic behavior across watersheds and time. Redundancy, however, is a concern with such a large number of indices when trying to determine which ones are appropriate for a particular management issue (Archfield and others, 2014). Analyses of a large number of available hydrologic indices have indicated a high degree of intercorrelation between many of the indices (Olden and Poff, 2003; Gao and others, 2009). A specific suite of hydrologic indices would need to be devised in a systematic way to address a particular hydrologic or ecological question. For this study, a set of hydrologic indices was selected to describe streamflow conditions that may be most useful in defining the suitability for a river or stream to sustain populations of priority aquatic species across the GCPO LCC. A comprehensive and spatially contiguous framework for generating hydrologic information can be developed from a contiguous hydrologic model of a region. In this study, the PRMS is used as the structural model framework.

The PRMS has been used for several modeling studies in the Southeastern United States for both historical and potential future climate and land-cover conditions. Hay and others (2011), Markstrom and others (2012), and Viger and others (2011) used output from the PRMS to simulate historical and potential future streamflow in the upper Flint River Basin in Georgia. LaFontaine and others (2013, 2015) used the PRMS to simulate historical and potential future streamflow, respectively, in the Apalachicola-Chattahoochee-Flint River Basin. Hunt and Garcia (2014) used the PRMS to simulate historical streamflow for all basins in the State of Alabama. Hydrologic simulations using the PRMS were included in two model intercomparison studies in the Southeastern United States (Farmer and others, 2014; Caldwell and others, 2015). In recent years, the spatial extent of hydrologic simulations using the PRMS has become larger. To facilitate the development of larger regional- to national-scale hydrologic assessments, the USGS developed the National Hydrologic Model (NHM; Regan and others, 2018). The NHM provides a consistent framework for the CONUS to apply hydrologic modeling methodologies and compute relevant hydrologic indices for use in characterizing hydrologic response. The initial configuration of PRMS for the modeling application described in the current report was extracted from the NHM.

The current study builds on a diverse set of past modeling and data-collection efforts in the region. New methodologies and frameworks developed as part of previous PRMS applications (for example, regional calibration, dynamic parameters, NHM) facilitate an application of this size. Previous studies show that land-cover change can have a substantial effect on hydrologic response. The availability of land-cover change products allows for the inclusion of landscape evolution within a continuous simulation. Past studies were limited to one realization of landscape characteristics or performing multiple simulations to analyze a range of landscape configurations. Research on potential redundancy of the many flow metrics that have been developed guided the selection of a subset of metrics for the current study. Flow metrics are used to assess potential effects on ecological processes and aquatic species. The construction of a daily time step hydrologic modeling application in the Southeastern United States that incorporates drivers of change (for example, climate and land cover) and provides outputs that are appropriate for a diverse set of management applications is motivated by current information needs across the natural resources community.

Hydrologic Description of the Study Area

The study area encompasses a diverse area of approximately 446,600 mi^2 in the Southeastern United States, including the majority of basins draining to the Gulf of Mexico (for example, lower Mississippi River Basin, Alabama-Coosa-Tallapoosa River Basin, Apalachicola-Chattahoochee-Flint River Basin) and two basins draining to the Atlantic Ocean (Altamaha and St. Mary's River Basins) (fig. 2). Altitude across the study area ranges from sea level at the coast to more than 5,400 feet in the southern Appalachian Mountains in western North Carolina and northeastern Georgia (fig. 2). Mean annual air temperature ranges from 70 to 75 degrees Fahrenheit (°F) in the southern part of the study area in central Florida to less than 50 °F in the southern Appalachian Mountains of western North Carolina, with a warm to cool distribution that varies with latitude (fig. 3). Mean annual precipitation is lowest in the northern and western parts of the study area, with accumulations less than 40 inches per year, and highest in the southern Appalachian Mountains of western North Carolina and northeastern Georgia, with accumulations of more than 90 inches per year (fig. 3). Precipitation accumulation for the majority of the study area ranges between 40 and 60 inches per year.

The study area includes all or part of six U.S. Environmental Protection Agency Level II ecoregions, including the Southeastern USA Plains (ecoregion 8.3), the Ozark, Ouachita-Appalachian Forests (ecoregion 8.4), the Mississippi Alluvial and Southeast USA Coastal Plains (ecoregion 8.5), the Temperate Prairies (ecoregion 9.2), the South Central Semi-Arid Prairies (ecoregion 9.4), and the Texas-Louisiana Coastal Plain (ecoregion 9.5) (fig. 2). Ecoregions were developed for North America to provide a geographic framework to facilitate ecosystem management and environmental understanding (Omernik and Griffith, 2014). The Southeastern USA Plains ecoregion has a mild, mid-latitude, humid subtropical climate with hot summers and mild winters. The hydrology of the Southeastern USA Plains ecoregion consists of low to moderate gradient perennial and intermittent streams (Omernik and Griffith, 2014). Land cover for the part of this ecoregion within the study area is predominantly forest (42.6 percent), with 13.4 percent covered with hay/pasture and 7.9 percent developed land cover (table 1; Omernik and Griffith, 2014). The Ozark, Ouachita-Appalachian Forests ecoregion has a mild, mid-latitude, humid subtropical climate with hot summers and mild winters. The hydrology of the Ozark, Ouachita-Appalachian Forests ecoregion is mostly high to moderate gradient perennial and intermittent streams with some parts of the ecoregion having low to moderate gradient streams of both dendritic and trellis type networks (Omernik and Griffith, 2014). Land cover for the part of this ecoregion within the study area is predominantly forest (60.6 percent), with 21.6 percent covered with hay/pasture and 7.4 percent developed land cover (table 1; Omernik and Griffith, 2014). The Mississippi Alluvial and Southeast USA Coastal Plains ecoregion has a mild, mid-latitude, humid subtropical climate with hot humid summers and warm to mild winters. The hydrology of the Mississippi Alluvial and Southeast USA Coastal Plains ecoregion consists of low gradient perennial streams and rivers (including the Mississippi River), swamps, marshes, and estuaries (Omernik and Griffith, 2014). Land cover for this ecoregion is predominantly cultivated crops (35.4 percent) and wetlands (32.8 percent), with 10.1 percent forest and 6.7 percent developed land cover (table 1; Omernik and Griffith, 2014).

The part of the Temperate Prairies ecoregion that is included in the study area has a humid subtropical climate with hot summers and mild to cold winters. The hydrology of the Temperate Prairies ecoregion consists of perennial streams with some large rivers (for example, the Missouri River) (Omernik and Griffith, 2014). Land cover for the part of the ecoregion that is included in the study area is predominantly hay/pasture (42.4 percent), with 27.6 percent cultivated crops, 15.2 percent forest, and 6.3 percent developed land cover (table 1; Omernik and Griffith, 2014). The part of the South Central Semi-Arid Prairies ecoregion that is included in the study area has a severe to mild, mid-latitude, humid subtropical climate with hot summers and mild to severe winters. The hydrology of the South Central Semi-Arid Prairies ecoregion consists of low to moderate gradient perennial and intermittent streams (Omernik and Griffith, 2014). Land cover for the part of the South Central Semi-Arid Prairies ecoregion that is included in the study area is predominantly shrub/scrub/herbaceous (34.1 percent), with 24.3 percent forest, 18.4 percent hay/pasture, 12.2 percent cultivated crops, and 8.2 percent developed land cover (table 1; Omernik and Griffith, 2014). The part of the Texas-Louisiana Coastal Plain ecoregion that is included in the study area has a mild, mid-latitude, humid subtropical climate with hot summers and mild winters. The hydrology of the Texas-Louisiana Coastal Plain ecoregion consists of low gradient intermittent and perennial streams (Omernik and Griffith, 2014). Land cover for the part of the Texas-Louisiana Coastal Plain ecoregion that is included in the study area is predominantly wetlands (25.2 percent) with 22.5 percent cultivated crops, 20.1 percent hay/pasture, and 16.8 percent developed land cover (table 1; Omernik and Griffith, 2014).

Impervious area is an important land-cover property that can have substantial implications for hydrologic response, most notably changes to infiltration of precipitation and increases in the magnitude and frequency of storm runoff events (Paul and Meyer, 2001). Figure 4 shows the distribution of 15 land-cover classes from the National Land Cover Database 2011 (NLCD2011; Homer and others, 2015). Impervious area is associated with the four developed land-cover classes in the NLCD2011 (Developed, Open Space; Developed, Low Intensity; Developed, Medium Intensity; and Developed, High Intensity). These land-cover classes are predominant in the urban centers located within the study area; examples include Atlanta, Georgia; Houston, Texas; and St. Louis, Missouri. This study incorporates changing land cover on an annual time step for the simulation period (1952–2099). Changes in impervious area and dominant land-cover type are discussed later in the report and in appendix 1.

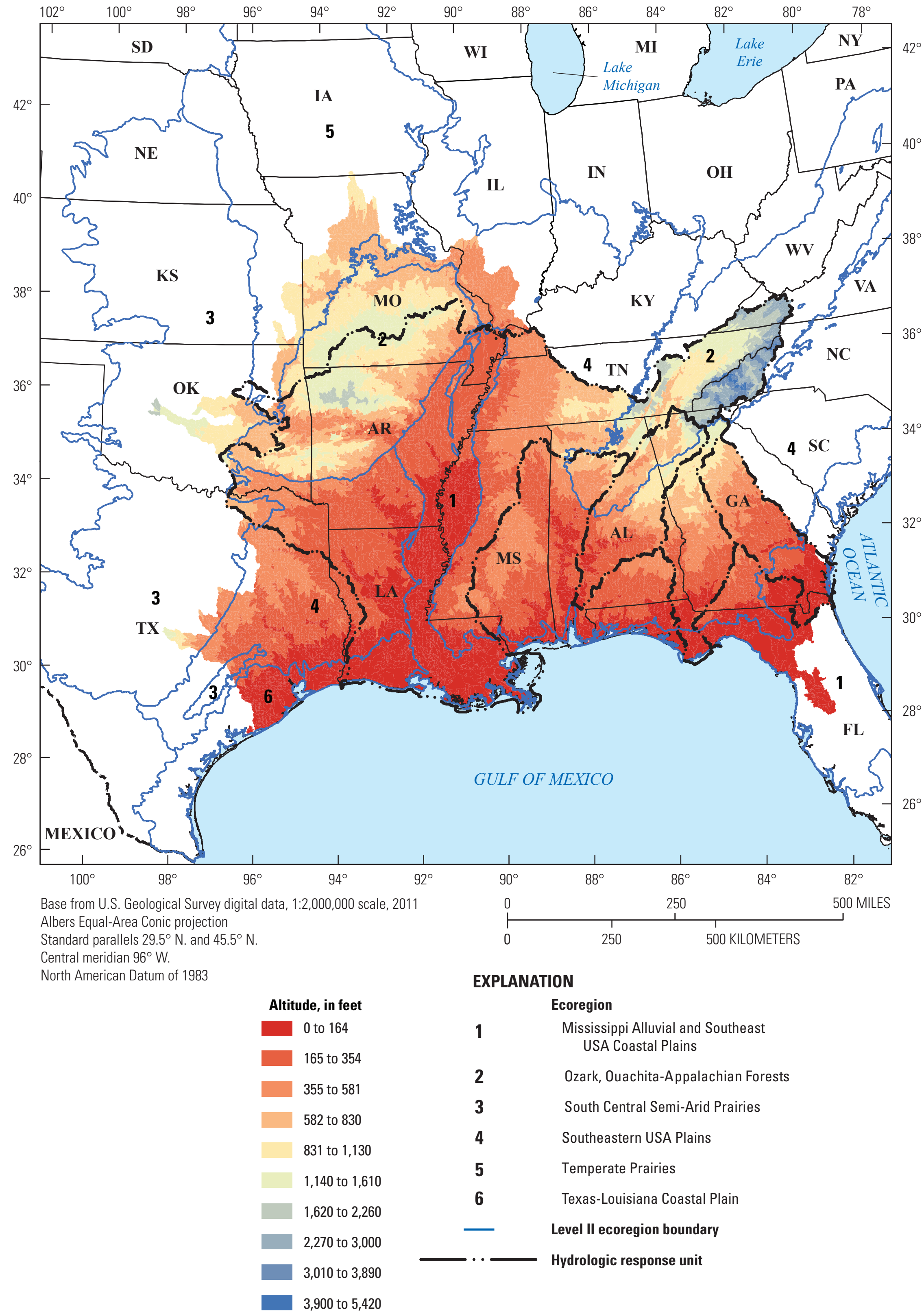

Figure 2. Map showing the range in altitude and U.S. Environmental Protection Agency Level II ecoregions included within the study area. Ecoregion names (EPA, 2016) are (*1*) Mississippi Alluvial and Southeast USA Coastal Plains, (*2*) Ozark, Ouachita-Appalachian Forests, (*3*) South Central Semi-Arid Prairies, (*4*) Southeastern USA Plains, (*5*) Temperate Prairies, and (*6*) Texas-Louisiana Coastal Plain. Altitude is shown using the Precipitation-Runoff Modeling System parameter hru_elev value for each hydrologic response unit (Markstrom and others, 2015). Altitude data are from the digital elevation model included with the National Hydrography Dataset version 1 (http://www.horizon-systems.com/NHDPlus/NHDPlusV1_home.php, accessed April 1, 2013).

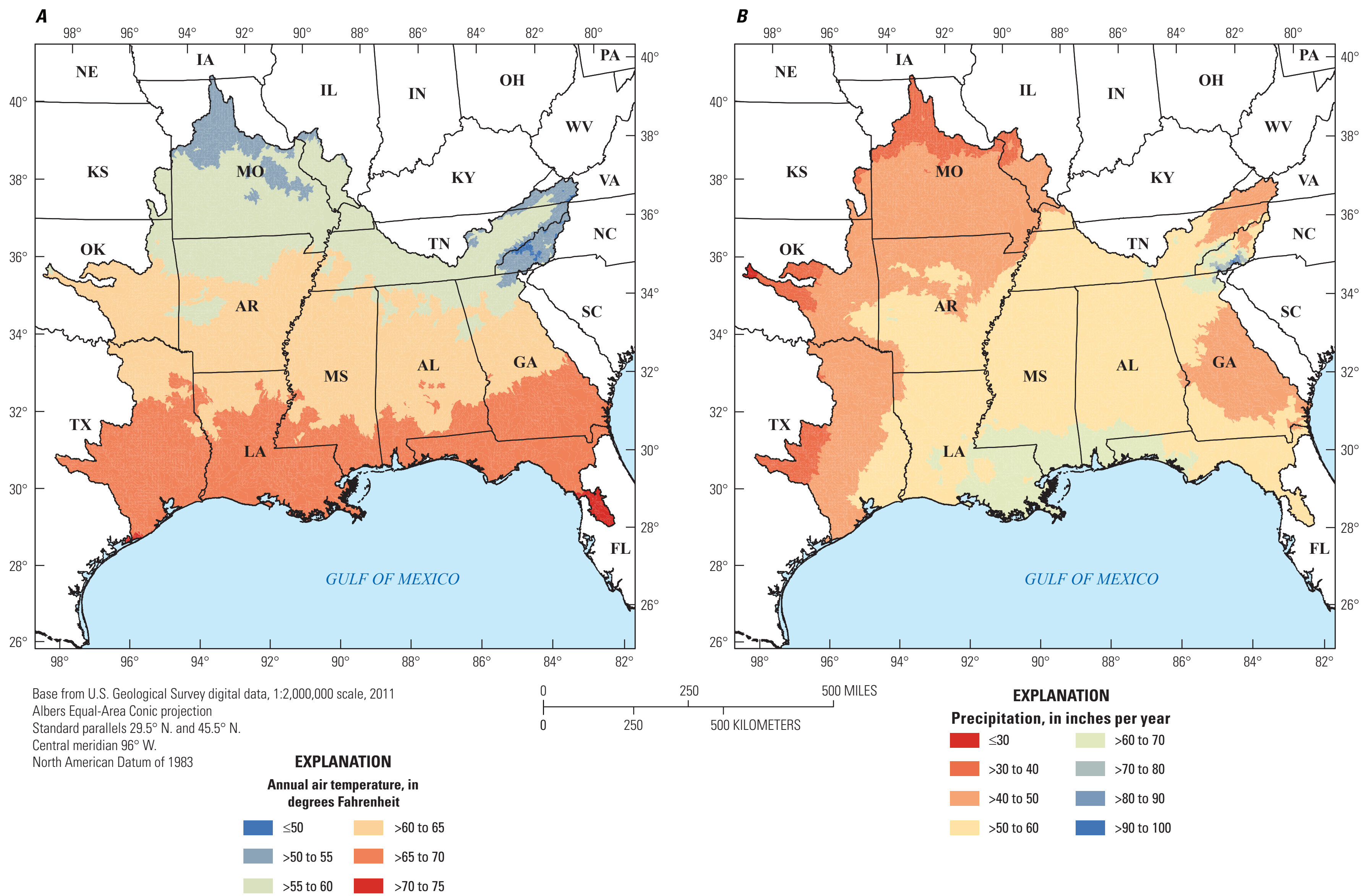

Figure 3. Maps showing the distribution of mean annual (*A*) air temperature, and (*B*) precipitation, summarized on the hydrologic response units for the period 1949–2010. Units of air temperature are degrees Fahrenheit and units of precipitation are inches per year. Precipitation and air temperature data are from the dataset developed by Maurer and others (2002).

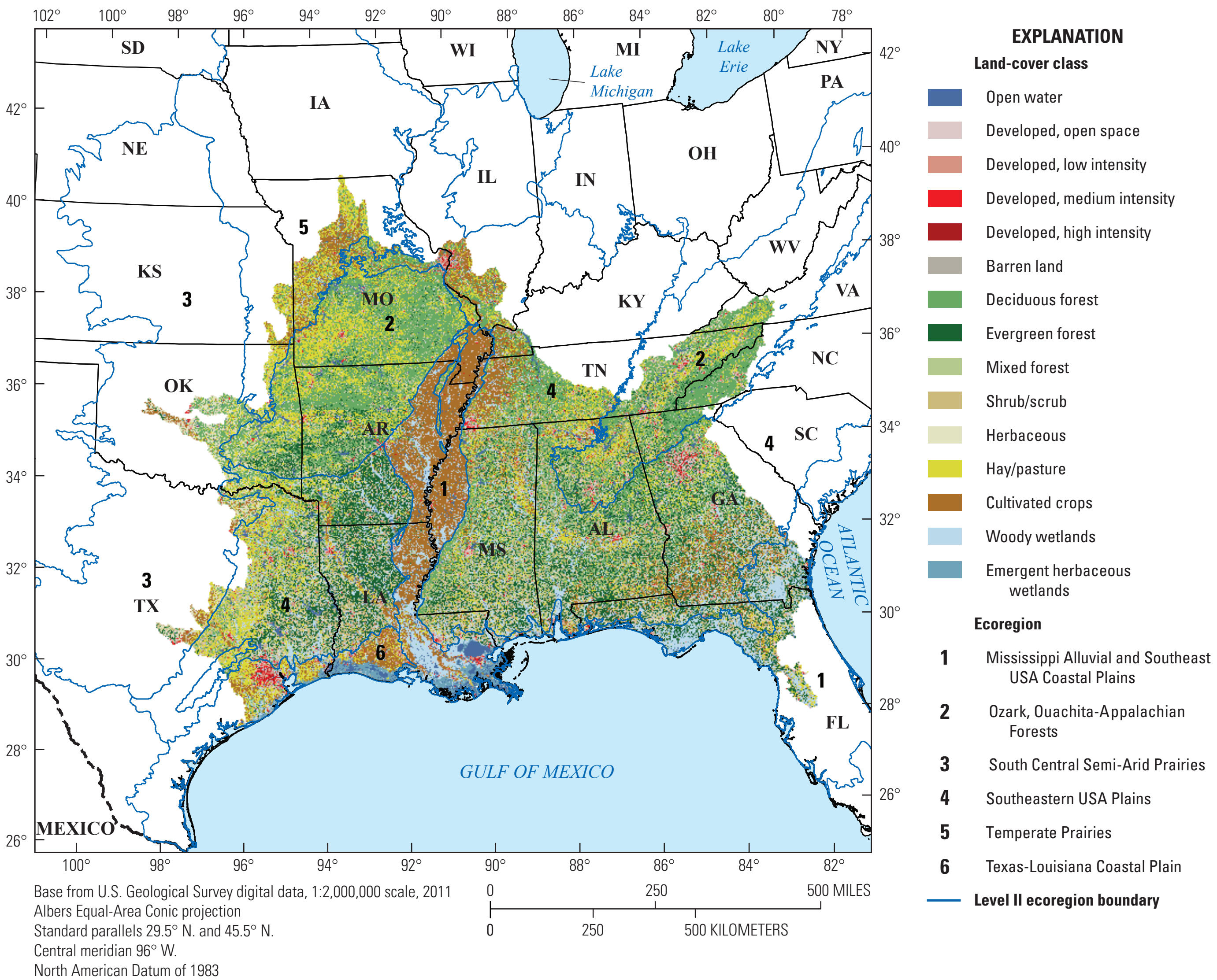

Figure 4. Map showing land-cover classes from the National Land Cover Database 2011 and U.S. Environmental Protection Agency Level II ecoregions included within the study area. Ecoregion names are (*1*) Mississippi Alluvial and Southeast USA Coastal Plains, (*2*) Ozark, Ouachita-Appalachian Forests, (*3*) South Central Semi-Arid Prairies, (*4*) Southeastern USA Plains, (*5*) Temperate Prairies, and (*6*) Texas-Louisiana Coastal Plain. National Land Cover Database 2011 data are from Homer and others, 2015.

Table 1. Land-cover percentages from the National Land Cover Database 2011 (Homer and others, 2015) for the study area, summarized by U.S. Environmental Protection Level II ecoregion (Omernik and Griffith, 2014).

[The land-cover percentages for each ecoregion are only for that part of the ecoregion in the study area]

	Level II ecoregion					
	1. (8.5) Mississippi Alluvial and Southeast USA Coastal Plains	2. (8.4) Ozark, Ouachita-Appalachian Forests	3. (9.4) South Central Semi-Arid Prairies	4. (8.3) Southeastern USA Plains	5. (9.2) Temperate Prairies	6. (9.5) Texas-Louisiana Coastal Plain
Area, in square miles	68,415	106,897	13,253	227,540	15,699	14,245
Fraction of study area	15.3	24.0	3.0	51.0	3.5	3.2
Land-cover type	Land-cover percentages					
Developed, total	6.7	7.4	8.2	7.9	6.3	16.8
Forest, total	10.1	60.6	24.3	42.6	15.2	4.1
Cultivated crops	35.4	1.4	12.2	8.3	27.6	22.5
Hay/pasture	2.5	21.6	18.4	13.4	42.4	20.1
Water	6.5	1.9	1.6	2.0	1.5	6.7
Barren	0.3	0.3	0.2	0.3	0.1	0.5
Shrub/scrub/herbaceous	5.7	6.1	34.1	14.4	3.8	4.1
Wetlands	32.8	0.7	1.2	11.1	3.1	25.2

Hydrologic Simulation Methods for Modeling the Southeastern United States

Providing reliable hydrologic simulations for a region as large as the study area requires multiple types of input and calibration datasets and a consistent hydrologic framework of modeling units. Because much of the study area does not have measurements of reference-quality streamflow (Kiang and others, 2013), other datasets were needed for the construction, calibration, and evaluation of the hydrologic model. The USGS developed an NHM framework consisting of hydrologic response units (HRUs) and stream segment spatial units, attributes of those spatial units, and default model parameters for a national application of the PRMS called the NHM-PRMS (Viger and Bock, 2014; Regan and others, 2018). A calibrated application of the MWBM, called the NHM-MWBM, has also been developed using the NHM (Bock and others, 2016a). Statistically based streamflow time series were simulated using the methods developed by Farmer (2016). These various tools were combined to provide hydrologic simulations for the study area. A description of the construction, calibration, and evaluation of the regional PRMS application is provided in appendix 1.

National Hydrologic Model

To support the efficient construction of local-, regional-, and national-scale hydrologic models for the CONUS, Viger and Bock (2014) developed the Geospatial Fabric for National Hydrologic Modeling. The Geospatial Fabric for National Hydrologic Modeling includes two main products: (1) geographic information system (GIS) files of spatial features (HRUs, stream segments, and points of interest) and (2) GIS-based tables of attributes describing the spatial features. The Geospatial Fabric for National Hydrologic Modeling spatial features include 109,951 HRUs and 56,460 stream segments. The HRUs for CONUS have a mean and median size of 28.7 and 12.8 mi^2, respectively. The HRUs used in the study area have a mean and median size of 22.0 and 12.4 mi^2, respectively. The stream segments for CONUS have a mean and median length of 9.1 and 8.5 miles, respectively. The stream segments used in the study area have a mean and median length of 8.8 and 8.4 miles, respectively. A description of the current version of the NHM-PRMS, including the derivation of the initial model parameters, is provided by Regan and others (2018).

Precipitation-Runoff Modeling System (PRMS)

The PRMS is a modular, deterministic, distributed-parameter, physical-process-based hydrologic simulation code. It was developed to evaluate the effects of various combinations of climate, physical characteristics, and simulation options on hydrologic response and water distribution at the watershed scale (Leavesley and others, 1983; Markstrom and others, 2015). The PRMS computes water flow and storage from and to the atmosphere, plant canopy, land surface, snowpack, surface depressions, shallow subsurface zone, saturated zone aquifers, stream segments, and lakes. Physical characteristics, including topography, soils, vegetation, geology, and land use, are used to characterize and derive parameters required in simulation algorithms, spatial discretization, and topological connectivity. Computations of the hydrologic processes use historical, current, and (or) potential future climate data consisting of daily precipitation and minimum and maximum air temperature. Other datasets, such as potential evapotranspiration, solar radiation, streamflow, plant transpiration period, wind speed, and humidity, can be incorporated into PRMS simulations, but are optional. The PRMS operates on a daily time step with simulation periods from days to centuries. A schematic of the PRMS conceptualization is shown in figure 5. A detailed schematic of the soil zone and its hydrologic connections to other parts of the PRMS is shown in figure 6.

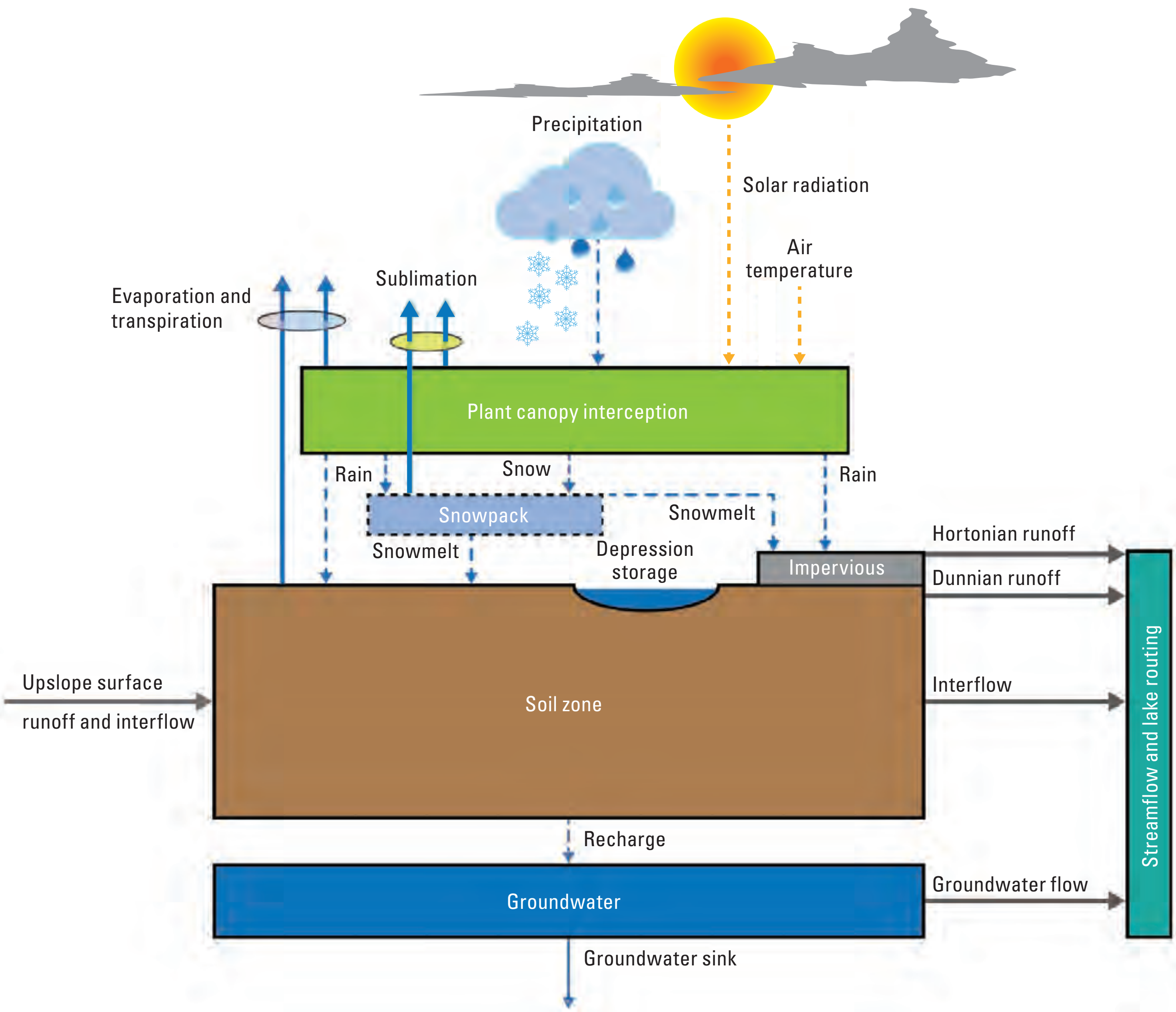

Figure 5. Conceptual schematic of the Precipitation-Runoff Modeling System (from Regan and LaFontaine, 2017).

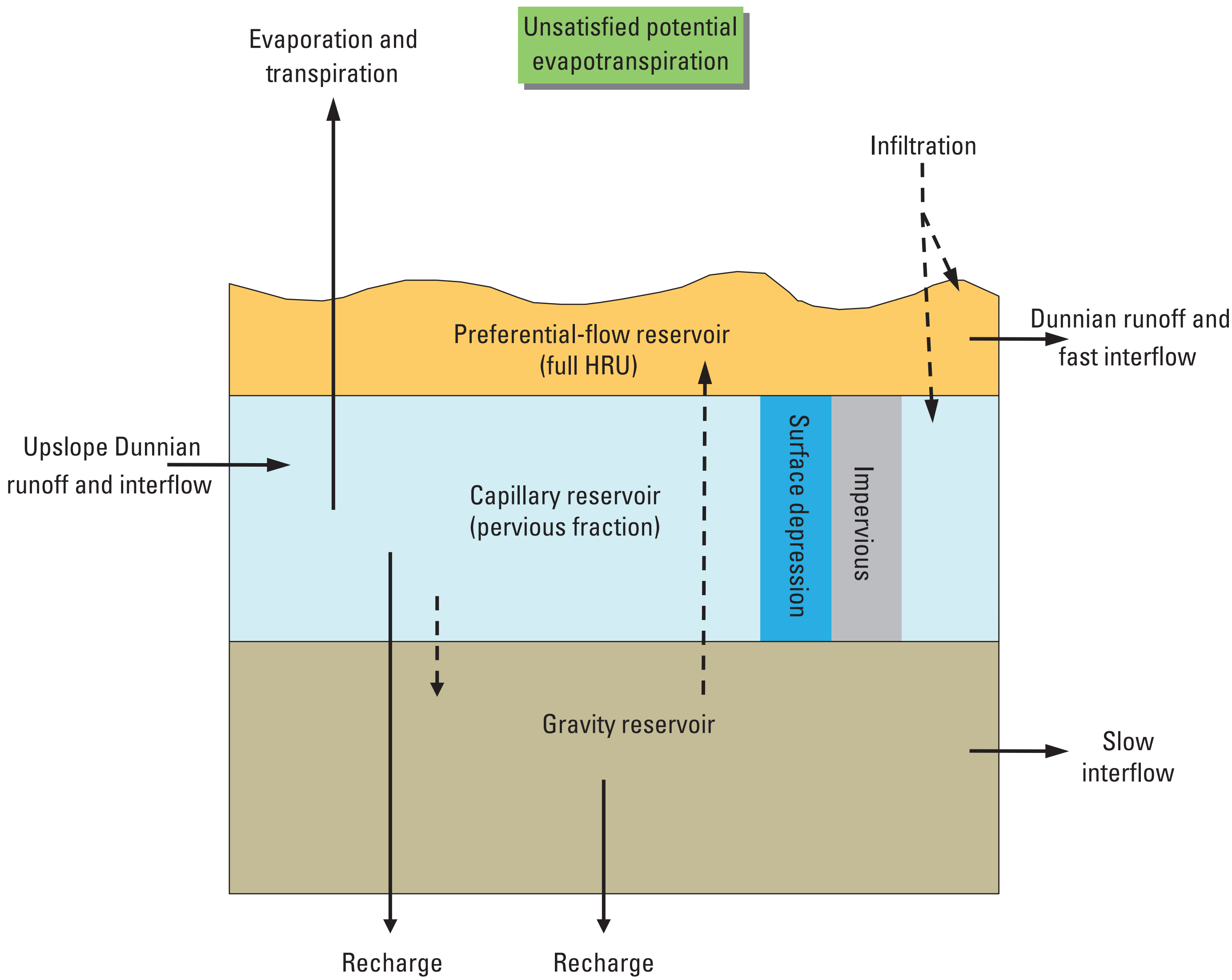

Figure 6. Conceptual schematic of the Precipitation-Runoff Modeling System including the detail of the soil zone (from Regan and LaFontaine, 2017).

The PRMS simulates the hydrologic response of a geographic area, called the model domain. The model domain is typically discretized into HRUs on which PRMS computes water flux and storage at a daily time step in response to inputs of climate, air temperature, and precipitation. Stream segments are used to represent channelized flow in the model domain and connect the network of HRUs to simulate accumulated streamflow from the upstream watershed. The PRMS computes flow components (surface runoff, shallow subsurface flow, and groundwater flow) generated on each HRU for each time step. These flow components then are directed to stream segments for flow aggregation. In addition, two types of water bodies are simulated by PRMS—on-channel lakes and off-channel surface-depression storage. On-channel lakes can be used to simulate features such as reservoirs, whereas surface depressions are conceptualized as water bodies that are not directly connected to the stream network, such as farm ponds. Regan and LaFontaine (2017) describe recent enhancements to the PRMS, including the use of dynamic parameters. This new capability allows for the simulation of changing landscape characteristics throughout a PRMS simulation and was used to vary dominant land-cover type, percent impervious area, and canopy interception on an annual time step for the model simulations. Appendix 1 of this report provides details about the PRMS model construction, calibration, and evaluation.

Monthly Water Balance Model (MWBM)

The Monthly Water Balance Model (MWBM) is a modular water accounting model that estimates components of the hydrologic cycle on a monthly time step (fig. 7; Wolock and McCabe, 1999; McCabe and Markstrom, 2007). Monthly estimates of runoff for each watershed for the period 1951–2010 were obtained from the application of the MWBM by Bock and others (2016a) using the NHM version of the MWBM (NHM-MWBM). This application of the NHM-MWBM was constructed using the same modeling units as the NHM-PRMS model. Monthly inputs of average air temperature and precipitation accumulation are used by the MWBM to compute seven model variables including potential evapotranspiration (PET), actual evapotranspiration (AET), snow water equivalent (SWE), direct runoff, soil moisture storage, and surplus runoff. Parameters used by the MWBM include latitude of the HRU, soil moisture storage capacity, and PET coefficients. The application of the NHM-MWBM by Bock and others (2016a) simulated hydrologic response using the climate forcings developed by Maurer and others (2002). Bock and others (2016a) summarized those climate forcings to the model HRUs using the USGS GeoData Portal. Soil moisture storage capacity was computed from the 1-km × 1-km gridded USGS dataset Soils Data for the Conterminous United States (STATSGO; Wolock, 1997). The PET coefficients were computed for the Hamon PET method using a mean monthly evapotranspiration product developed by Farnsworth and Thompson (1982). A detailed description of the development of the PET coefficients is provided by McCabe and others (2015). The MWBM was calibrated by Bock and others (2016a) for the CONUS using a regional grouping scheme (49 calibration regions) and 1,575 streamgages. The calibration resulted in group Nash-Sutcliffe Index values greater than 0.6 for most of the Eastern United States and the west coast of the United States. Nash-Sutcliffe Index values less than 0.6 for most of the Central and Southwestern parts of the United States (Bock and others, 2016a, fig. 14) for the outputs of monthly runoff, AET, and SWE (where applicable) from the MWBM were used as calibration targets for the application of the Precipitation-Runoff Modeling System in the Southeastern United States (GCPO-PRMS) (see appendix 1 for further details).

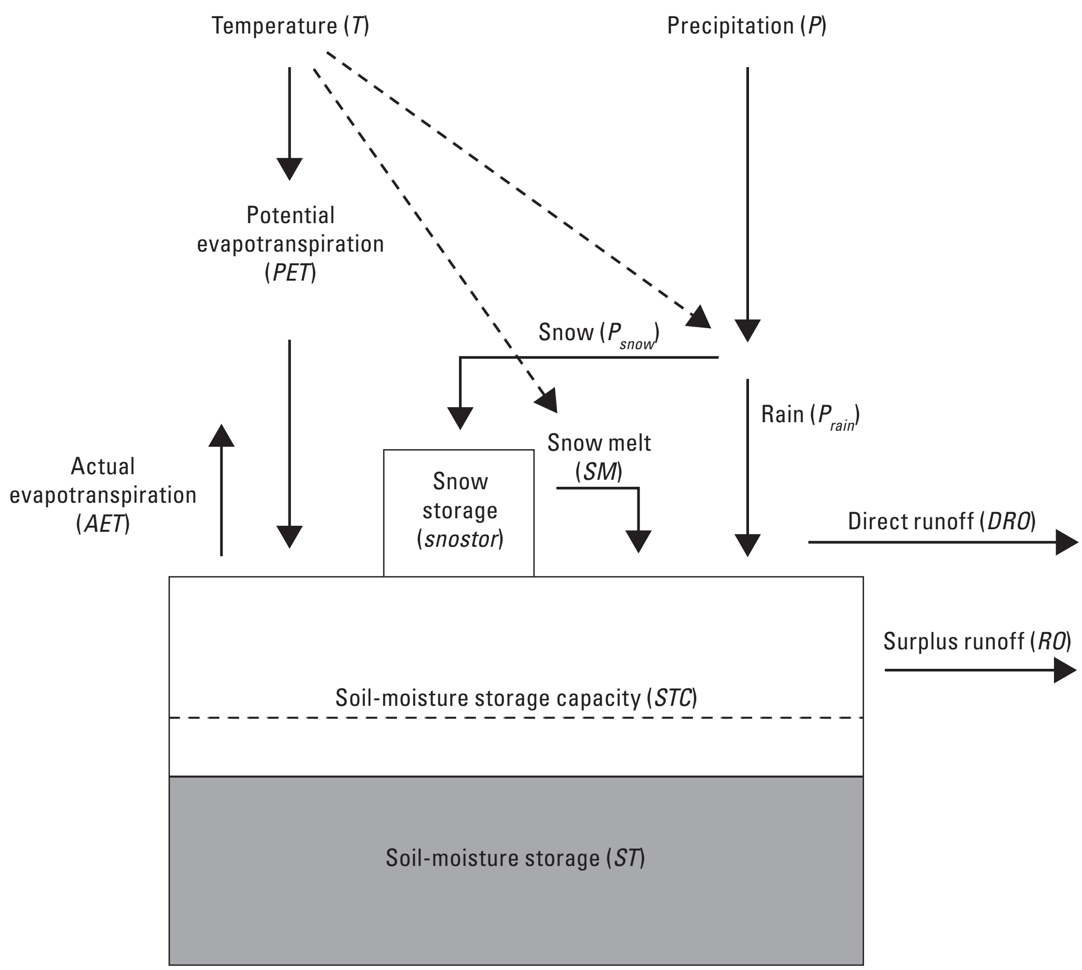

Figure 7. Schematic of the Monthly Water Balance Model (from McCabe and Markstrom, 2007).

Statistical Time Series of Streamflow

Statistically based streamflow simulations were constructed using an application of ordinary kriging developed by Farmer (2016). These simulations were developed for 1,262 headwater watersheds in the study area and were used as calibration targets for the extraction from the NHM-PRMS for this study in the Southeastern United States, referred to as the GCPO-PRMS. The headwater watersheds are defined for this study as areas less than 1,158 mi^2 (3,000 square kilometers) in drainage areas that contribute to the large mainstem rivers of the study area. Ordinary kriging is a geostatistical tool that uses the distance between two points to predict the semivariance of a dependent variable. A buffer of 186 miles (300 km) around the study area was used for streamgage selection from the GAGES-II dataset developed by Falcone (2011). Streamflow data from 482 reference-quality streamgages were used in the ordinary kriging methodology to simulate daily time step streamflow at the outlets of the 1,262 headwater watersheds for 1981–2010. A leave-one-out validation procedure, where simulated daily streamflow time series were developed for each headwater watershed using 481 of the 482 total streamgages, was used resulting in a range of simulations for each headwater watershed. The maximum, minimum, and median simulated daily streamflows from the leave-one-out analysis were used for PRMS model calibration (as part of the streamflow timing objective function) as described in appendix 1 of this report. The performance of the statistical streamflow time series compared to reference-quality streamgages that coincided with headwater outlets had a median Nash-Sutcliffe model efficiency index of approximately 0.78 (Nash and Sutcliffe, 1970). The statistically based daily streamflow simulation data are documented in the accompanying data release (LaFontaine and others, 2019).

Historical and Potential Future Climate Inputs

Climate inputs of both historical and potential future precipitation and air temperature data were used in this study. Observation-based historical climate inputs developed by Maurer and others (2002) for the period 1949–2010 were used for the calibration of the NHM-MWBM developed by Bock and others (2016a) and the GCPO-PRMS application described in this report. Historical and future climate projection inputs from 13 statistically downscaled GCMs developed as part of CMIP5 were used to simulate potential future hydrologic response computed as the difference between the GCM-based historical simulations and the GCM-based future simulations (table 2; Meehl and others, 2009; Hurrell and others, 2011; Taylor and others, 2012). The GCMs were downscaled by the Bureau of Reclamation (2013), using the Daily Bias Correction Constructed Analogs method (Hidalgo and others, 2008; Maurer and Hidalgo, 2008; Maurer and others, 2010). The original downscaled GCM datasets are available at https://gdo-dcp.ucllnl.org/downscaled_cmip_projections/ (accessed October 20, 2014). A total of 45 future scenarios grouped by four representative concentration pathways (RCPs) were used to assess potential changes in hydrologic response for the study area (table 2). The four RCPs represent potential changes in emissions of greenhouse gases, air pollutants, and land use based on various socioeconomic assumptions about the future and defined in terms of the resulting change in radiative forcing levels by the year 2100 (Vuuren and others, 2011). The GCMs and RCPs used from the CMIP5 for the hydrologic simulations were limited to those available through the USGS GeoData Portal—a web interface developed to process gridded datasets, such as climate inputs, to study units of interest (Blodgett and others, 2011). The historical time period available for the GCM-based climate inputs is 1950–2005. The GCM-based future scenario datasets are available for the period 2006–2099. A future period of analysis for 2045–2075 (centered on year 2060) was compared to the historical period (1952–2005) to assess potential changes in hydrologic response for this study. This future window was chosen to coincide with the target time frame of conservation planning activities in the GCPO LCC region in the Southeastern United States.

Historical and Potential Future Land-Cover Inputs

Land-cover vegetation type and the amount of impervious area in a watershed can substantially affect streamflow and other parts of the water budget such as evapotranspiration and soil moisture. Vegetation and impervious area can affect precipitation interception, infiltration into the soil zone, and runoff timing and magnitude. Using the dynamic parameters module in the PRMS, annual inputs of both historical and potential future land-cover type and percent impervious area were used to incorporate the evolution of the study area landscape for the period 1950–2099. Further details about the source of the land-cover data and the conversion to PRMS parameters are provided in appendix 1.

Figure 8 shows the distribution of dominant land-cover class as used in the PRMS for the years 1950, 2005, and 2060. Most of the study area is classified as tree, with grass being dominant in the northwestern part of the study area and in the Mississippi Alluvial Plain. Change in dominant land-cover class through the year 2060 consists mostly of conversion from tree to bare or tree to grass (fig. 8*C* and 8*D*). The tree to bare conversion is mostly associated with areas surrounding urban centers such as Atlanta, Georgia, and Houston, Texas.

Table 2. List of statistically downscaled general circulation model climate scenarios (historical and future representative concentration pathways) of precipitation and air temperature from the Coupled Model Intercomparison Project Phase 5 used for hydrologic simulations in the Southeastern United States.

[Historical datasets are for the period 1950–2005. Representative concentration pathway datasets are for the period 2006–2099. These general circulation models (GCMs) were downscaled by the Bureau of Reclamation (2013), using the Daily Bias Correction Constructed Analogs method (Hidalgo and others, 2008; Maurer and Hidalgo, 2008; Maurer and others, 2010). The downscaled GCM datasets are available at https://gdo-dcp.ucllnl.org/downscaled_cmip_projections/, accessed October 20, 2014. x, available; —, not available]

GCM	Historical	Representative concentration pathway				Modeling center
		2.6	4.5	6.0	8.5	
ACCESS1-0	x	—	x	—	x	Commonwealth Scientific and Industrial Research Organization and Bureau of Meteorology, Australia
bcc-csm1-1	x	x	—	x	x	Beijing Climate Center, China Meteorological Adminstration, China
BNU-ESM	x	—	x	—	x	College of Global Change and Earth System Science, Beijing Normal University, China
CCSM4 (run 1)	x	x	x	x	x	National Center for Atmospheric Research, USA
GFDL-ESM2G	x	x	x	x	x	National Oceanic and Atmospheric Administration Geophysical Fluid Dynamics Laboratory, USA
GFDL-ESM2M	x	x	x	x	x	
IPSL-CM5A-LR	x	x	x	—	x	Institut Pierre Simon Laplace, France
IPSL-CM5A-MR	x	x	x	x	x	
MIROC5	x	x	—	x	x	Japan Agency for Marine-Earth Science and Technology, Atmosphere and Ocean Research Institute (The University of Tokyo), and National Institute for Environmental Studies, Japan
MIROC-ESM	x	x	x	x	x	
MIROC-ESM-CHEM	x	x	x	x	x	
MRI-CGCM3	x	x	x	x	x	Meteorological Research Institute, Japan
NorESM1-M	x	x	x	x	x	Norwegian Climate Centre, Norway
GCM Count	13	11	11	10	13	

The tree to grass conversion in the northwestern part of the study area and the Mississippi Alluvial Plain is most likely associated with conversion to agricultural and pasture land-cover types, which both would be classified as grass in the PRMS land-cover classification system. From a hydrologic perspective, less tree land-cover type could lead to a decoupling of the current interception capacity–infiltration relation in the system, resulting in potential changes in the water balance (Bosch and Hewlett, 1982; Andreassian, 2004).

Figure 9 shows the distribution of the amount of impervious area across the study area. Percent impervious area by HRU is incorporated into PRMS simulations as described by Markstrom and others (2015). Most of the study area HRUs have less than 5 percent impervious area. Urban centers such as Atlanta, Houston, and St. Louis have the highest levels of impervious area in the 1950 period (fig. 9*A*). By year 2060, many of the urban areas that had been relatively small are projected to substantially increase in size (fig. 9*C*). The change in percent impervious area from 2005 to 2060 is shown in figure 9*D*. The change in impervious area is most noticeable in the areas surrounding existing urban centers such as Atlanta and Houston. Atlanta is projected to sprawl in all directions, whereas Houston is projected to mostly expand to the north. From a hydrologic perspective, these increases in impervious area can lead to reduced infiltration and increases in the number and magnitude of storm runoff events. To offset some of these effects, the use of best management practices, such as detention and retention structures, could be incorporated into future simulations but are beyond the scope of this study.

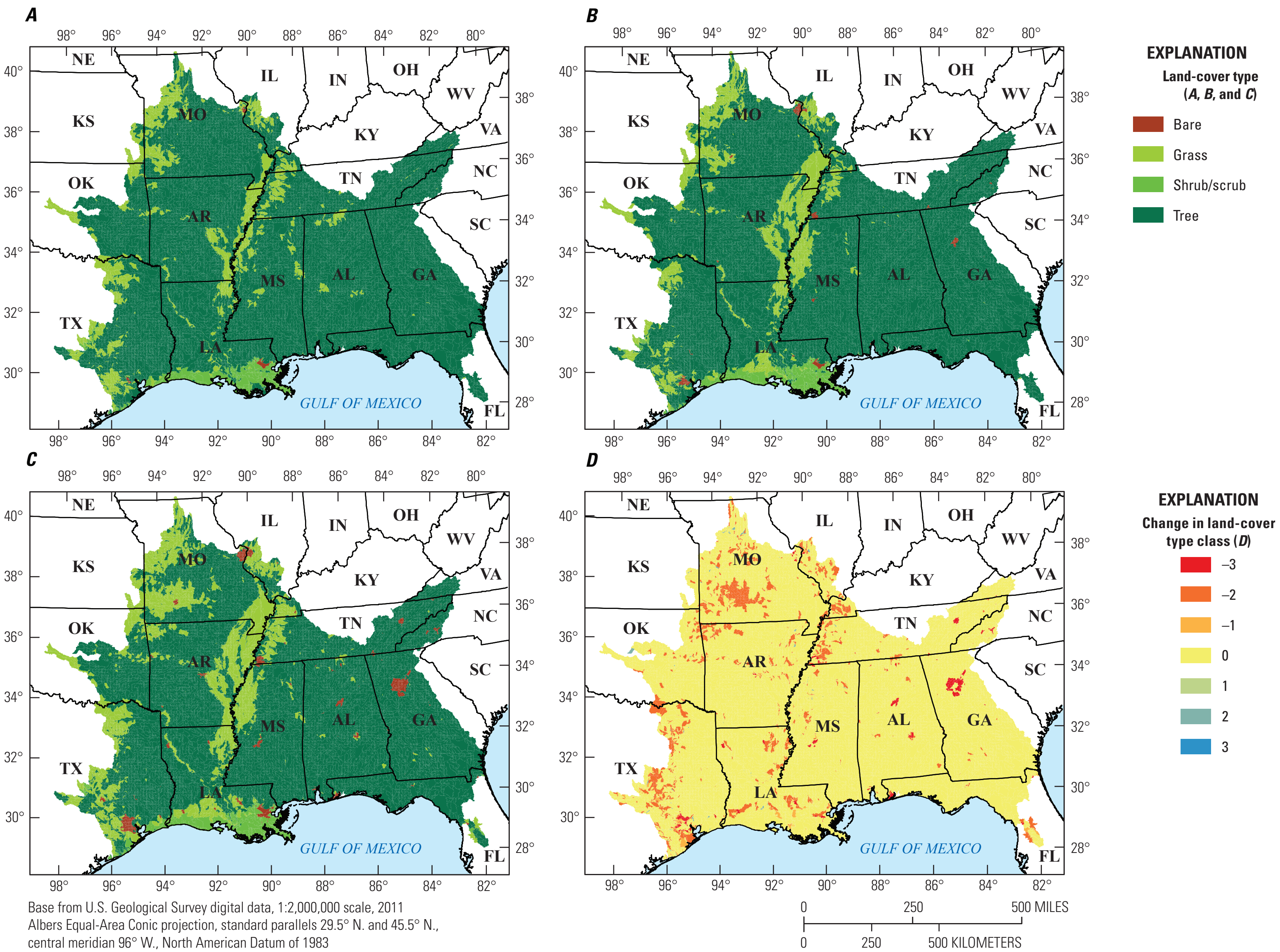

Figure 8. Maps showing the distribution of the Precipitation-Runoff Modeling System (PRMS) parameter **cov_type**, which describes the dominant land-cover type for each hydrologic response unit for years (*A*) 1950, (*B*) 2005, and (*C*) 2060. Land-cover types (and parameter values) within the PRMS include bare (0), grass (1), shrub/scrub (2), and tree (3). Change in land-cover type class from 2005 to 2060 is shown in figure part *D*. For the change in land-cover type class, a negative value means cov_type changed from a more vegetated state to a less vegetated state (for example, tree changing to bare due to urbanization). A positive value for change in land-cover type means that cov_type moved from a less vegetated state to a more vegetated state (for example, grass changing to tree). A zero value for change in land-cover type means that cov_type remained the same between 2005 and 2060.

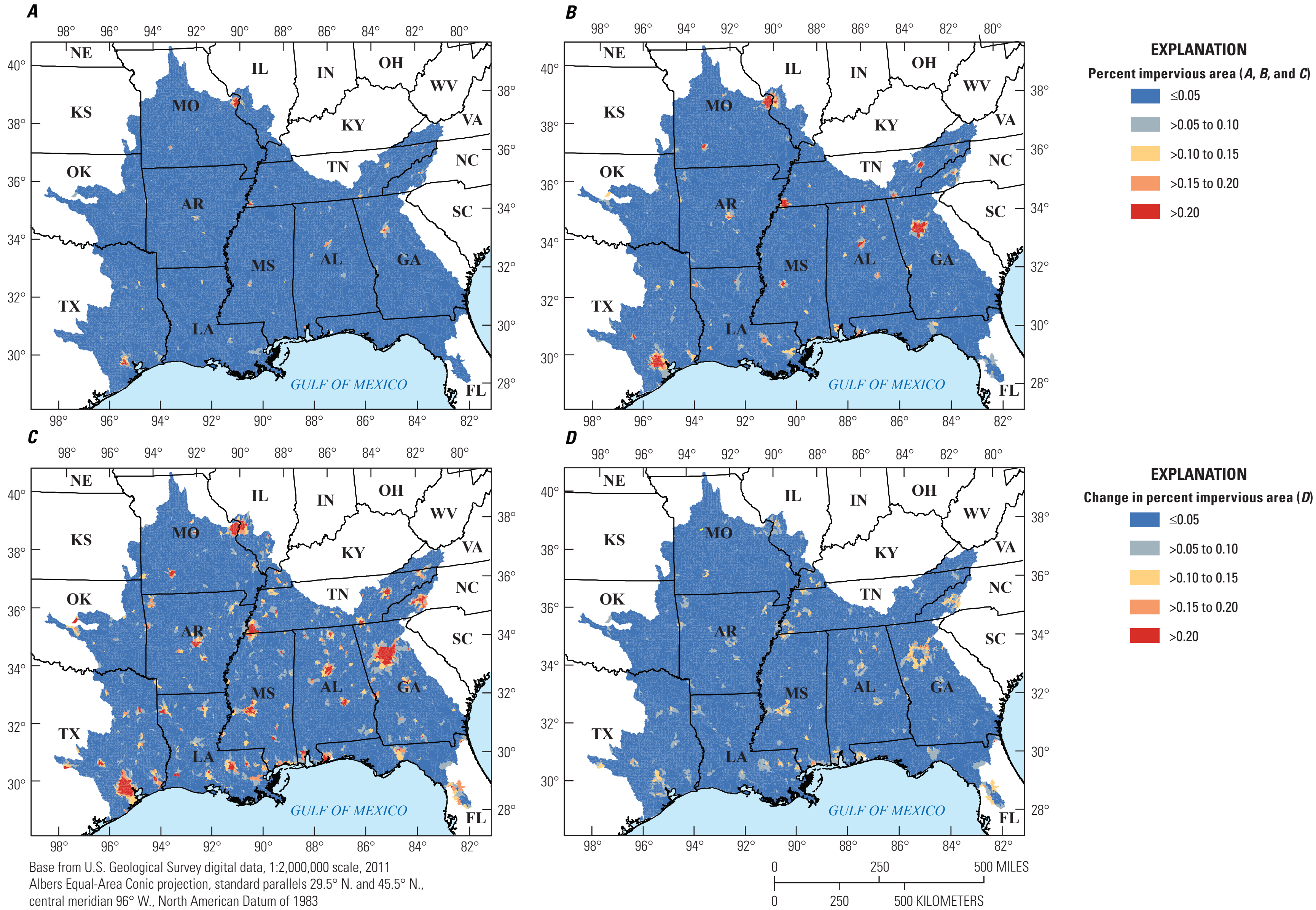

Figure 9. Maps showing the distribution of the Precipitation-Runoff Modeling System parameter **hru_percent_imperv**, describing the percent impervious area for each hydrologic response unit for years (*A*) 1950, (*B*) 2005, and (*C*) 2060. Change in percent impervious area from 2005 to 2060 is shown in figure part *D*.

Model Application and Hydrologic Simulations in the Southeastern United States

The GCPO-PRMS application simulates daily time step streamflow for 20,251 HRUs and 10,742 stream segments in the study area for the period 1952–2099 (fig. 1–1). The HRUs and stream segments and associated default parameters were obtained from the USGS NHM (Viger and Bock, 2014; Regan and others, 2018; Driscoll and others, 2017). Outputs from the MWBM developed by Bock and others (2016a), statistical streamflow simulations using ordinary kriging, USGS measured streamflow data, and remotely sensed data products of AET and SWE were used to calibrate the GCPO-PRMS application in a multistep process (fig. 1–3). Details about the construction, calibration, and evaluation of the GCPO-PRMS model and supporting datasets are provided in appendix 1 of this report. Historical and potential future climate and land-cover datasets were used for the simulations. Historical simulations used observations of precipitation and air temperature from the dataset developed by Maurer and others (2002) and 13 historical simulations of precipitation and air temperature from downscaled GCMs from CMIP5 (table 2). Future hydrologic simulations used 45 datasets of precipitation and air temperature from the downscaled GCMs from CMIP5 for four RCPs.

A wide diversity of river systems is present within the GCPO LCC geography—high-gradient streams in the Ozark, Ouachita-Appalachian Forests, medium-low gradient meandering rivers in the Southeast USA Coastal Plains, and mainstem rivers draining into the Gulf of Mexico. Aquatic organisms inhabiting these systems have evolved to require an equally diverse set of streamflow conditions to successfully survive and reproduce. The GCPO Technical Advisory Team for this modeling project identified a suite of 52 streamflow metrics that may be most useful in defining the suitability for each river or stream to support sustaining populations of priority aquatic species across the GCPO LCC. These metrics were computed using daily outputs of runoff from HRUs (PRMS variable *hru_outflow*) and streamflow from the model stream segments (PRMS variable *seg_outflow*) for all historical and future GCPO-PRMS simulations (table 3). These streamflow statistics describe the duration, frequency, magnitude, rate of change, and timing of streamflows computed for each calendar year of simulation. The mean or median values of the annual statistics (see table 3) for the periods 1952–2005 and 2045–2075 were computed as the representative historical and potential future value, respectively, of each statistic for each of the hydrologic simulations. In addition, percentiles of the computed changes between the historical baseline and future periods across the model units, using the median GCM response for each RCP, were computed for each statistic.

Table 3. List of statistics computed using runoff (hydrologic response unit based) and streamflow (stream segment based) time series.

[MHIT, statistic was computed using the Matlab Hydrological Index Tool developed by Abouali and others (2016); Matlab, statistic was computed using Matlab software based on methods developed by Henriksen and others (2006); Difference, specifies how the differences between historical and future simulations were computed]

Statistic short name	Method	Difference	Description
			Duration
DH1	MHIT	percent	Annual maximum daily flow. Compute the maximum of a 1-day moving average flow for each year. DH1 is the median of these values (cubic feet per second – temporal).
DH2	MHIT	percent	Annual maximum of 3-day moving average flows. Compute the maximum of a 3-day moving average flow for each year. DH2 is the median of these values (cubic feet per second – temporal).
DH3	MHIT	percent	Annual maximum of 7-day moving average flows. Compute the maximum of a 7-day moving average flow for each year. DH3 is the median of these values (cubic feet per second – temporal).
DH4	MHIT	percent	Annual maximum of 30-day moving average flows. Compute the maximum of 30-day moving average flows. Compute the maximum of a 30-day moving average flow for each year. DH4 is the median of these values (cubic feet per second – temporal).
DH5	MHIT	percent	Annual maximum of 90-day moving average flows. Compute the maximum of a 90-day moving average flow for each year. DH5 is the median of these values (cubic feet per second – temporal).
DH15	MHIT	percent	High flow pulse duration. Compute the average duration for flow events with flows above a threshold equal to the 75th percentile value for each year in the flow record. DH15 is the median of the yearly average durations (days/year – temporal).
DL1	MHIT	percent	Annual minimum daily flow. Compute the minimum 1-day average flow for each year. DL1 is the median of these values (cubic feet per second – temporal).
DL2	MHIT	percent	Annual minimum of 3-day moving average flow. Compute the minimum of a 3-day moving average flow for each year. DL2 is the median of these values (cubic feet per second – temporal).
DL3	MHIT	percent	Annual minimum of 7-day moving average flow. Compute the minimum of a 7-day moving average flow for each year. DL3 is the median of these values (cubic feet per second – temporal).
DL4	MHIT	percent	Annual minimum of 30-day moving average flow. Compute the minimum of a 30-day moving average flow for each year. DL4 is the median of these values (cubic feet per second – temporal).
DL5	MHIT	percent	Annual minimum of 90-day moving average flow. Compute the minimum of a 90-day moving average flow for each year. DL5 is the median of these values (cubic feet per second – temporal).
DL16	MHIT	percent	Low flow pulse duration. Compute the average pulse duration for each year for flow events below a threshold equal to the 25th percentile value for the entire flow record. DL16 is the median of the yearly average durations (days/year – temporal).
LF1	Matlab	absolute	Number of days per year below a threshold of 0.1 cubic feet per second per square mile. LF1 is the median annual number of days below the threshold (number of days/year – temporal).
SPR_DUR3	Matlab	percent	Spring (April-June) maximum of 3-day moving average flows. Compute the maximum of a 3-day moving average flow for each year. SPR_DUR3 is the median of these values (cubic feet per second – temporal).
SPR_DUR7	Matlab	percent	Spring (April-June) maximum of 7-day moving average flows. Compute the maximum of a 7-day moving average flow for each year. SPR_DUR7 is the median of these values (cubic feet per second – temporal).
SUM_DUR3	Matlab	percent	Summer (July-September) minimum of 3-day moving average flow. Compute the minimum of a 3-day moving average flow for each year. SUM_DUR3 is the median of these values (cubic feet per second – temporal).
SUM_DUR7	Matlab	percent	Summer (July-September) minimum of 7-day moving average flow. Compute the minimum of a 7-day moving average flow for each year. SUM_DUR7 is the median of these values (cubic feet per second – temporal).
			Frequency
FH1	Matlab	absolute	High flood pulse count. Compute the average number of flow events with flows above a threshold equal to the 75th percentile value for the entire flow record. FH1 is the median number of events (number of events/year – temporal).

Table 3. List of statistics computed using runoff (hydrologic response unit based) and streamflow (stream segment based) time series.—Continued

[MHIT, statistic was computed using the Matlab Hydrological Index Tool developed by Abouali and others (2016); Matlab, statistic was computed using Matlab software based on methods developed by Henriksen and others (2006); Difference, specifies how the differences between historical and future simulations were computed]

Statistic short name	Method	Difference	Description
			Frequency—Continued
FH5	Matlab	absolute	Flood frequency. Compute the average number of flow events with flows above a threshold equal to the median flow value for the entire flow record. FH5 is the median number of events (number of events/year – temporal).
FH6	Matlab	absolute	Flood frequency. Compute the average number of flow events with flows above a threshold equal to three times the median flow value for the entire flow record. FH6 is the median number of events (number of events/year – temporal). threshold equal to three times the median flow value for the entire flow record. FH6 is the median number of events (number of events/year – temporal).
FH7	Matlab	absolute	Flood frequency. Compute the average number of flow events with flows above a threshold equal to seven times the median flow value for the entire flow record. FH7 is the median number of events (number of events/year – temporal).
FL1	Matlab	absolute	Low flood pulse count. Compute the average number of flow events with flows below a threshold equal to the 25th percentile value for the entire flow record. FL1 is the median number of events (number of events/year – temporal).
FL3	Matlab	absolute	Frequency of low pulse spells. Compute the average number of flow events with flows below a threshold equal to 5 percent of the mean flow value for the entire flow record. FL3 is the median number of events (number of events/year – temporal).
SPR_FREQ	Matlab	absolute	Flood frequency for April-June. Compute the average number of flow events with flows above a threshold equal to the 10th percentile for the entire flow record. SPR_FREQ is the median number of events (number of events/year - temporal).
SUM_FREQ	Matlab	absolute	Flood frequency for July-September. Compute the average number of flow events with flows below a threshold equal to the 90th percentile for the entire flow record. SUM_FREQ is the median number of events (number of events/year - temporal).
			Magnitude
MA3	MHIT	percent	Coefficient of variation (standard deviation/mean) for each year. Compute the coefficient of variation for each year of daily flows. Compute the median of the annual coefficients of variation (percent - temporal).
MA4	MHIT	percent	Standard deviation of the percentiles of the logs of the entire flow record divided by the mean of percentiles of the logs. Compute the log10 of the daily flows for the entire record. Compute the 5th, 10th, 15th, 20th, 25th, 30th, 35th, 40th, 45th, 50th, 55th, 60th, 65th, 70th, 75th, 80th, 85th, 90th, and 95th percentiles for the logs of the entire flow record. Percentiles are computed by interpolating between the ordered (ascending) logs of the flow values. Compute the standard deviation and mean for the percentile values. Divide the standard deviation by the mean (percent - spatial).
MA12	MHIT	percent	Mean of monthly flow values for January.
MA13	MHIT	percent	Mean of monthly flow values for February.
MA14	MHIT	percent	Mean of monthly flow values for March.
MA15	MHIT	percent	Mean of monthly flow values for April.
MA16	MHIT	percent	Mean of monthly flow values for May.
MA17	MHIT	percent	Mean of monthly flow values for June.
MA18	MHIT	percent	Mean of monthly flow values for July.
MA19	MHIT	percent	Mean of monthly flow values for August.
MA20	MHIT	percent	Mean of monthly flow values for September.
MA21	MHIT	percent	Mean of monthly flow values for October.
MA22	MHIT	percent	Mean of monthly flow values for November.

Table 3. List of statistics computed using runoff (hydrologic response unit based) and streamflow (stream segment based) time series.—Continued

[MHIT, statistic was computed using the Matlab Hydrological Index Tool developed by Abouali and others (2016); Matlab, statistic was computed using Matlab software based on methods developed by Henriksen and others (2006); Difference, specifies how the differences between historical and future simulations were computed]

Statistic short name	Method	Difference	Description
			Magnitude—Continued
MA23	MHIT	percent	Mean of monthly flow values for December.
MH14	MHIT	percent	Median of annual maximum flows. Compute the annual maximum flows from monthly maximum flows. Compute the ratio of annual maximum flow to median annual flow for each year. MH14 is the median of these ratios (dimensionless – temporal).
MH20	MHIT	percent	Specific mean annual maximum flow. MH20 is the median of the annual maximum flows divided by the drainage area (cubic feet per second/square mile – temporal).
ML17	MHIT	percent	Base flow. Compute the mean annual flows. Compute the minimum of a 7-day moving average flow for each year and divide them by the mean annual flow for that year. ML17 is the median of those ratios (dimensionless – temporal).
SPR_MAG	Matlab	percent	Specific mean spring (April-June) maximum flow. MH20 is the median of the annual maximum flows divided by the drainage area (cubic feet per second/square mile – temporal).
SUM_CV	Matlab	percent	Coefficient of variation (standard deviation/mean) for each year for the summer (July-September). Compute the coefficient of variation for each year of daily flows. Compute the median of the annual coefficients of variation (percent - temporal).
SUM_MAG	Matlab	percent	Minimum of the summer (July-September) flows divided by the drainage area (cubic feet per second/square mile – temporal).
			Rate of Change
RA1	MHIT	percent	Rise rate. Compute the change in flow for days in which the change is positive for the entire flow record. RA1 is the median of these values (cubic feet per second/day – temporal).
RA3	MHIT	percent	Fall rate. Compute the change in flow for days in which the change is negative for the entire flow record. RA3 is the median of these values (cubic feet per second/day – temporal).
RA8	MHIT	percent	Number of reversals. Compute the number of days in each year when the change in flow from one day to the next changes direction. RA8 is the median of the yearly values (days - temporal).
			Timing
SPR_ORD	Matlab	absolute	Julian date of spring (April-June) maximum. Determine the Julian date that the maximum flow occurs for each year. SPR_ORD is the median of these values (Julian day – temporal).
SUM_ORD	Matlab	absolute	Julian date of summer (July-September) minimum. Determine the Julian date that the minimum flow occurs for each water year. SUM_ORD is the median of these values (Julian day – temporal).
TH1	MHIT	absolute	Julian date of annual maximum. Determine the Julian date that the maximum flow occurs for each year. TH1 is the median of these values (Julian day – temporal).
TL1	MHIT	absolute	Julian date of annual minimum. Determine the Julian date that the minimum flow occurs for each water year. TL1 is the median of these values (Julian day – temporal).

Simulated Change in Climate Forcings and Evapotranspiration

Climate datasets used in this study include projections of potential future change in air temperature and precipitation for 13 downscaled GCMs for four RCP scenarios. Potential changes in maximum and minimum air temperature from the historical baseline period of 1952–2005 are shown in figure 10. All GCM-RCP combinations show some increase in air temperature into the future with a median increase of approximately 5 °F by 2099. The seasonal by-HRU distributions of average daily air temperature in figure 11 show the northern and northwestern parts of the study area having the highest increases in maximum air temperature and the southern and southeastern parts of the study area having the lowest increases in air temperature during the four seasonal periods. The increases in average daily air temperature are most pronounced during July to September (summer season; fig. 11*C*).

Potential changes in annual precipitation accumulation are less consistent than air temperature over time and across the different GCMs, RCPs, and seasons. The median of the RCP scenario 11-year moving averages shows a slight increase in precipitation through 2099, with the full range of GCMs depicting potential change in precipitation accumulation of +20 percent (fig. 12). Seasonal and spatial differences of potential change in precipitation accumulation could result in more extreme localized effects than the long-term study area averages shown in figure 13. Seasonal change in precipitation at the HRU scale for the period 2045–2075 for the median of all RCP scenarios is shown in figure 13. The seasonal by-HRU distributions of precipitation in figure 13 show the northern part of the study area having the highest increases in precipitation during January to March (winter season; fig. 13*A*), the southwestern part of the study area having the highest decreases in precipitation during January to March (winter season) and April to June (spring season; fig. 13*B*). The eastern part of the study area has potential increases in precipitation during July to September (summer season; fig. 13*C*).

Potential changes in annual PET and AET are shown in figure 14. The median of the RCP scenario 11-year moving averages shows increasing PET thorough year 2099, consistent with the potential increases in air temperature, and a relatively stable increase in AET for the entire future period. When considering increases in both air temperature and potential evapotranspiration coupled with uncertain precipitation changes and land-cover change into the future, the simulations resulted in a relatively small increase in actual evapotranspiration (fig. 14*B*). The increases of actual evapotranspiration of approximately 5 percent are not in proportion to the increases in potential evapotranspiration, suggesting a water-limiting condition on changes in future evapotranspiration. The seasonal by-HRU distributions of AET are shown in figure 15. These seasonal distributions show the result of complex interactions of climate and land-cover changes on the hydrology of the study area. The northwestern part of the study area is projected to have increases in AET for January to March (winter season; fig. 15*A*) and October to December (fall season; fig. 15*D*), relatively no change in AET for April to June (spring season; fig. 15*B*), and a mix of increases and decreases in AET for July to September (summer season; fig. 15*C*). The southern part of the study area is projected to have decreases or relatively no change in AET for all seasons. Changes in dominant land cover, impervious area, and vegetation cover density can all affect simulations of AET. Increases in air temperature and precipitation generally produce more AET in response to more PET as long as sufficient water is available. Changes in the seasonality and sequencing of precipitation events, however, can affect AET simulations through changes in how much water is available for evapotranspiration and how the water moves through the hydrologic system.

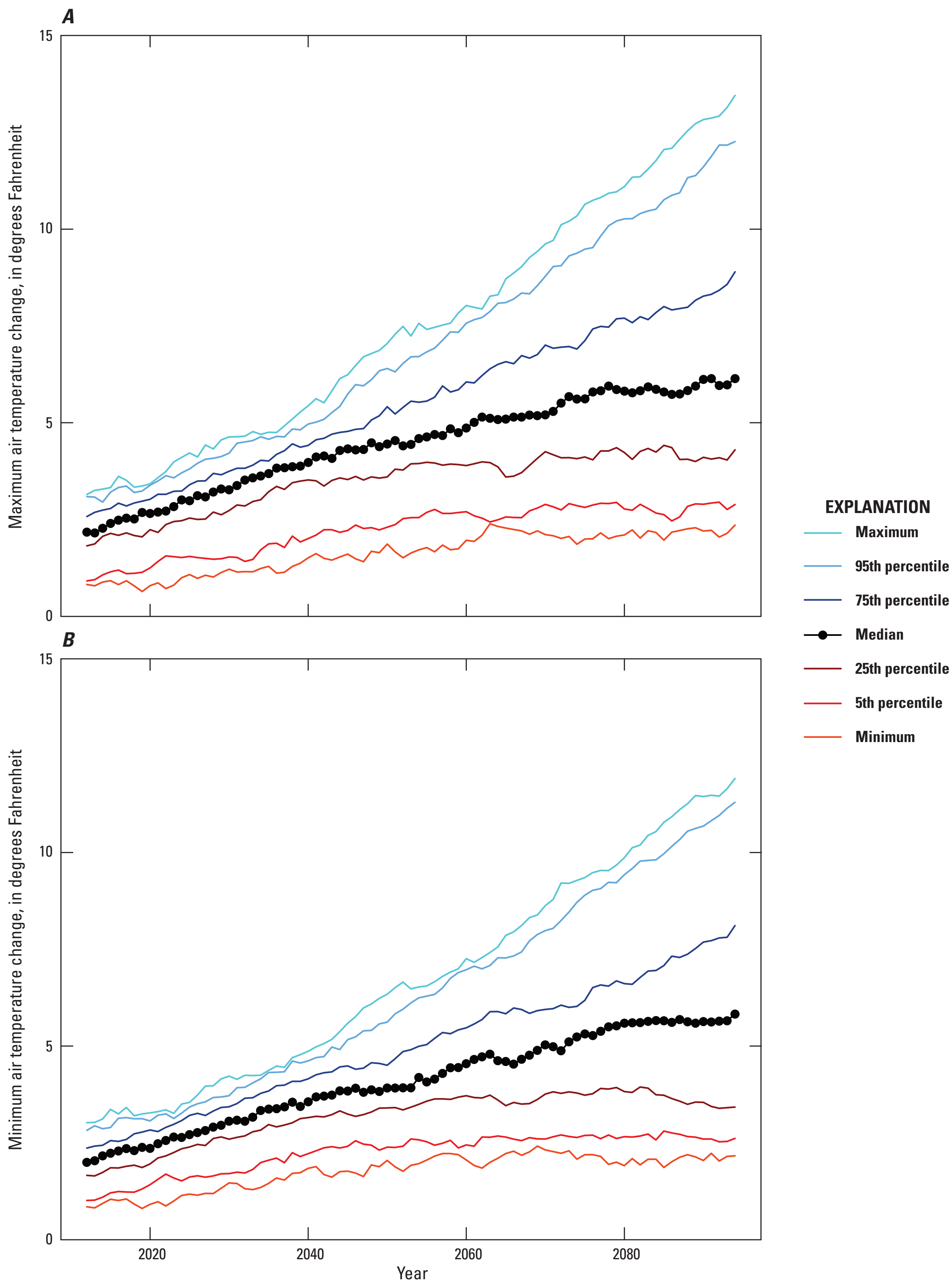

Figure 10. Graphs showing potential changes relative to the 1952–2005 baseline in (*A*) maximum daily air temperature and (*B*) minimum daily air temperature using an 11-year moving average for the period 2012–2094. The black lines with symbols represent the median of all future simulations for the four representative concentration pathways (RCPs). The color-coded solid lines represent the range across all downscaled general circulation model- (GCM-) based simulations for a range of percentiles. See table 2 for a list of which GCMs are available for each RCP.

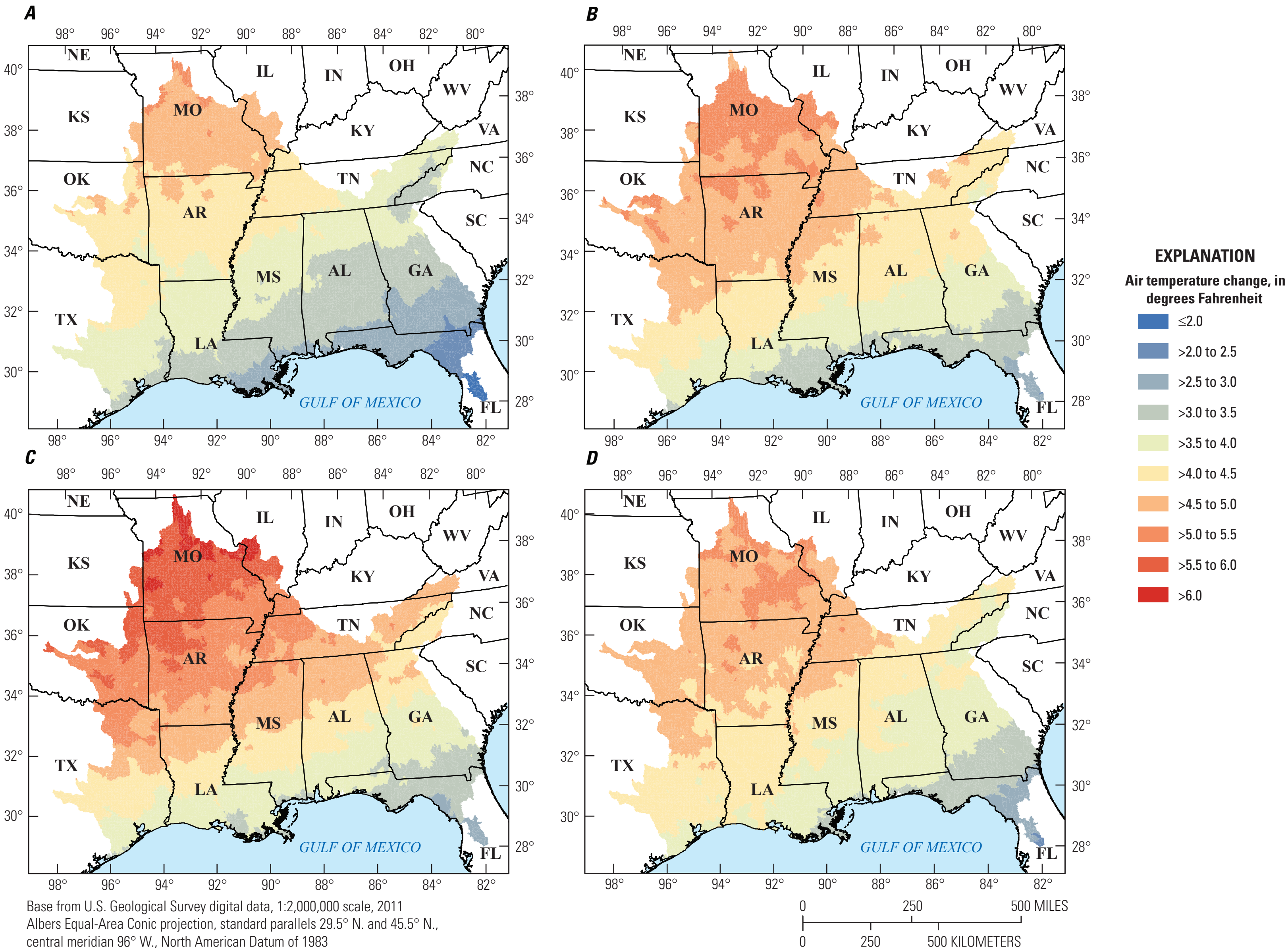

Figure 11. Maps showing the distribution of absolute difference in future average air temperature, in degrees Fahrenheit, for the median of the 45 future simulations for the period 2045–2075 compared to the historical temperature period of 1952–2005 by hydrologic response unit. The maps show seasonal periods (*A*) January to March, (*B*) April to June, (*C*) July to September, and (*D*) October to December.

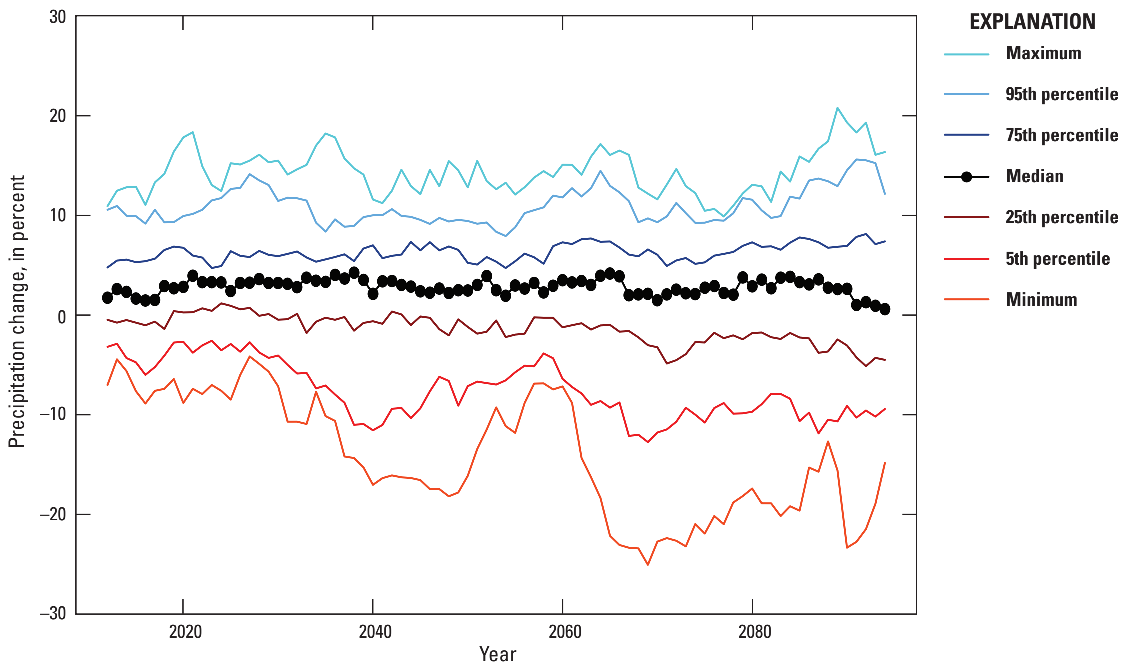

Figure 12. Graph showing potential changes relative to 1952–2005 baseline in annual precipitation accumulation using an 11-year moving average for the period 2012–2094. The black lines with symbols represent the median of all future simulations for the four representative concentration pathways (RCPs). The color-coded solid lines represent the range across all downscaled general circulation model- (GCM-) based simulations for a range of percentiles. See table 2 for a list of which GCMs are available for each RCP.

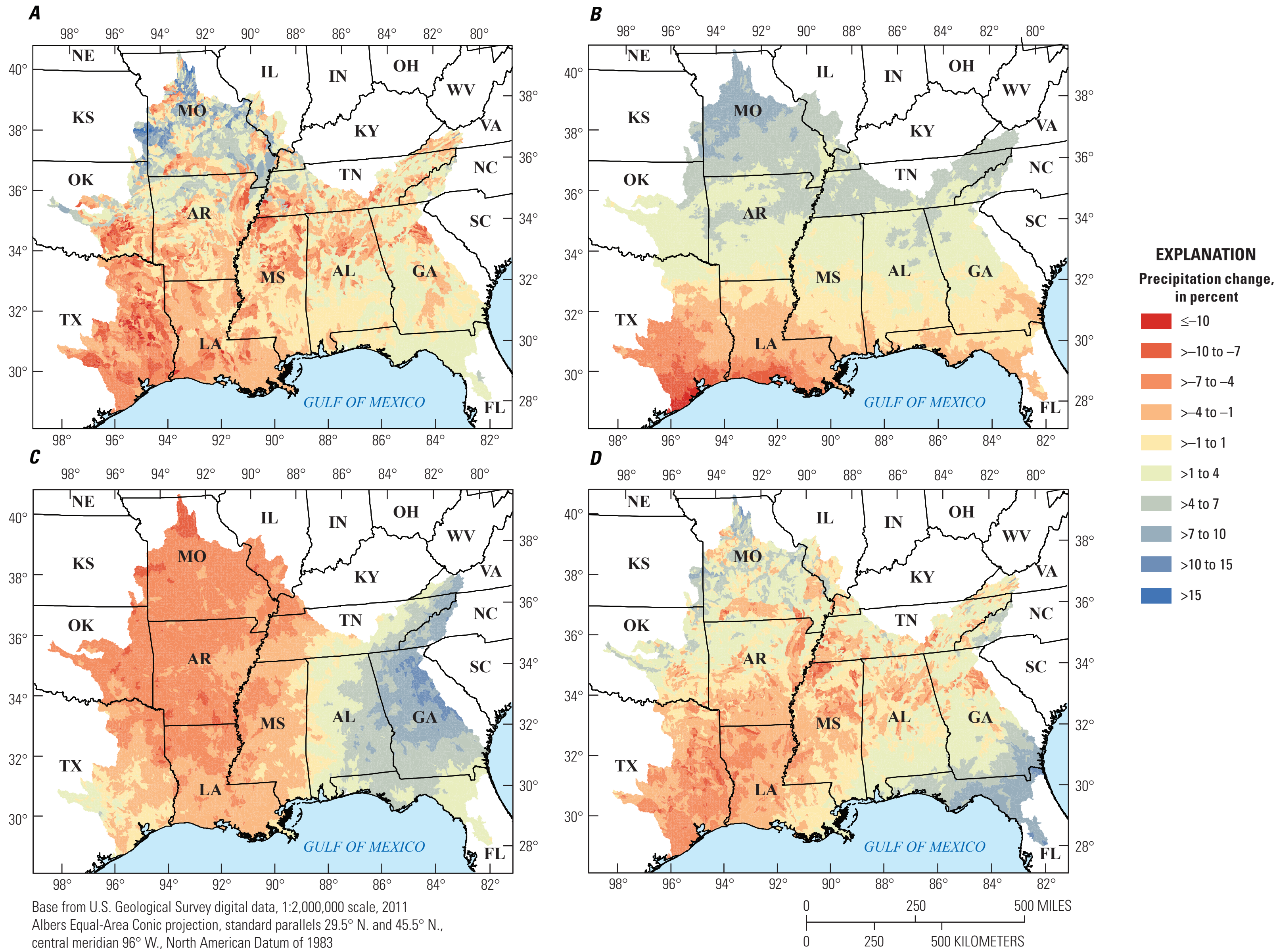

Base from U.S. Geological Survey digital data, 1:2,000,000 scale, 2011
Albers Equal-Area Conic projection, standard parallels 29.5° N. and 45.5° N.,
central meridian 96° W., North American Datum of 1983

Figure 13. Maps showing the distribution of percent difference in future precipitation for the median of the 45 future simulations for the period 2045–2075 compared to the historical precipitation period of 1952–2005 by hydrologic response unit. The maps show seasonal periods (*A*) January to March, (*B*) April to June, (*C*) July to September, and (*D*) October to December.

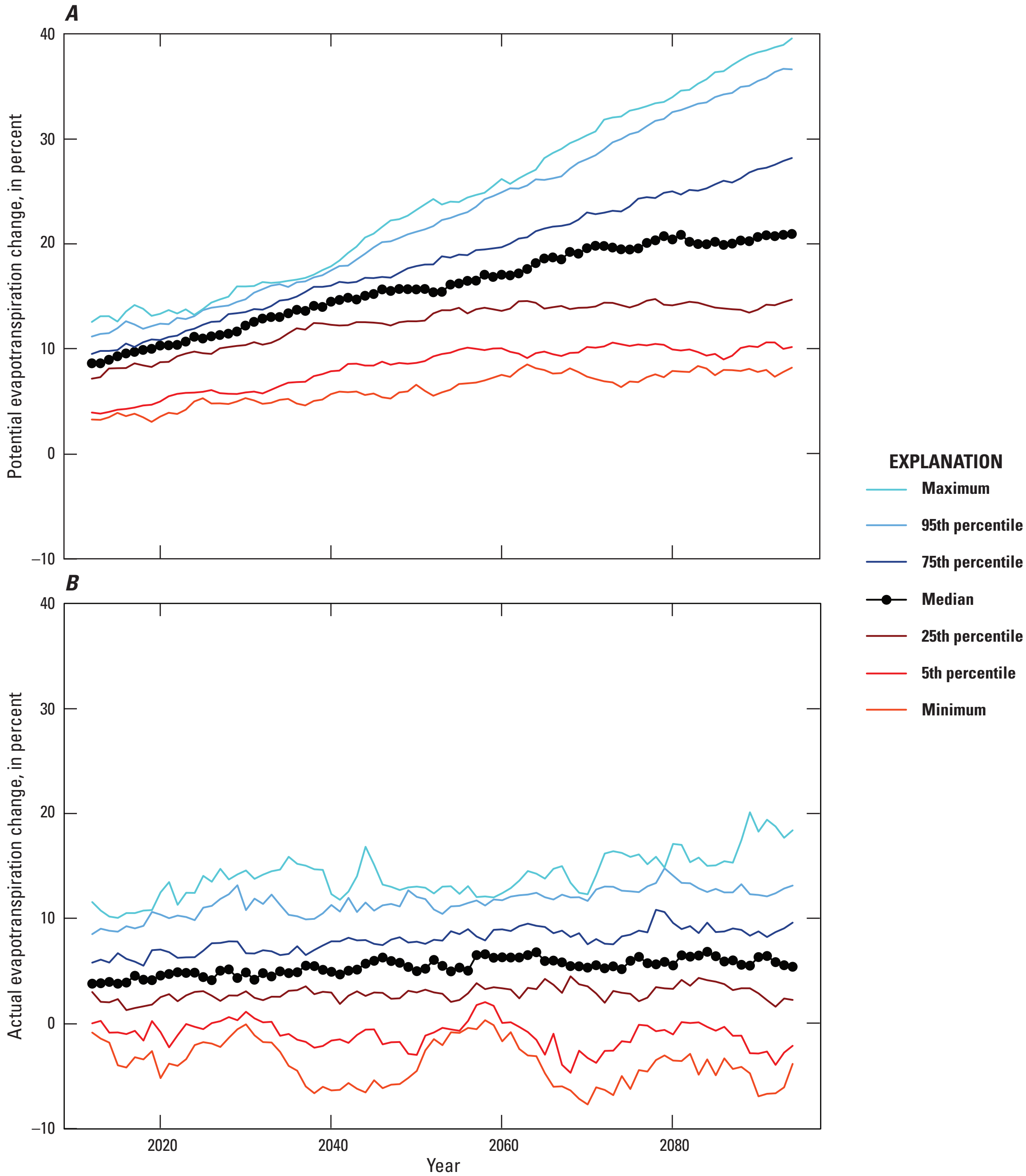

Figure 14. Graphs showing potential changes relative to the 1952–2005 baseline in (*A*) potential evapotranspiration and (*B*) actual evapotranspiration using an 11-year moving average for the period 2012–2094. The black lines with symbols represent the median of all future simulations for the four representative concentration pathways (RCPs). The color-coded solid lines represent the range across all downscaled general circulation model- (GCM-) based simulations for a range of percentiles. See table 2 for a list of which GCMs are available for each RCP.

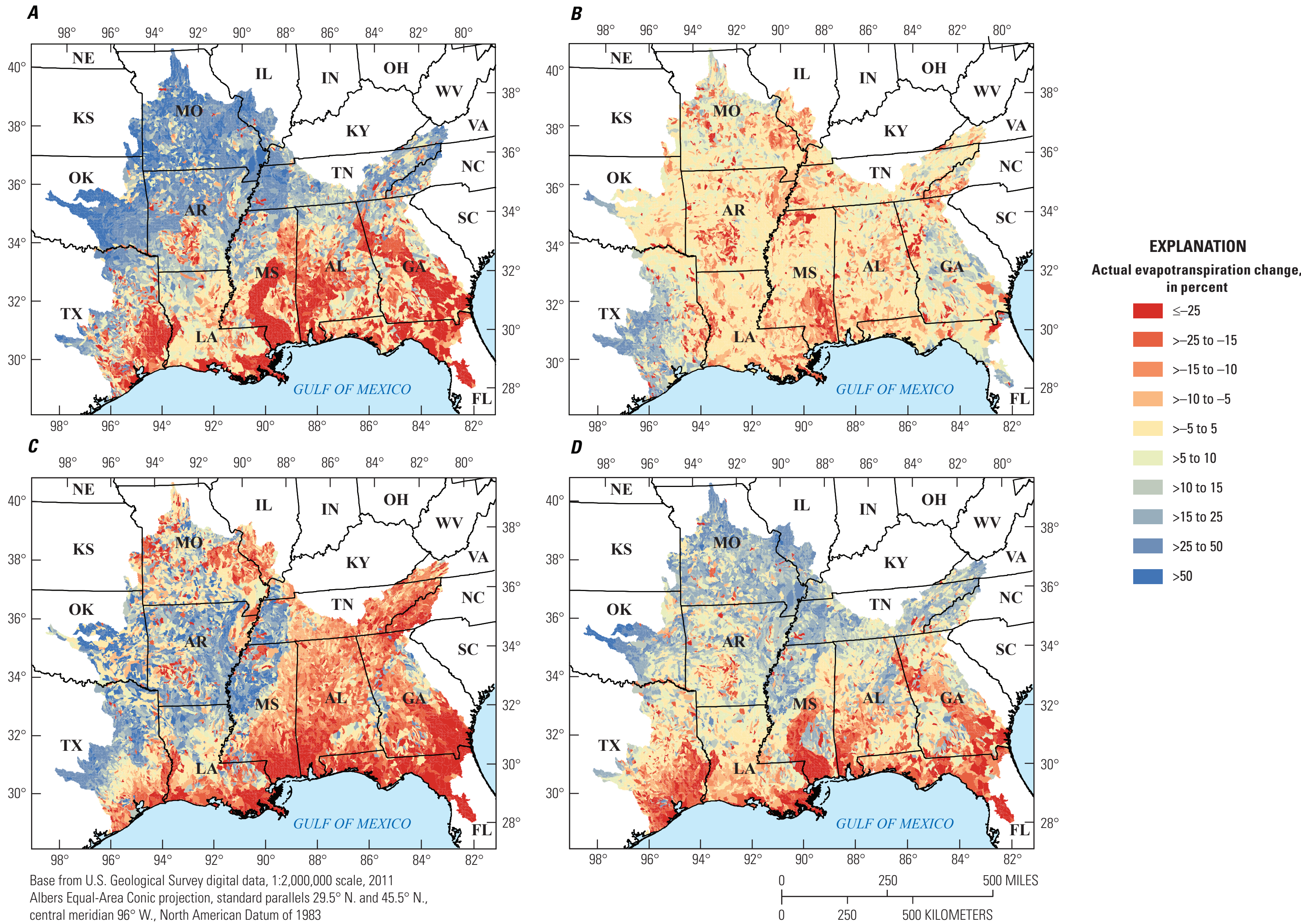

Figure 15. Maps showing the distribution of percent difference in future actual evapotranspiration for the median of the 45 future simulations for the period 2045–2075 compared to historical actual evapotranspiration period of 1952–2005 by hydrologic response unit. The maps show seasonal periods (*A*) January to March, (*B*) April to June, (*C*) July to September, and (*D*) October to December.

Simulated Runoff for Historical and Potential Future Conditions

The spatial distribution of mean annual runoff yield (runoff normalized to the HRU drainage area) at the HRU scale for the GCPO-PRMS model for the period 1952–2010 is shown in figure 16; mean monthly runoff yield is available in LaFontaine and others (2019). Runoff yield is highest in the northeastern part of the study area—in the southern Appalachian Mountains—and lowest along the northwestern, western, and southeastern edges of the study area. These patterns of high and low runoff yield correspond to the long-term pattern of high and low precipitation accumulation in the study area (fig. 3*B*). The spatial distribution of streamflow at the stream segment scale for the GCPO-PRMS model for the period 1952–2010 is shown in figure 17, which provides a visualization of how streamflow accumulates through the study area. Much of the study area consists of tributaries that have average streamflows less than 50 cubic feet per second (ft^3/s), with average segment streamflow ranging from near zero to approximately 180,000 ft^3/s. The streamflows shown in figure 17 only represent accumulations from contributing watersheds within the study area. These streamflows are, therefore, less than the actual accumulations for larger rivers that flow into the study area from the north and west (for example, the Mississippi, Missouri, and Red Rivers).

Hydrologic simulations of potential future runoff from HRUs, streamflow in stream segments, and streamflow statistics were developed using daily time series inputs of maximum and minimum air temperature and precipitation accumulation from 13 historical GCM-based and 45 future GCM-based datasets (table 2). The hydrologic simulations include changes in land-cover parameters as described in appendix 1—specifically, percent impervious area, dominant land-cover type, and vegetation interception parameters. The median of the 45 GCM-RCP scenario 11-year moving averages shows a decrease in runoff of approximately 10 percent through year 2099 for the study area, with individual GCM-based simulations ranging across approximately +30 to −60 percent change (fig. 18). The spatial distribution of median seasonal change in runoff at the HRU scale for the study area for the period 2045–2075, including potential land-cover change, is shown in figure 19. Runoff for most of the study area is projected to decrease or remain within 5 percent of the historical period 1952–2005, except for those areas projected to have substantial increases in impervious area (fig. 9). Past studies have noted that increases in impervious area can reduce evapotranspiration and infiltration resulting in increases in runoff (Paul and Meyer, 2001; Caldwell and others, 2012; Salavati and others, 2015; Shrestha and others, 2018; Suttles and others, 2018). The western part of the study area has the largest decreases in runoff for the January to March and July to September seasonal periods, with the southern part of the study area having the largest decreases in runoff for the April to June seasonal period. The areas surrounding cities such as Atlanta, Georgia; Houston, Texas; and St. Louis, Missouri are projected to have the highest increases in runoff into the future due to the potential effects of urbanization, which generally includes increases in impervious area and decreases in vegetation land cover (Paul and Meyer, 2001). One caveat to these results is that the effects of new storm retention or detention structures, or other best management practices, designed to mitigate increased storm runoff volume from urbanized areas are not included in the simulations. As regulations and guidelines for the implementation of such structures vary by locality (LaFontaine and others, 2015), these results are intended to provide potential future flow volumes that managers could use to plan for such best management practices.

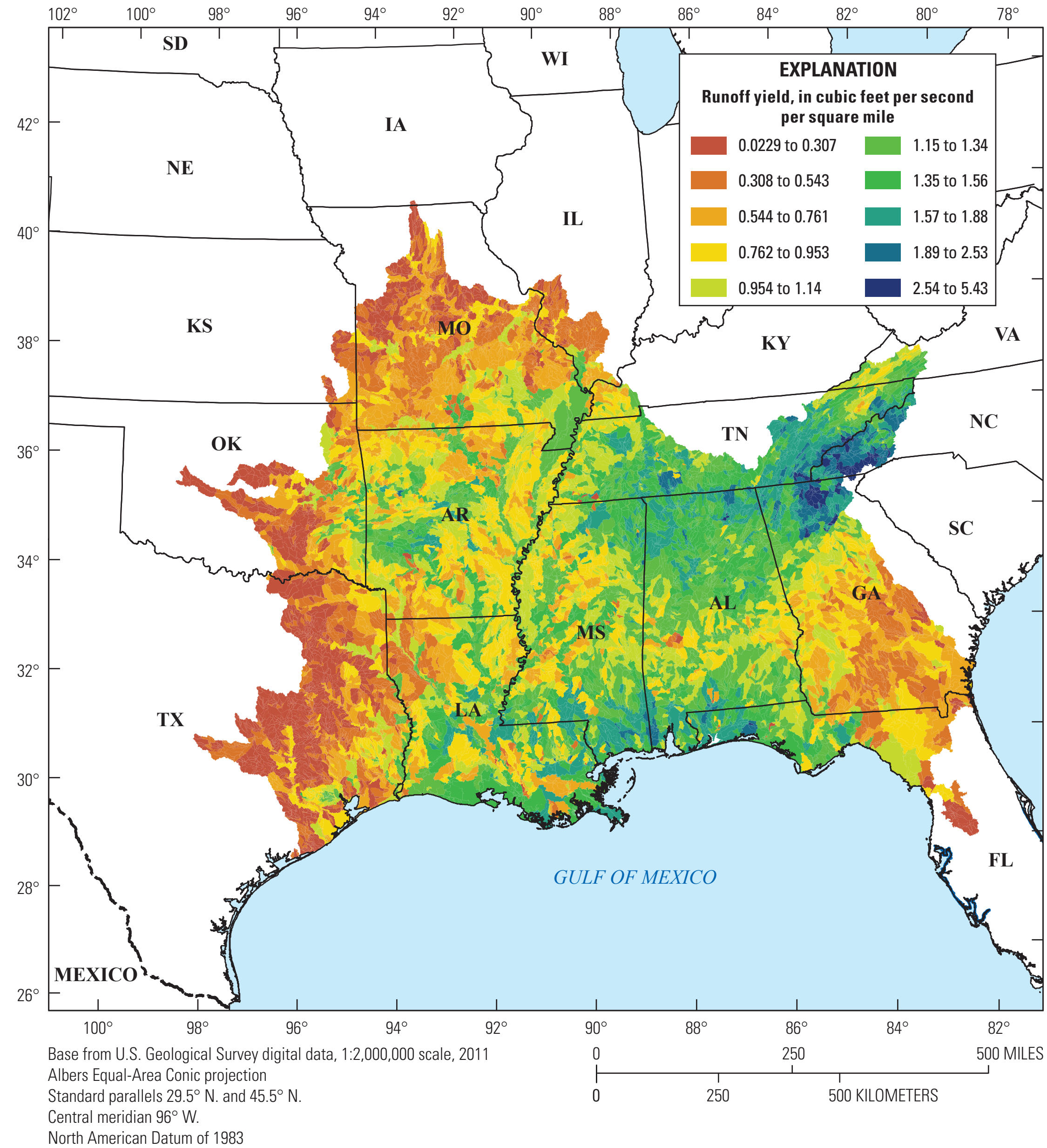

Figure 16. Map showing the simulated long-term runoff yield (runoff divided by drainage area) by hydrologic response unit for the historical period 1952–2010, in cubic feet per second per square mile.

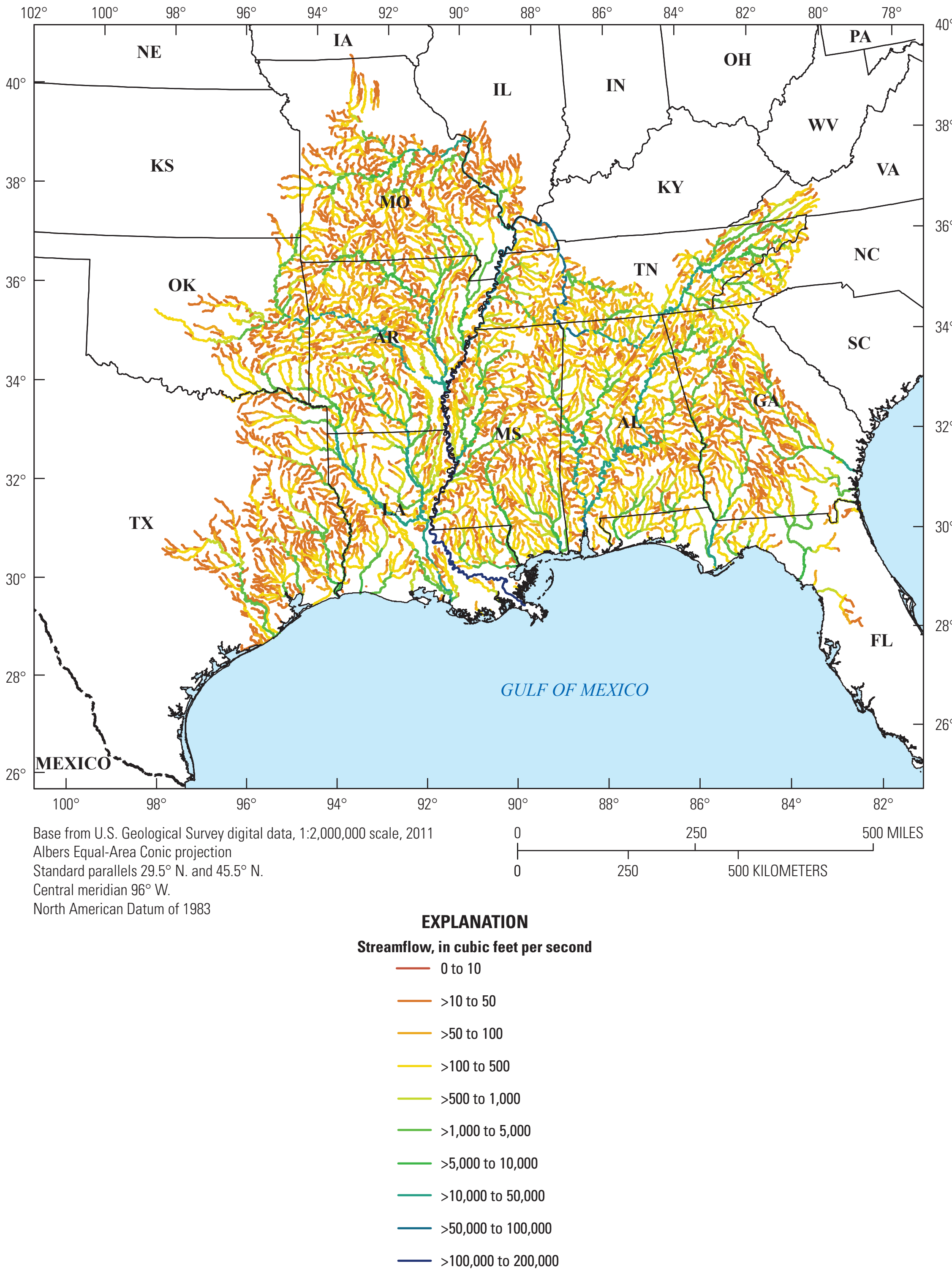

Figure 17. Map showing the simulated long-term average streamflow for the historical period 1952–2010, by stream segment, in cubic feet per second. Values are averages of the 59-year period 1952–2010.

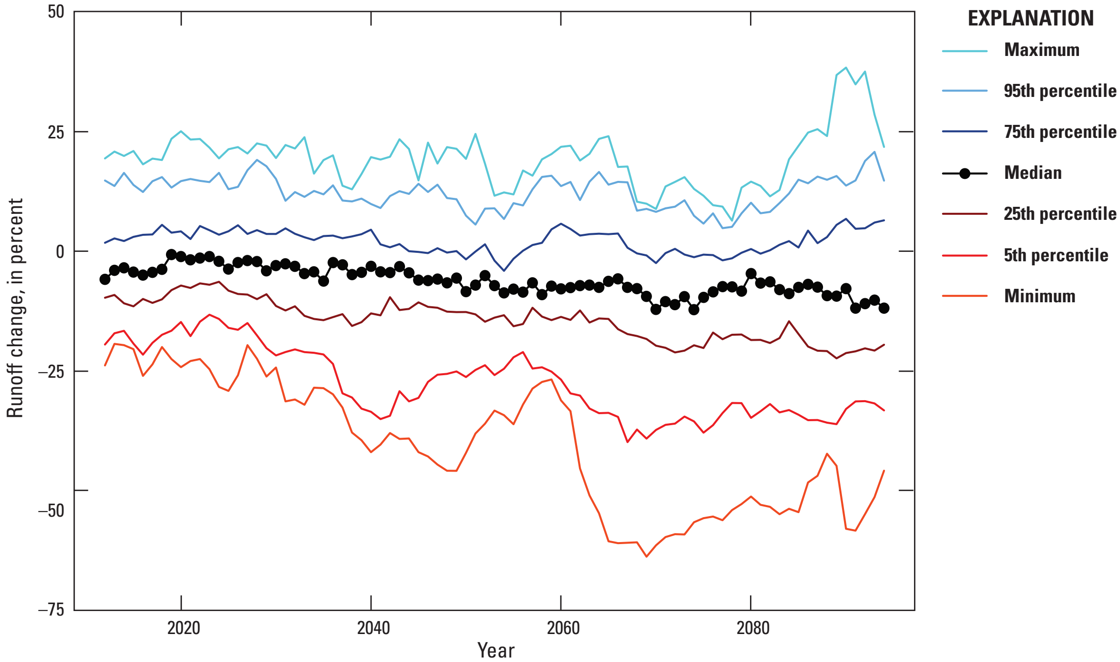

Figure 18. Graph showing potential changes relative to 1952–2005 baseline in runoff using an 11-year moving average for the period 2012–2094. The black line with symbols represents the median of all future simulations for the four representative concentration pathways (RCPs). The color-coded solid lines represent the range across all downscaled general circulation model- (GCM-) based simulations for a range of percentiles. See table 2 for a list of which GCMs are available for each RCP.

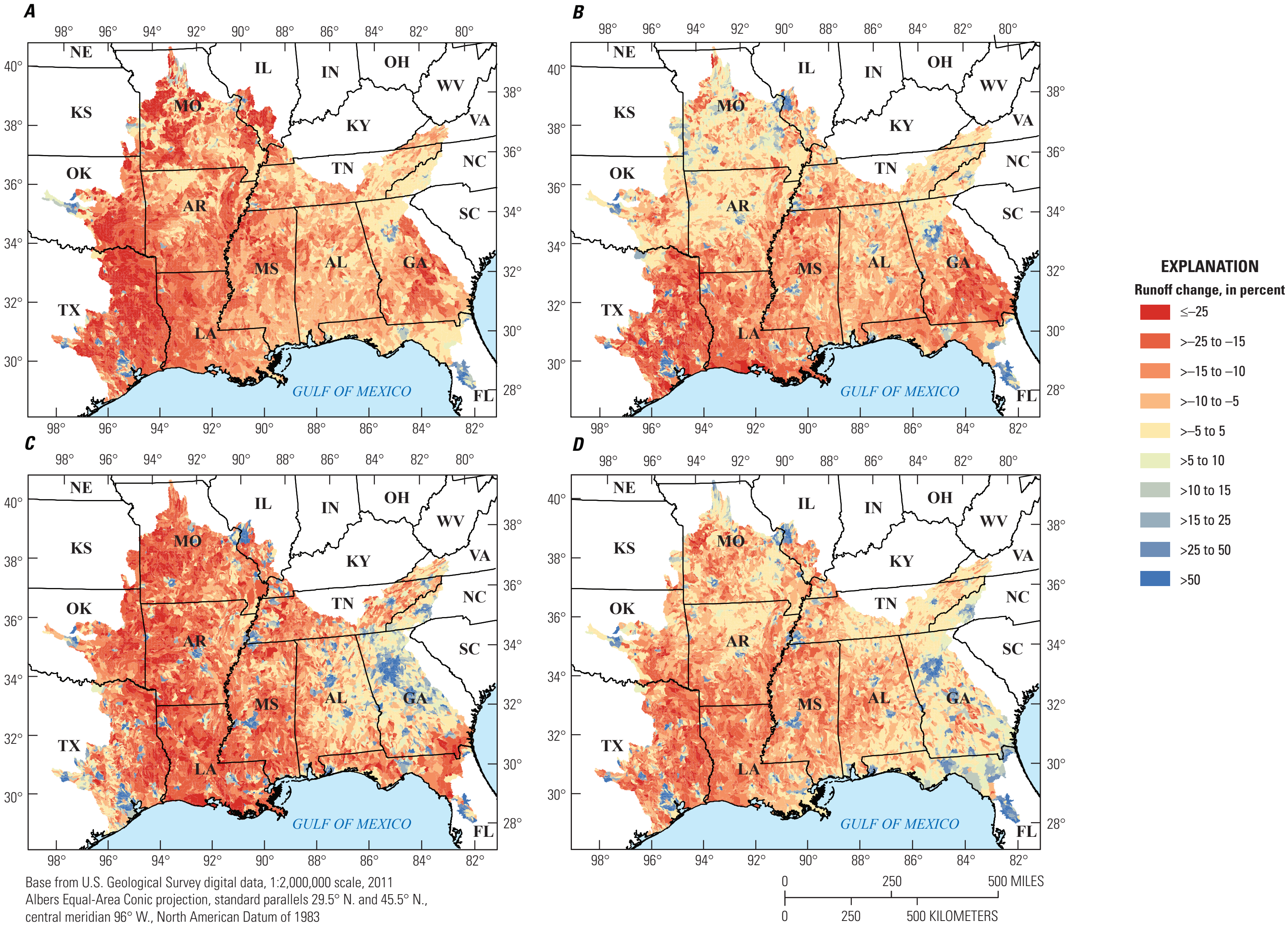

Figure 19. Maps showing the distribution of percent difference in future runoff for the median of all 45 representative concentration pathway scenarios for the period 2045–2075 compared to the historical runoff period of 1952–2005 by hydrologic response unit. The maps show seasonal periods (*A*) January to March, (*B*) April to June, (*C*) July to September, and (*D*) October to December.

Streamflow Statistics for Historical and Potential Future Conditions

The streamflow statistics described in table 3 were computed for runoff from the 20,251 HRUs and streamflow from the 10,690 of the 10,742 stream segments in the study area for the historical periods 1952–2010 (observation-based simulations) and 1952–2005 (GCM-based simulations), and for the future period 2045–2075 (GCM-based simulations). Fifty-two model stream segments were left out of the analysis because they are inflow boundary segments with no connected hydrologic response units. These statistics were computed for each period from daily time-step-simulated runoff (PRMS variable *hru_outflow*) and streamflow (PRMS variable *seg_outflow*) outputs. The statistics were computed for each calendar year and then were summarized for each period and model simulation (13 historical and 45 future) using a mean or median of the yearly values based on the statistic type (table 3). Summaries of the 52 streamflow statistics across the HRUs and stream segments for the observation-based historical period 1952–2010 are shown in table 4. Many of the statistics have units of cubic feet per second and range over several orders of magnitude because the drainage areas of the model HRUs and stream segments also vary substantially across the study area. In addition, the TH1 and TL1 timing statistics, which describe the Julian day of the annual maximum and minimum streamflows, respectively, have wide ranges in values across the year as well. The TL1 statistic is more consistent than the TH1 statistic because at least 75 percent of the model units have a median TL1 value occurring during the fall season (October to December). A discussion of the ability of GCM-based simulations to reproduce the historical distribution of observation-based simulations is included in this section. The annual streamflow statistic values used for historical period summaries are documented in LaFontaine and others (2019).

Future differences in the 52 streamflow statistics were computed by comparing the future simulations for a particular GCM to the corresponding historical simulation for the same GCM (for example, all future ACCESS1-0 simulations [RCP 4.5 and 8.5] were compared to the historical ACCESS1-0 simulation). Two types of differences were computed on the basis of the statistic of interest—percent difference or absolute difference (table 3). The potential future change results for the HRUs and stream segments are shown in table 5 and table 6, respectively, and are discussed in the following sections of this report. The statistics are grouped by the categories of streamflow duration, frequency, magnitude, rate of change, and timing. Some change statistics of duration and frequency have “Inf” values, which are the result of a zero value in the historical period. These instances would need to be interpreted as a qualitative increase into the future, without a quantitative value. The annual streamflow statistic values used for the future period summaries are documented in LaFontaine and others (2019).

Duration of Streamflow

A total of 17 streamflow duration statistics, and the difference between the historical baseline period 1952–2005 and the future period 2045–2075, were computed for the HRUs and stream segments that describe streamflow duration characteristics (table 3). The duration statistics describe the length of time that a specific water condition exists. A decrease in a duration statistic means a shorter length of time that a specific water condition exists compared to the historical baseline, and an increase in a duration statistic means a longer length of time that a specific water condition exists compared to the historical baseline. A median decrease was computed for eight of the duration type statistics across the HRUs (DH3, DH4, DH5, DL1, DL2, DL3, DL4, and DL5), a median increase for three of the duration type statistics (DH1, DH2, and LF1), and no change for the median response for the remaining six statistics (DH15, DL16, SPR_DUR3, SPR_DUR7, SUM_DUR3, and SUM_DUR7) (table 5). Decreases in high-flow-duration statistics are clustered mostly in the southwestern and northern parts of the study area. Decreases in low-flow duration statistics occur across the majority of the study area, with localized areas of increases in low-flow duration in areas of projected urbanization. Additionally, the median decrease in low-flow-duration statistics is substantially larger than the median decrease in high-flow-duration statistics. Changes in the segment-based statistics are similar to the HRU-based ranges and distributions except for the SPR_DUR3, SPR_DUR7, SUM_DUR3, and SUM_DUR7 statistics where the HRUs have more instances of no change and the segments have more instances of a quantitative or qualitative increase (“Inf” value) into the future (table 6). Maps of the distribution of duration type streamflow statistics and their differences into the future are provided in LaFontaine and others (2019).

Frequency of Streamflow

A total of eight streamflow frequency statistics, and the difference between the historical baseline period 1952–2005 and the future period 2045–2075, were computed for the HRUs and stream segments that describe streamflow frequency characteristics (table 3). The frequency statistics describe the occurrence of extreme water conditions, such as droughts or floods. An increase in a frequency statistic means more events of a particular flow extreme are occurring compared to the historical baseline, and a decrease in a frequency statistic means fewer events of a particular flow extreme are occurring compared to the historical baseline.

A median decrease was computed for two of the frequency type statistics across the HRUs (FH1 and FH5), a median increase for four of the frequency type statistics (FH6, FH7, FL1, and FL3), and no change for the median response for the remaining two statistics (SPR_FREQ and SUM_FREQ) (table 5). Changes for the interquartile range of HRU-based values for the frequency type statistics are generally less than 10 events per year when comparing the historical and future periods. Note that the change in the frequency type statistics is measured in events per year. Decreases in high flood pulse frequency (FH1) mostly occur in the western part of the study area. Decreases in the frequency of flow events above the median daily discharge (FH5) are concentrated in the southwestern part of the study area, with relatively little change occurring in the eastern part of the study area. Changes in the segment-based statistics are similar to the HRU-based ranges and distributions except for the SPR_FREQ and SUM_FREQ statistics where the HRUs have a median of no change and the segments have mostly increases into the future (table 6). Maps of the distribution of the frequency type streamflow statistics and their differences into the future are provided in LaFontaine and others (2019).

Magnitude of Streamflow

A total of 20 streamflow statistics, and the difference between the historical baseline period 1952–2005 and the future period 2045–2075, were computed for the HRUs and stream segments that describe streamflow magnitude characteristics (table 3). This set of statistics includes mean monthly streamflow for each calendar month and several flow variation metrics. A median decrease was computed for 15 of the magnitude type statistics across the HRUs (MA12, MA13, MA14, MA15, MA16, MA17, MA18, MA19, MA20, MA21, MA22, MA23, ML17, SPR_MAG, and SUM_MAG) and a median increase for 5 of the magnitude type statistics (MA3, MA4, MH14, MH20, and SUM_CV) (table 5). In general, the projected decreases are for the volume-related metrics, and the increases are for the flow-variability and flow-extremes-related metrics. The coefficient of variation (MA3) is projected to increase for much of the study area, with localized decreases in MA3 for the urbanizing areas. Monthly streamflows are projected to increase in the urbanizing areas around the fringes of the metropolitan areas across the study area due to potential increases in impervious area and decreases in forested land cover. This type of land-cover conversion can cause reductions in evapotranspiration and infiltration and result in potentially more runoff (Paul and Meyer, 2001; Bosch and Hewlett, 1982; Andreassian, 2004). Most monthly streamflows are projected to be less than or similar to historical volumes across much of the study area, except in areas with substantial increases in urbanization where streamflow volumes are projected to increase across all months. Reduced streamflows across the study area are affected by projected increases in air temperature and evapotranspiration, which can reduce the quantity of water storage available to generate runoff. The median of annual maximum flows (MH14) is projected to increase across most of the study area, suggesting a change in the magnitude or intensity of precipitation events compared to the historical period. The specific mean annual maximum flow (MH20) is projected to decrease in the southwestern part of the study area and increase in the northeastern part of the study area. This result coincides with the pattern of the annual maximum daily flow statistic (DH1). The specific mean summer minimum flow (SUM_MAG) is projected to decrease across most of the study area, with localized increases for urbanizing areas. The simulated increases in the SUM_MAG statistic for urbanizing areas is contrary to the general acceptance that infiltration decreases with urbanization, leading to decreased low flows (Paul and Meyer, 2001). The configuration and development of dynamic land-cover parameters in the PRMS simulations, which for many HRUs changed dominant land cover in urbanizing areas from tree to bare, may have inadvertently caused increased streamflow across the entire flow regime. This phenomenon should be the focus of future research for these types of hydrologic studies. Changes in the segment-based statistics are similar to the HRU-based ranges for all 20 metrics in the magnitude category (table 6). Maps of the distribution of the magnitude type streamflow statistics and their differences into the future are provided in LaFontaine and others (2019).

Rate of Change of Streamflow

A total of three streamflow statistics, and the difference between the historical baseline period 1952–2005 and the future period 2045–2075, were computed for the HRUs and stream segments that describe streamflow rate of change characteristics (table 3). The rate of change statistics describe how much change in streamflow occurs from one day to the next (RA1 and RA3 in table 3) as well as how many times a hydrograph switches between increasing and decreasing from one day to the next (RA8 in table 3). A decrease in the RA1 or RA3 statistic (rise rate and fall rate, respectively) means that the hydrograph is not as dynamic from one day to the next compared to the historical baseline, and an increase means that the hydrograph is changing faster from one day to the next compared to the historical baseline. A decrease in the RA8 statistic (average number of reversals per year) means that the hydrograph is not changing from increasing to decreasing, or decreasing to increasing, as often when compared to the historical baseline. An increase in the RA8 statistic means that the hydrograph is reversing from increasing to decreasing, or decreasing to increasing, more often than the historical baseline. A median decrease was computed for all of the rate of change type statistics across the HRUs (RA1, RA3, and

RA8) (table 5). The median change in rise rate (RA1) and fall rate (RA3) of streamflow has similar patterns across the study area, with decreases projected in the southwestern and northern parts of the study area and in the Coastal Plain of Georgia. The median change in RA1 and RA3 is projected to increase in the urbanizing areas and in the southern Appalachian Mountains region of the upper Tennessee River Basin. The number of reversals (RA8) is not expected to change substantially into the future except in localized areas across the study area, primarily in urbanizing areas. Due to increases in impervious area, smaller storms that may not have generated a stormflow event may now result in a response due to less infiltration and more surface runoff. Changes in the segment-based statistics are similar to the HRU-based ranges for all 20 metrics (table 6). Maps of the distribution of the rate-of-change type streamflow statistics and their differences into the future are provided in LaFontaine and others, (2019).

Timing of Streamflow

A total of four streamflow statistics, and the difference between the historical baseline period 1952–2005 and the future period 2045–2075, were computed for the HRUs and stream segments that describe streamflow timing characteristics (table 3). A median decrease was computed for two of the timing type statistics across the HRUs (SUM_ORD and TL1), a median increase for the TH1 timing type statistic, and no change for the median response for the SPR_ORD statistic (table 5). No substantial changes in the timing of the spring maximum (−3.0 to 4.5 days) or summer minimum flow (−6.3 to 1.0 days) are projected for at least 90 percent of the HRUs. The Julian date of the annual maximum flow (TH1) is projected to occur later in the year in the western and northern parts of the study area and around the same time as the historical period for the remainder of the study area. Conversely, the Julian date of the annual minimum flow (TL1) is projected to not change or to occur earlier in the year compared to historical baseline conditions, with decreases distributed across most of the study area, excluding the northeastern part. Changes in the segment-based statistics are similar to the HRU-based ranges for all 20 metrics (table 6). Maps of the distribution of the timing type streamflow statistics and their differences into the future are provided in LaFontaine and others (2019).

Table 4. Summary statistics of the 52 streamflow statistics computed for the model hydrologic response units and stream segments for the observation-based historical period 1952–2010.

[The computed percentiles used all 20,251 hydrologic response units and 10,690 of the 10,742 stream segments in the study area. There are 52 model stream segments that are inflow boundary segments with no connected hydrologic response units; these stream segments are not included in the statistical analysis. Statistical values are summarized for the following distribution: minimum, 5th percentile, 25th percentile, median, 75th percentile, 95th percentile, and maximum. ft^3/s, cubic foot per second; mi^2, square mile]

Statistic	Units	Hydrologic response units							Stream segments						
		MIN	5th	25th	50th	75th	95th	MAX	MIN	5th	25th	50th	75th	95th	MAX
Duration statistics															
DH1	ft^3/s	0.016	4.82	62.5	261	715	2,210	28,800	1.02	134	670	1,860	6,500	41,200	437,000
DH2	ft^3/s	0.007	2.51	30.4	126	345	1,030	15,400	0.696	91.2	462	1,320	5,180	40,000	435,000
DH3	ft^3/s	0.004	1.49	17.1	70.4	193	564	7,970	0.392	53.2	272	785	3,420	35,600	432,000
DH4	ft^3/s	0.002	0.658	7.56	31.0	85.9	248	3,510	0.155	22.0	121	357	1,580	22,800	395,000
DH5	ft^3/s	0.001	0.398	4.51	18.8	53.2	159	2,310	0.085	12.1	74.2	225	985	16,300	321,000
DH15	days/year	2	2	3	5	7	10	46	2	3	5	6	9	18	30
DL1	ft^3/s	0	0.001	0.033	0.192	0.880	6.69	114	0	0.122	1.11	5.87	38.4	1,150	42,800
DL2	ft^3/s	0	0.002	0.036	0.203	0.921	6.93	116	0	0.129	1.17	6.07	39.4	1,180	43,300
DL3	ft^3/s	0	0.002	0.043	0.231	1.04	7.36	119	0.001	0.150	1.31	6.66	42.4	1,240	44,500
DL4	ft^3/s	0	0.009	0.124	0.535	1.97	10.4	157	0.009	0.387	2.62	11.5	66.1	1,570	51,700
DL5	ft^3/s	0	0.030	0.375	1.53	5.25	21.1	268	0.021	1.02	7.07	27.0	140	2,780	82,200
DL16	days/year	3	5	6	7	8	13	30	4	6	7	9	11	18	30
LF1	days/year	0	0	26	88	169	299	362	0	0	0	52	130	264	358
SPR_DUR3	ft^3/s	0	2.00	5.50	7.00	9.00	11.0	17.0	0	2.00	5.50	7.00	8.00	9.50	12.5
SPR_DUR7	ft^3/s	0	0	5.50	7.50	10.0	14.0	26.0	0	0.0	5.00	7.00	8.00	10.5	17.5
SUM_DUR3	ft^3/s	0	0	0	0	0	4.00	8.00	0	0	0	0	0	3.85	8.00
SUM_DUR7	ft^3/s	0	0	0	0	0	0.500	5.00	0	0	0	0	0	0.50	5.50
Frequency statistics															
FH1	events/year	18	69	82	88	92	98	117	26	74	83	88	93	99	116
FH5	events/year	71	171	181	186	192	201	243	110	173	181	187	192	201	235
FH6	events/year	0	12	38	64	92	121	171	0	16	40	58	79	106	151
FH7	events/year	0	3	11	19	41	77	152	0	0	9	18	30	57	123
FL1	events/year	0	62	77	83	88	94	113	0	63	76	82	87	94	109
FL3	events/year	0	0	0	38	79	156	275	0	0	0	0	36	88	209
SPR_FREQ	events/year	0	2	5	6	8	9	11	0	3	6	7	8	9	11

Table 4. Summary statistics of the 52 streamflow statistics computed for the model hydrologic response units and stream segments for the observation-based historical period 1952–2010.—Continued

[The computed percentiles used all 20,251 hydrologic response units and 10,690 of the 10,742 stream segments in the study area. There are 52 model stream segments that are inflow boundary segments with no connected hydrologic response units; these stream segments are not included in the statistical analysis. Statistical values are summarized for the following distribution: minimum, 5th percentile, 25th percentile, median, 75th percentile, 95th percentile, and maximum. ft^3/s, cubic foot per second; mi^2, square mile]

Statistic	Units	Hydrologic response units							Stream segments						
		MIN	5th	25th	50th	75th	95th	MAX	MIN	5th	25th	50th	75th	95th	MAX
SUM_FREQ	events/year	0	0	0	0	1	6	11	0	0	0	0	1	5	10
Magnitude statistics															
MA3	percent	5.23	102	198	261	336	448	878	23.7	75.2	123	170	227	314	596
MA4	percent	3.98	52.7	87.5	110	149	219	307	9.35	58.2	82.8	105	130	171	257
MA12	ft^3/s	0.001	0.251	2.96	12.3	36.8	116	1,440	0.072	7.49	48.7	151	668	10,700	213,000
MA13	ft^3/s	0.001	0.302	3.47	14.4	43.3	135	1,590	0.044	8.82	60.5	183	806	13,000	254,000
MA14	ft^3/s	0.001	0.291	3.37	14.4	43.6	136	1,640	0.047	7.91	59.9	185	806	14,200	291,000
MA15	ft^3/s	0.001	0.282	3.16	12.9	37.2	113	1,350	0.084	8.15	53.0	160	710	13,700	303,000
MA16	ft^3/s	0	0.231	2.64	10.6	29.4	87.2	1,290	0.079	7.89	43.4	131	632	10,600	281,000
MA17	ft^3/s	0	0.167	1.87	7.19	19.9	61.0	746	0.094	5.73	29.1	89.2	422	7,150	229,000
MA18	ft^3/s	0	0.113	1.28	5.16	15.4	49.9	1,240	0.039	3.36	21.5	70.0	322	5,580	153,000
MA19	ft^3/s	0	0.074	0.879	3.43	10.7	38.5	1,820	0.033	2.34	14.3	48.2	232	4,410	113,000
MA20	ft^3/s	0.001	0.092	1.10	4.14	12.2	41.4	1,820	0.069	3.35	16.9	55.0	258	3,760	80,700
MA21	ft^3/s	0	0.094	1.13	4.08	11.6	38.2	1,140	0.066	3.67	16.2	52.9	245	4,360	76,900
MA22	ft^3/s	0	0.130	1.51	5.72	16.8	52.6	800	0.084	4.42	22.8	73.6	341	4,760	85,400
MA23	ft^3/s	0.001	0.216	2.43	9.88	29.6	92.2	1,170	0.061	6.12	39.2	123	549	8,710	149,000
MH14	none	1.33	14.2	45.2	81.6	177	610	7,290	2.20	5.95	16.3	32.4	66.1	176	1,220
MH20	$(ft^3/s)/mi^2$	0.236	4.95	16.1	26.2	37.2	53.0	95.0	0.271	2.58	6.90	12.1	18.4	29.5	60.8
ML17	none	0	0.003	0.014	0.032	0.085	0.298	0.921	0	0.012	0.032	0.070	0.148	0.290	0.848
SPR_MAG	$(ft^3/s)/mi^2$	0.083	1.10	5.55	10.3	16.3	29.0	53.1	0.142	1.01	3.09	5.41	8.54	14.6	50.6
SUM_CV	percent	0.034	0.419	0.909	1.36	1.98	2.88	5.61	0.093	0.375	0.647	0.940	1.33	1.97	4.08
SUM_MAG	$(ft^3/s)/mi^2$	0	0.003	0.015	0.042	0.125	0.440	3.13	0	0.008	0.026	0.078	0.192	0.463	2.57
Rate of change statistics															
RA1	$(ft^3/s)/day$	0.001	0.248	3.14	12.9	35.9	111	1,400	0.082	5.19	25.8	71.5	212	925	5,150
RA3	$(ft^3/s)/day$	–531	–35.8	–11.1	–3.85	–0.899	–0.072	0	–3,550	–588	–105	–30.3	–10.0	–1.82	–0.018
RA8	days	30	92	104	114	125	138	164	29	56	81	93	102	114	141

Table 4. Summary statistics of the 52 streamflow statistics computed for the model hydrologic response units and stream segments for the observation-based historical period 1952–2010.—Continued

[The computed percentiles used all 20,251 hydrologic response units and 10,690 of the 10,742 stream segments in the study area. There are 52 model stream segments that are inflow boundary segments with no connected hydrologic response units; these stream segments are not included in the statistical analysis. Statistical values are summarized for the following distribution: minimum, 5th percentile, 25th percentile, median, 75th percentile, 95th percentile, and maximum. ft^3/s, cubic foot per second; mi^2, square mile]

Statistic	Units	Hydrologic response units							Stream segments						
		MIN	5th	25th	50th	75th	95th	MAX	MIN	5th	25th	50th	75th	95th	MAX
Timing statistics															
SPR_ORD	Julian day	91	104	115	121	127	136	162	94	105	113	121	126	136	160
SUM_ORD	Julian day	189	241	260	267	271	273	273	201	247	261	266	270	272	273
TH1	Julian day	36	73	92	111	127	164	263	45	72	89	105	126	160	254
TL1	Julian day	42	220	273	278	294	310	328	51	242	273	284	296	310	325

Table 5. Difference in streamflow statistics across the hydrologic response units for the 13 general circulation models (GCMs) for the four representative concentration pathways.

[Percentiles presented are across the range of values for the hydrologic response units based on the median computed difference between the future period 2045–2075 and the historical baseline period of 1952–2005. Blue boxes indicate an increase, red boxes indicate a decrease, and white boxes indicate no difference. Metrics in green boxes are those that were acceptable based on the Kolmogorov-Smirnov test described in the "Reproducibility of Observation-Based Streamflow Statistics Using GCM-Based Simulations" section of this report. A value of "Inf" indicates that the change was computed with a zero in the denominator. Statistical values are summarized for the following distribution: minimum, 5th percentile, 25th percentile, median, 75th percentile, 95th percentile, and maximum. ft³/s, cubic foot per second; mi², square mile]

Statistic	Units	Difference metric	Representative concentration pathway percentiles						
			MIN	5th	25th	50th	75th	95th	MAX
Duration type statistics									
DH1	ft³/s	percent	–82	–28	–4.4	3.4	8.9	19	990
DH2	ft³/s	percent	–77	–27	–6.5	0.7	6.3	16	910
DH3	ft³/s	percent	–74	–27	–8.1	–1.3	4.2	13	780
DH4	ft³/s	percent	–72	–28	–11	–4.5	0.5	9.0	740
DH5	ft³/s	percent	–69	–29	–14	–7.2	–2.0	7.5	600
DH15	days/year	percent	–87	–33	–6.7	0	4.4	13	360
DL1	ft³/s	percent	–83	–39	–26	–17	–9.6	8.7	Inf
DL2	ft³/s	percent	–81	–39	–25	–17	–9.6	9.2	Inf
DL3	ft³/s	percent	–79	–38	–25	–17	–9.8	9.9	4,800
DL4	ft³/s	percent	–80	–35	–24	–16	–7.1	36	1,400
DL5	ft³/s	percent	–91	–34	–24	–17	–7.8	47	1,100
DL16	days/year	percent	–75	–20	–7.1	0	0	8.3	120
LF1	days/year	absolute	–360	–2.5	3.5	13	22	38	150
SPR_DUR3	ft³/s	percent	–100	–23	–8.3	0	0	33	Inf
SPR_DUR7	ft³/s	percent	–100	–23	–6.7	0	0	50	Inf
SUM_DUR3	ft³/s	percent	–100	0	0	0	0	60	Inf
SUM_DUR7	ft³/s	percent	–100	0	0	0	0	0	Inf
Frequency type statistics									
FH1	events/year	absolute	–35	–13	–8.0	–5.0	–3.0	0	41
FH5	events/year	absolute	–55	–14	–6.0	–3.5	–1.5	2.0	180
FH6	events/year	absolute	–84	–11	–3.0	0.5	4.0	12	71
FH7	events/year	absolute	–53	–6.5	–0.5	1.0	3.0	11	90
FL1	events/year	absolute	–91	–4.5	–1.0	1.0	2.5	6.5	110
FL3	events/year	absolute	–100	–6.5	0	4.0	10	19	200
SPR_FREQ	events/year	absolute	–6.5	–1.0	–0.5	0	0	1.5	10
SUM_FREQ	events/year	absolute	–7.5	–0.5	0	0	0	1.5	8.0
Magnitude type statistics									
MA3	percent	percent	–60	–6.7	6.1	10	13	19	140
MA4	percent	percent	–52	–4.7	1.4	4.2	7.3	14	250
MA12	ft³/s	percent	–62	–32	–19	–12	–6.8	4.0	530
MA13	ft³/s	percent	–68	–37	–21	–13	–7.2	1.8	340
MA14	ft³/s	percent	–69	–34	–19	–10	–4.4	4.9	380
MA15	ft³/s	percent	–79	–30	–16	–9.7	–3.7	9.1	460
MA16	ft³/s	percent	–73	–26	–12	–5.9	0	18	500
MA17	ft³/s	percent	–84	–28	–18	–12	–4.9	21	610
MA18	ft³/s	percent	–90	–34	–24	–17	–8.4	25	600

Table 5. Difference in streamflow statistics across the hydrologic response units for the 13 general circulation models (GCMs) for the four representative concentration pathways.—Continued

[Percentiles presented are across the range of values for the hydrologic response units based on the median computed difference between the future period 2045–2075 and the historical baseline period of 1952–2005. Blue boxes indicate an increase, red boxes indicate a decrease, and white boxes indicate no difference. Metrics in green boxes are those that were acceptable based on the Kolmogorov-Smirnov test described in the “Reproducibility of Observation-Based Streamflow Statistics Using GCM-Based Simulations” section of this report. A value of “Inf” indicates that the change was computed with a zero in the denominator. Statistical values are summarized for the following distribution: minimum, 5th percentile, 25th percentile, median, 75th percentile, 95th percentile, and maximum. ft^3/s, cubic foot per second; mi^2, square mile]

Statistic	Units	Difference metric	Representative concentration pathway percentiles						
			MIN	5th	25th	50th	75th	95th	MAX
Magnitude type statistics—Continued									
MA19	ft^3/s	percent	–89	–31	–21	–14	–5.3	34	630
MA20	ft^3/s	percent	–80	–32	–17	–5.1	8.0	48	730
MA21	ft^3/s	percent	–87	–32	–20	–10	3.4	41	860
MA22	ft^3/s	percent	–77	–28	–15	–6.5	1.0	30	710
MA23	ft^3/s	percent	–51	–21	–13	–7.4	–1.5	14	640
MH14	ft^3/s	percent	–84	–14	14	24	35	54	640
MH20	$(ft^3/s)/mi^2$	percent	–82	–28	–4.4	3.4	8.9	19	990
ML17	none	percent	–84	–28	–13	–5.4	2.1	25	2,300
SPR_MAG	$(ft^3/s)/mi^2$	percent	–98	–32	–12	–1.9	6.3	37	1,600
SUM_CV	percent	percent	–83	–8.9	0.5	4.1	9.9	38	530
SUM_MAG	$(ft^3/s)/mi^2$	percent	–85	–39	–23	–16	–9.4	6.1	2,100
Rate of change type statistics									
RA1	(ft^3/s)/day	percent	–68	–25	–8.7	–1.7	4.4	39	870
RA3	(ft^3/s)/day	percent	–69	–27	–11	–3.1	3.3	41	850
RA8	days	percent	–33	–4.7	–2.9	–1.7	–0.5	2.7	80
Timing type statistics									
SPR_ORD	Julian day	absolute	–23	–3.0	–1.0	0	1.5	4.5	22
SUM_ORD	Julian day	absolute	–75	–6.3	–2.5	–1.0	0	1.0	35
TH1	Julian day	absolute	–75	–3.0	2.0	6.0	11	22	97
TL1	Julian day	absolute	–140	–16	–8.0	–3.5	–1.0	3.0	130

Table 6. Difference in streamflow statistics across the stream segments for the 13 general circulation models (GCMs) for the four representative concentration pathways.

[Percentiles presented are across the range of values for the stream segments based on the median computed difference between the future period 2045–2075 and the historical baseline period of 1952–2005. Blue boxes indicate an increase, red boxes indicate a decrease, and white boxes indicate no difference. Metrics in green boxes are those that were acceptable based on the Kolmogorov-Smirnov test described in the “Reproducibility of Observation-Based Streamflow Statistics Using GCM-Based Simulations” section of this report. A value of “Inf” indicates that the change was computed with a zero in the denominator. Statistical values are summarized for the following distribution: minimum, 5th percentile, 25th percentile, median, 75th percentile, 95th percentile, and maximum. ft^3/s, cubic foot per second; mi^2, square mile]

Statistic	Units	Difference metric	Representative concentration pathway percentiles						
			MIN	5th	25th	50th	75th	95th	MAX
Duration									
DH1	ft^3/s	percent	–73	–23	–5.8	0.9	6.1	14	540
DH2	ft^3/s	percent	–72	–24	–6.8	0	4.7	13	500
DH3	ft^3/s	percent	–69	–24	–8.4	–1.7	2.8	10	450
DH4	ft^3/s	percent	–67	–26	–11	–4.6	–0.5	6.5	380
DH5	ft^3/s	percent	–65	–27	–14	–7.4	–2.8	4.7	370
DH15	days/year	percent	–77	–25	–7.1	0	0	7.8	38
DL1	ft^3/s	percent	–71	–31	–21	–15	–7.1	16	2,200
DL2	ft^3/s	percent	–70	–31	–21	–15	–7.2	16	2,100
DL3	ft^3/s	percent	–67	–31	–21	–15	–7.3	15	1,900
DL4	ft^3/s	percent	–62	–30	–21	–14	–5.0	24	640
DL5	ft^3/s	percent	–51	–30	–21	–14	–5.5	25	450
DL16	days/year	percent	–62	–20	–8.3	0	0	7.1	17
LF1	days/year	absolute	–190	–7.0	0	10	20	35	120
SPR_DUR3	ft^3/s	percent	–8.3	11	29	45	80	Inf	Inf
SPR_DUR7	ft^3/s	percent	–26	4.8	20	40	130	Inf	Inf
SUM_DUR3	ft^3/s	percent	0	100	Inf	Inf	Inf	Inf	Inf
SUM_DUR7	ft^3/s	percent	–50	Inf	Inf	Inf	Inf	Inf	Inf
Frequency									
FH1	events/year	absolute	–24	–11	–6.0	–3.5	–2.0	1.0	23
FH5	events/year	absolute	–37	–12	–6.5	–3.5	–1.5	1.5	47
FH6	events/year	absolute	–33	–12	–3.5	0.5	3.0	7.0	41
FH7	events/year	absolute	–27	–5.5	0	1.0	2.5	6.0	59
FL1	events/year	absolute	–93	–2.0	1.0	2.5	4.5	8.0	48
FL3	events/year	absolute	–66	–5.5	0	0	5.0	14	130
SPR_FREQ	events/year	absolute	0	1.0	2.0	3.0	4.0	8.0	9.0
SUM_FREQ	events/year	absolute	0	4.0	8.5	9.0	9.0	9.0	9.0
Magnitude									
MA3	percent	percent	–43	–4.7	3.9	8.1	11	16	82
MA4	percent	percent	–41	–4.8	1.2	4.2	6.8	11	89
MA12	ft^3/s	percent	–60	–29	–18	–11	–6.6	2.7	300
MA13	ft^3/s	percent	–62	–36	–21	–14	–7.9	0.4	290
MA14	ft^3/s	percent	–62	–34	–20	–12	–6.8	0.6	340
MA15	ft^3/s	percent	–51	–28	–15	–9.3	–4.3	5.0	370
MA16	ft^3/s	percent	–43	–22	–9.8	–4.2	0.7	12	360
MA17	ft^3/s	percent	–42	–25	–16	–9.7	–4.0	11	360
MA18	ft^3/s	percent	–54	–32	–21	–14	–6.6	13	350

Table 6. Difference in streamflow statistics across the stream segments for the 13 general circulation models (GCMs) for the four representative concentration pathways.—Continued

[Percentiles presented are across the range of values for the stream segments based on the median computed difference between the future period 2045–2075 and the historical baseline period of 1952–2005. Blue boxes indicate an increase, red boxes indicate a decrease, and white boxes indicate no difference. Metrics in green boxes are those that were acceptable based on the Kolmogorov-Smirnov test described in the "Reproducibility of Observation-Based Streamflow Statistics Using GCM-Based Simulations" section of this report. A value of "Inf" indicates that the change was computed with a zero in the denominator. Statistical values are summarized for the following distribution: minimum, 5th percentile, 25th percentile, median, 75th percentile, 95th percentile, and maximum. ft^3/s, cubic foot per second; mi^2, square mile]

Statistic	Units	Difference metric	Representative concentration pathway percentiles						
			MIN	5th	25th	50th	75th	95th	MAX
			Magnitude—Continued						
MA19	ft^3/s	percent	–46	–28	–19	–13	–5.0	21	370
MA20	ft^3/s	percent	–57	–28	–15	–3.3	8.2	36	430
MA21	ft^3/s	percent	–52	–28	–18	–8.7	4.2	29	440
MA22	ft^3/s	percent	–46	–25	–13	–6.2	0.5	22	400
MA23	ft^3/s	percent	–42	–19	–11	–6.2	–1.0	12	320
MH14	none	percent	–60	–8.5	9.3	19	28	42	530
MH20	$(ft^3/s)/mi^2$	percent	–73	–23	–5.8	0.9	6.1	14	540
ML17	none	percent	–84	–17	–8.4	–3.2	3.4	24	740
SPR_MAG	$(ft^3/s)/mi^2$	percent	–71	–24	–8.3	–0.5	5.7	24	570
SUM_CV	percent	percent	–47	–6.3	0.8	4.4	9.4	27	230
SUM_MAG	$(ft^3/s)/mi^2$	percent	–63	–30	–20	–14	–7.5	11	770
			Rate of change						
RA1	(ft^3/s)/day	percent	–53	–21	–7.4	–0.7	4.4	24	600
RA3	(ft^3/s)/day	percent	–52	–23	–9.0	–2.0	3.5	28	790
RA8	days	percent	–14	–4.6	–3.0	–2.0	–0.4	6.4	56
			Timing						
SPR_ORD	Julian day	absolute	–10	–2.5	–1.0	0.5	2.0	4.5	19
SUM_ORD	Julian day	absolute	–31	–6.0	–3.0	–1.5	–0.5	0.5	26
TH1	Julian day	absolute	–40	–1.0	4.5	8.0	13	23	72
TL1	Julian day	absolute	–86	–14	–7.5	–4.0	–1.0	1.5	49

Reproducibility of Observation-Based Streamflow Statistics Using GCM-Based Simulations

A concern when using the GCM output to drive hydrologic models at the basin scale is that the scale of the GCMs is too large to sufficiently represent hydrologically important physical processes (Intergovernmental Panel on Climate Change, 2007). To transfer outputs from the GCMs to a scale that may be useful for basin-scale hydrologic characterization, downscaling procedures have been used. Various downscaling techniques have been developed, including statistical and dynamical techniques. An overview of those techniques is described by Fowler and others (2007). Ideally, an analysis of potential future change would include multiple downscaling methods, but that is beyond the scope of this study. Accurately representing historical hydrologic conditions with the downscaled GCM climate inputs may be considered either a minimum condition or a necessity when evaluating whether a particular hydrologic application can be considered useful (Wood and others, 2004; Tebaldi and Knutti, 2007). Bock and others (2018) evaluated the accuracy of hydrologic simulations (average monthly temperature, monthly precipitation accumulation, and average monthly runoff) using downscaled GCMs for historical conditions (1950–2005) and an application of the MWBM for the CONUS. Bock and others (2018) found that the CMIP5 GCM-based simulations generally produced accurate estimates of temperature, precipitation, and runoff distributions at the monthly time step for most of the Southeastern United States. Hay and others (2014) evaluated an application of the PRMS and a stream temperature model (SNTemp) in the Apalachicola-Chattahoochee-Flint River Basin that used both observation-based and the statistically downscaled GCM-based climate inputs to produce hydrologic simulations for historical conditions. That study used the Kolmogorov-Smirnov test (KS test; Massey, 1951) to evaluate inputs of air temperature and precipitation from the downscaled GCMs and outputs of streamflow and water temperature from the process-based models PRMS and SNTemp to determine if simulations that used historical observations of climate conditions were similar to those that used the downscaled GCM outputs. A similar analysis was performed for this study for the 52 streamflow statistics that were computed for each HRU and stream segment. For this study, a particular GCM was considered acceptable for representing a streamflow statistic for historical conditions if at least 75 percent of the modeling units (HRU or stream segments) did not reject the null hypothesis of the KS test at an alpha of 0.05 when compared to the observation-based streamflow statistics. A streamflow statistic was considered acceptable overall if at least 10 of the GCMs passed the 75 percent criteria. The results of the KS test for the 52 streamflow statistics for the HRUs and stream segments are shown in table 7 and table 8, respectively.

Using the criteria described in the previous paragraph, a total of 16 streamflow statistics were acceptable for both the HRU and stream segment modeling units. Nine of the 16 were in the magnitude category, 5 were in the duration category, and 2 were in the frequency category. None of the rate of change or timing statistics passed the 75 percent criteria. An additional four statistics—DL1, DL2, MA18, and MA19—passed the criteria for the HRUs, but not the stream segments. An additional six statistics—DL16, SPR_DUR3, SPR_DUR7, FL1, SUM_FREQ, and ML17—passed the criteria for the stream segments, but not the HRUs. A total of 26 statistics did not pass the criteria for either the HRUs or the stream segments. Guidance for selecting or culling GCMs for use in these types of studies is limited and is an area of ongoing research. Future guidance may allow for a reevaluation of these results to provide further refinement to the model projections.

In general, the GCM-based simulations passed the established criteria when compared to the observation-based simulations for longer duration, low-flow statistics. Four of the five statistics that passed the criteria for both HRUs and stream segments were low-flow statistics (DL4, DL5, SUM_DUR3, and SUM_DUR7). The only high-flow statistic that passed the criteria in the duration category was DH5, which describes the annual maximum 90-day moving average flow. Two high-flow frequency statistics were acceptable based on the established criteria, FH1 and FH5, which are metrics of moderately high flows as opposed to the extreme high-flow-event metrics described by DH1 and DH2 (table 3). The nine magnitude category statistics that passed the criteria for both HRUs and stream segments were mean monthly flow values for January to June and October to December. These flows occur during the non-summer months when precipitation events are primarily frontal and of longer duration than the convective type precipitation events that occur in the Southeastern United States in the months of June to September. No statistics from the rate of change or timing categories passed the established criteria. This finding points to a limitation of the downscaled GCM-based climate datasets not reliably reproducing precipitation event characteristics at short time steps. The rate of change statistics describe the rise rate (RA1), fall rate (RA3), and number of reversals (RA8) of a hydrograph. Although the downscaled GCMs may be able to reproduce precipitation volumes over long periods, these short time step hydrologic processes are still not adequately represented in the downscaled GCM-based simulations. The timing category of statistics are quite variable across the model units. Whereas the timing of the annual low flow generally occurs during the fall in the Southeastern United States, the stochastic nature of rainfall-type precipitation events prevents timing of the annual high-flow statistic from being more closely grouped across the study area. The timing statistics may be more valuable for snowmelt-dominated watersheds where the peak streamflow for the year is during the spring snowmelt period and mostly controlled by air temperature. Further support for this finding is that the GCMs match historical air temperature observations more reliably than historical precipitation observations.

Not all GCMs had equal skill in reproducing historical distributions of the 52 streamflow statistics. The bcc-csm1-1, BNU-ESM, GFDL-ESM2G, GFDL-ESM2M, and IPSL-CM5A-LR GCMs had the most statistical comparisons fail to reject the null hypothesis of the KS tests for the HRU-based statistics and were, therefore, statistically similar to the observation-based statistics—at least 26 of the 52 metrics. The ACCESS1-0, bcc-csm1-1, BNU-ESM, IPSL-CM5A-LR, MIROC-ESM-CHEM, and MIROC-ESM GCMs had the most statistics fail to reject the null hypothesis of the KS test for the stream segment-based statistics—at least 29 of the 52 metrics. For both HRU-based and stream segment-based statistics, the MRI-CGCM3 GCM had the fewest statistics fail to reject the null hypothesis of the KS test. Additionally, more statistics failed to reject the null hypothesis of the KS test for the stream segment-based statistics than the HRU-based statistics and, therefore, were considered acceptable. The difference in performance of the two different output types can be explained partly as a function of the configuration of the HRUs versus stream segments. The HRUs are discrete spatial units that are not affected by neighboring or upstream HRUs. The stream segment values are accumulated from upstream HRUs and segments and, therefore, represent larger areas that are not as susceptible to small-scale precipitation problems at the HRU scale. The HRU-based values are less similar than the segment-based values between the observation-based and GCM-based simulations. The GCMs that performed better than others in the study area may not be as reliable for other areas across the CONUS or the world; local evaluations would need to be performed as part of any modeling application. Results of the KS test by GCM, HRU, and stream segment for the historical period 1952–2005 are provided in LaFontaine and others (2019).

Table 7. Results of the Kolmogorov-Smirnov (KS) statistical test for distribution similarity between the observation-based and downscaled general circulation model- (GCM-) based simulations for the model hydrologic response units.

[The KS test was used on the distribution of each computed hydrologic statistic for the period 1952–2005. A statistical threshold of alpha = 0.05 was used to determine similarity. Rows shaded green are those metrics that were acceptable based on the KS test described in the “Reproducibility of Observation-Based Streamflow Statistics Using GCM-Based Simulations” section of this report. GCMs shaded green in the column headings are those that were acceptable based on the KS test and had the most metrics. x, acceptable; —, not acceptable; ROC, rate of change]

Statistic	General circulation model													
	ACCESS1-0	bcc-csm1-1	BNU-ESM	CCSM4	GFDL-ESM2G	GFDL-ESM2M	IPSL-CM5A-LR	IPSL-CM5A-MR	MIROC5	MIROC-ESM-CHEM	MIROC-ESM	MRI-CGCM3	NorESM1-M	Total
Duration														
DH1	—	—	—	—	—	—	—	—	—	—	—	—	—	0
DH2	—	—	—	—	—	—	—	—	—	—	—	—	—	0
DH3	—	—	—	—	—	—	—	—	—	—	—	—	—	0
DH4	—	x	x	x	x	—	x	—	—	—	—	—	x	6
DH5	x	x	x	x	x	x	x	x	x	x	x	—	x	12
DH15	x	—	—	—	—	—	—	—	x	x	x	x		6
DL1	x	x	x	x	x	x	x	x	—	x	x	—	x	11
DL2	x	x	x	x	x	x	x	x	—	—	x	—	x	10
DL3	—	x	x	x	x	x	x	x	—	—	x	—	x	9
DL4	x	x	x	x	x	x	x	x	x	x	x	—	x	12
DL5	x	x	x	x	x	x	x	x	x	x	x	—	x	12
DL16	—	—	—	—	x	x	x	x	—	—	—	—	x	5
LF1	—	—	—	—	—	—	—	—	—	—	—	—	—	0
SPR_DUR3	x	x	x	—	x	—	x	—	x	—	x	x	x	9
SPR_DUR7	—	—	—	—	—	—	—	—	—	—	—	—	—	0
SUM_DUR3	—	x	x	—	x	x	x	x	x	x	x	—	x	10
SUM_DUR7	x	x	x	x	x	x	x	x	x	x	x	x	x	13
Frequency														
FH1	x	x	x	x	x	x	x	x	x	x	x	—	x	12
FH5	x	x	x	x	x	x	x	x	x	x	x	x	x	13
FH6	—	—	—	—	—	—	—	—	—	—	—	—	—	0
FH7	—	—	—	—	—	—	—	—	—	—	—	—	—	0
FL1	—	—	x	—	—	x	—	—	—	—	—	—	—	2
FL3	—	—	—	—	—	—	—	—	—	—	—	—	—	0
SPR_FREQ	—	—	—	—	—	—	—	—	—	—	—	—	—	0
SUM_FREQ	—	x	x	—	x	x	x	x	—	x	—	—	—	7

Table 7. Results of the Kolmogorov-Smirnov (KS) statistical test for distribution similarity between the observation-based and downscaled general circulation model- (GCM-) based simulations for the model hydrologic response units.—Continued

[The KS test was used on the distribution of each computed hydrologic statistic for the period 1952–2005. A statistical threshold of alpha = 0.05 was used to determine similarity. Rows shaded green are those metrics that were acceptable based on the KS test described in the “Reproducibility of Observation-Based Streamflow Statistics Using GCM-Based Simulations” section of this report. GCMs shaded green in the column headings are those that were acceptable based on the KS test and had the most metrics. x, acceptable; —, not acceptable; ROC, rate of change]

Statistic	General circulation model													
	ACCESS1-0	bcc-csm1-1	BNU-ESM	CCSM4	GFDL-ESM2G	GFDL-ESM2M	IPSL-CM5A-LR	IPSL-CM5A-MR	MIROC5	MIROC-ESM-CHEM	MIROC-ESM	MRI-CGCM3	NorESM1-M	Total
Magnitude														
MA3	—	—	—	—	—	—	—	—	—	—	—	—	—	0
MA4	—	—	—	—	—	—	—	—	—	—	—	—	—	0
MA12	x	x	x	x	x	x	x	x	x	x	x	x	x	13
MA13	x	x	x	x	x	x	x	x	x	x	x	x	x	13
MA14	x	x	x	x	x	x	x	x	x	x	x	x	x	13
MA15	x	x	x	x	x	x	x	x	x	x	x	x	x	13
MA16	x	x	x	x	x	x	x	x	x	x	x	x	x	13
MA17	x	x	x	x	x	x	x	x	x	x	x	—	x	12
MA18	x	x	x	x	x	—	x	x	x	x	x	—	x	11
MA19	x	x	x	x	x	x	x	x	x	x	x	—	x	12
MA20	x	x	x	—	x	x	x	x	—	x	x	—	—	9
MA21	x	x	x	x	x	x	x	x	x	x	x	—	x	12
MA22	x	x	x	x	x	x	x	x	x	x	x	x	x	13
MA23	x	x	x	x	x	x	x	x	x	x	x	x	x	13
MH14	—	—	—	—	—	—	—	—	—	—	—	—	—	0
MH20	—	—	—	—	—	—	—	—	—	—	—	—	—	0
ML17	—	x	x	—	x	x	x	x	—	—	x	—	x	8
SPR_MAG	—	—	—	—	—	—	—	—	—	—	—	—	—	0
SUM_CV	—	—	—	—	—	—	—	—	—	—	—	—	—	0
SUM_MAG	—	—	—	—	—	—	—	—	—	—	—	—	—	0
ROC														
RA1	—	—	—	—	—	—	—	—	—	—	—	—	—	0
RA3	—	—	—	—	—	—	—	—	—	—	—	—	—	0
RA8	—	—	—	—	—	—	—	—	—	—	—	—	—	0

Table 7. Results of the Kolmogorov-Smirnov (KS) statistical test for distribution similarity between the observation-based and downscaled general circulation model- (GCM-) based simulations for the model hydrologic response units.—Continued

[The KS test was used on the distribution of each computed hydrologic statistic for the period 1952–2005. A statistical threshold of alpha = 0.05 was used to determine similarity. Rows shaded green are those metrics that were acceptable based on the KS test described in the "Reproducibility of Observation-Based Streamflow Statistics Using GCM-Based Simulations" section of this report. GCMs shaded green in the column headings are those that were acceptable based on the KS test and had the most metrics. x, acceptable; —, not acceptable; ROC, rate of change]

Statistic	General circulation model													
	ACCESS1-0	bcc-csm1-1	BNU-ESM	CCSM4	GFDL-ESM2G	GFDL-ESM2M	IPSL-CM5A-LR	IPSL-CM5A-MR	MIROC5	MIROC-ESM-CHEM	MIROC-ESM	MRI-CGCM3	NorESM1-M	Total
							Timing							
SPR_ORD	—	—	—	—	—	—	—	—	—	—	—	—	—	0
SUM_ORD	—	x	—	—	—	—	—	—	—	—	—	—	—	1
TH1	—	—	—	—	—	—	—	—	—	—	—	—	—	0
TL1	—	—	—	—	—	—	—	—	—	—	—	—	—	0
Total	**22**	**27**	**27**	**21**	**27**	**26**	**27**	**25**	**20**	**22**	**25**	**11**	**25**	**—**

Table 8. Results of the Kolmogorov-Smirnov (KS) statistical test for distribution similarity between the observation-based and downscaled general circulation model- (GCM-) based simulations for the model stream segments.

[The KS test was used on the distribution of each computed hydrologic statistic for the period 1952–2005. A statistical threshold of alpha = 0.05 was used to determine similarity. Rows shaded green are those metrics that were acceptable based on the KS test described in the "Reproducibility of Observation-Based Streamflow Statistics Using GCM-Based Simulations" section of this report. GCMs shaded green in the column headings are those that were acceptable based on the KS test and had the most metrics. x, acceptable; — not acceptable; ROC, rate of change]

Statistic	General circulation model													
	ACCESS1-0	bcc-csm1-1	BNU-ESM	CCSM4	GFDL-ESM2G	GFDL-ESM2M	IPSL-CM5A-LR	IPSL-CM5A-MR	MIROC5	MIROC-ESM-CHEM	MIROC-ESM	MRI-CGCM3	NorESM1-M	Total
							Duration							
DH1	—	—	—	—	—	—	—	—	—	—	—	—	—	0
DH2	—	—	—	—	—	—	—	—	—	—	—	—	—	0
DH3	—	—	—	—	—	—	—	—	—	—	—	—	x	1
DH4	—	x	x	x	x	—	x	x	—	x	x	—	x	9
DH5	x	x	x	x	x	x	x	x	x	x	x	—	x	12
DH15	x	—	—	—	—	x	—	—	x	—	x	x	—	5
DL1	x	x	x	—	—	—	x	—	—	x	x	—	—	6
DL2	x	x	x	—	x	—	x	—	—	x	x	—	—	7

Table 8. Results of the Kolmogorov-Smirnov (KS) statistical test for distribution similarity between the observation-based and downscaled general circulation model- (GCM-) based simulations for the model stream segments.—Continued

[The KS test was used on the distribution of each computed hydrologic statistic for the period 1952–2005. A statistical threshold of alpha = 0.05 was used to determine similarity. Rows shaded green are those metrics that were acceptable based on the KS test described in the "Reproducibility of Observation-Based Streamflow Statistics Using GCM-Based Simulations" section of this report. GCMs shaded green in the column headings are those that were acceptable based on the KS test and had the most metrics. x, acceptable; — not acceptable; ROC, rate of change]

Statistic	General circulation model													
	ACCESS1-0	bcc-csm1-1	BNU-ESM	CCSM4	GFDL-ESM2G	GFDL-ESM2M	IPSL-CM5A-LR	IPSL-CM5A-MR	MIROC5	MIROC-ESM-CHEM	MIROC-ESM	MRI-CGCM3	NorESM1-M	Total
Duration—Continued														
DL3	x	x	x	—	x	—	x	—	—	x	x	—	—	7
DL4	x	x	x	x	x	—	x	—	x	x	x	—	x	10
DL5	x	x	x	x	x	—	x	x	x	x	x	—	x	11
DL16	x	—	—	x	x	x	x	x	x	x	x	—	x	10
SPR_DUR3	x	x	x	x	x	—	x	x	x	x	x	x	x	12
SPR_DUR7	x	x	x	x	x	—	x	—	x	x	x	x	x	11
SUM_DUR3	x	x	x	x	x	x	x	x	x	x	x	x	x	13
SUM_DUR7	x	x	x	x	x	x	x	x	x	x	x	x	x	13
Frequency														
FH1	x	x	x	x	x	x	x	x	x	x	x	x	x	13
FH5	x	x	x	x	x	x	x	x	x	x	x	x	x	13
FH6	—	—	—	—	—	—	—	—	—	—	—	—	—	0
FH7	—	—	—	—	—	—	—	—	—	—	—	—	—	0
FL1	x	—	x	x	x	x	x	x	x	x	—	—	x	10
FL3	—	—	—	—	—	—	—	—	—	—	—	—	—	0
LF1	—	—	—	—	—	—	—	—	—	—	—	—	—	0
SPR_FREQ	x	x	—	—	—	—	x	—	x	—	x	x	x	7
SUM_FREQ	x	x	x	x	x	x	x	x	x	x	x	—	x	12
Magnitude														
MA3	—	—	—	—	—	—	—	—	—	—	—	—	—	0
MA4	—	x	x	—	—	—	x	x	—	—	—	—	x	5
MA12	x	x	x	x	x	x	x	x	x	x	x	x	x	13
MA13	x	x	x	x	x	x	x	x	x	x	x	x	x	13
MA14	x	x	x	x	x	x	x	x	x	x	x	x	x	13
MA15	x	x	x	x	x	x	x	x	x	x	x	x	x	13

Table 8. Results of the Kolmogorov-Smirnov (KS) statistical test for distribution similarity between the observation-based and downscaled general circulation model- (GCM-) based simulations for the model stream segments.—Continued

[The KS test was used on the distribution of each computed hydrologic statistic for the period 1952–2005. A statistical threshold of alpha = 0.05 was used to determine similarity. Rows shaded green are those metrics that were acceptable based on the KS test described in the "Reproducibility of Observation-Based Streamflow Statistics Using GCM-Based Simulations" section of this report. GCMs shaded green in the column headings are those that were acceptable based on the KS test and had the most metrics. x, acceptable; — not acceptable; ROC, rate of change]

Statistic	General circulation model													
	ACCESS1-0	bcc-csm1-1	BNU-ESM	CCSM4	GFDL-ESM2G	GFDL-ESM2M	IPSL-CM5A-LR	IPSL-CM5A-MR	MIROC5	MIROC-ESM-CHEM	MIROC-ESM	MRI-CGCM3	NorESM1-M	Total
Magnitude—Continued														
MA16	x	x	x	x	x	x	x	x	x	x	x	x	x	13
MA17	x	x	x	x	x	x	x	x	x	x	x	—	x	12
MA18	x	x	x	—	x	—	x	x	x	x	x	—	—	9
MA19	x	x	x	—	x	—	x	x	—	x	x	—	—	8
MA20	x	x	x	—	x	—	x	—	—	x	x	—	—	7
MA21	x	x	x	x	x	x	x	x	x	x	x	—	x	12
MA22	x	x	x	x	x	x	x	x	x	x	x	—	x	12
MA23	x	x	x	x	x	x	x	x	x	x	x	x	x	13
MH14	—	—	—	—	—	—	—	—	—	—	—	—	—	0
MH20	—	—	—	—	—	—	—	—	—	—	—	—	—	0
ML17	x	x	x	x	x	x	x	x	x	x	x	—	x	12
SPR_MAG	—	—	—	—	—	—	—	—	—	—	—	—	—	0
SUM_CV	—	—	—	—	—	—	—	—	—	—	—	—	—	0
SUM_MAG	—	—	—	—	—	—	—	—	—	—	—	—	—	0
ROC														
RA1	—	—	—	—	—	—	—	—	—	—	—	—	—	0
RA3	—	—	—	—	—	—	—	—	—	—	—	—	—	0
RA8	—	—	—	—	—	—	—	—	—	—	—	—	—	0
Timing														
SPR_ORD	—	—	—	—	—	—	—	—	—	—	—	—	—	0
SUM_ORD	—	x	—	—	—	—	—	—	—	—	—	—	—	1
TH1	—	—	—	—	—	—	—	—	—	—	—	—	—	0
TL1	—	—	—	—	—	—	—	—	—	—	—	—	—	0
Total	**30**	**30**	**29**	**23**	**28**	**19**	**31**	**24**	**25**	**29**	**30**	**14**	**26**	—

Limitations and Assumptions

The PRMS model that was developed for this study provides simulations of streamflow conditions and potential changes to those streamflow conditions into the future for the Southeastern United States. The experiences gained from this modeling effort indicate that improvements could be made (1) to calibrate or evaluate hydrologic models by increasing the pool of available observed data, (2) to calibrate hydrologic models to match individual streamgage observations as well as provide acceptable representations of ungaged basins, (3) to include water-use information in hydrologic simulations, and (4) to simulate the hydrology of large mainstem rivers that have substantial anthropogenic effects. These concerns are described in detail in the following sections. As with any hydrologic modeling study, the assumptions and simplifications inherent in the representation of the physical processes and the statistical representation of the state of the hydrologic variables limit the accuracy and applicability of the results. The following discussion addresses these limitations and is arranged according to key topics that play a substantial role in the interpretation of the results.

Limitations of the Model Structure and Development

The use of both statistically based and physical process-based modeling approaches is more robust than methods that use only one of these approaches. For example, applications of statistical models—although perhaps sufficient for characterizing historical conditions—cannot readily incorporate projections of landscape or climate change and typically assume stationarity (Milly and others, 2008). The scale of modeling units chosen for this study (an aggregation of the National Hydrography Dataset version 1 [NHDPlus] drainage basins) is appropriate based on available datasets for model development. Finer resolution modeling of the region (for example, actual NHDPlus drainage basins) as a first, foundational step may be overly complicated and resource-intensive and should wait until better models of ungaged basins are developed and until input datasets of sufficient detail are available to parametrize those model applications. Simulating streamflow at other points of interest in the study area (for example, the actual NHDPlus flowlines) can be accomplished by applying a drainage area ratio to the hydrologic simulations for the HRU or stream segment that contains the point of interest. If finer resolution information is necessary in a particular part of the study area, the current modeling units could be further discretized within the existing Geospatial Fabric HRU, without expending the resources needed to develop a new fine-resolution model for the entire study area. Modeling with the Geospatial Fabric spatial units also allows the study to be linked to a broader scale product (for example, the USGS National Hydrologic Model documented in Regan and others, 2018), which is being used in the USGS National Water Census and for local hydrologic applications across the CONUS. A caveat to the projected changes in runoff in this study is that these simulations do not consider the effects of best management practices such as storm retention and detention structures or specifics of vegetation succession in an urban setting. The modeling structure may need further refinement to accurately represent hydrologic dynamics in urbanizing environments.

Limitations of the Calibration Methodology

The calibration methodology used for this study was intended to provide a consistent representation of the hydrologic response across the entire study area. Because there is a limited coverage of reference-quality (that is, with minimal anthropogenic effects) streamflow information available in the study area (Kiang and others, 2013), calibration of watersheds not upstream from such streamgages was informed by proximal gaged watersheds of sufficient quality. Individual gaged watersheds could have been calibrated to better match a single measured streamflow time series compared to the current model calibration, but would have lost the relative distribution of the regional parameterization. By coupling the calibration of both gaged and ungaged areas, initial parameters for the model application are realistically adjusted together. This regional similarity approach to calibration was previously used by Bock and others (2016a) in the development of a national-scale application of the MWBM (McCabe and Markstrom, 2007). Additionally, the calibration methodology employed for this study used several types of hydrologic information (measured streamflow, simulated streamflow, actual evapotranspiration, and snow water equivalent) to optimize the PRMS model parameters. As other datasets become available at the national scale (for example, soil moisture), that information can also be used to better constrain the parameter optimization scheme beyond its current capabilities to more parts of the hydrologic cycle, as opposed to just optimizing for streamflow, AET, and SWE.

This study used only reference-quality streamgages from the GAGES-II database as identified by Falcone (2011) for calibration. Based on the results of the model simulations, there appear to be many more streamgages that could potentially be used for calibration. Non-reference-quality streamgages with acceptable Nash-Sutcliffe Index (>0.6) and percent bias (within +25 percent) values could be used for calibration of future applications in the study area or to refine this application (figs. 1–6 and 1–7). The majority of the streamgages that meet those criteria are located in the eastern part of the study area. Additionally, the exclusion of non-reference gages in urban areas could influence how those parts of the study are projected to respond to potential changes in climate and land cover, since the model parameters were optimized for non-urban hydrologic response.

Limitations of the Model Structure and Calibration Due to Water Use

Water-use data were not readily available at the spatial or temporal scales required for use in these model simulations. As part of the USGS National Water Census, the USGS is currently populating a Site-Specific Water Use Data System, a part of the USGS National Water Information System (U.S. Geological Survey, 2017), that could provide these types of information for inclusion in future modeling efforts. An example of where these types of data have been included at the model unit scale is provided in LaFontaine and others (2017). That study incorporated monthly estimates of site-specific surface-water withdrawals and return flows, and groundwater withdrawals. Those types of water-use information could allow modeling simulations to better represent the actual hydrologic cycle for a particular study area instead of just the "natural" hydrologic response to climate and land-cover conditions.

Limitations of the Streamflow Routing and Reservoir Simulation

The streamflow simulations developed in this study do not include the effects of flow regulation (for example, dam operations) on hydrologic response. Recent enhancements to the PRMS provide mechanisms to include lakes in the stream routing process (Regan and LaFontaine, 2017). The available options for including lakes in the routing process, however, do not include the complex rule-curve-based methodology used by the U.S. Army Corps of Engineers for many of the large reservoirs in the Southeastern United States. A coupling of the PRMS simulations with software such as HEC-ResSim (Hydrologic Engineering Center Reservoir System Simulation software) could be a method to provide more realistic hydrographs of those stream segments that are affected by dam operations. One option allows for the replacement of simulated streamflow with observed streamflow at the dam location. This option may be useful for historical simulations, but not for projecting future hydrologic response as in this study.

The hydrologic simulations in this study do not simulate the process of water moving from the stream channel to the subsurface or groundwater zones. Currently, runoff components are computed on the HRUs, fed to the stream network, and then the stream network routes the flow out of the basin. To simulate this process within the current PRMS structure, estimates of water loss across the streambed would need to be computed for each stream segment using some other process and applied to the simulations using the PRMS Water Use module, or a new algorithm that would simulate this process directly would have to be developed for the PRMS.

Web Mapping Service of Simulated Streamflow Statistics

Selected results presented in this report of the potential change in the 52 streamflow statistics for each HRU and stream segment for the period 2045–2075 are also available through the GCPO LCC Conservation Planning Atlas (https://gcpolcc.databasin.org/maps/c3423bb56f9c44c4bcd478a092ed3c28/active, accessed May 5, 2018), an online science-based mapping platform built specifically for land managers and planners. The Conservation Planning Atlas shows the median response of the potential change in the 52 streamflow metrics listed in table 3 for the 13 GCMs and four RCPs (2.6, 4.5, 6.0, and 8.5) listed in table 2. The median response for each HRU or stream segment is color coded on the Conservation Planning Atlas to represent the departure from the historical baseline (1952–2005) as either percent difference or absolute difference. Model agreements based on the KS test by HRU and stream segment are also included on the Conservation Planning Atlas presentation for each streamflow statistic. This map presentation of model results allows the user to understand and visualize model results and uncertainty at the local, regional, and landscape scales. The GCPO LCC Conservation Planning Atlas allows a user to select one or several statistics of interest for viewing, zoom in/out or pan to any part of the study area, and (or) export the screen view in one of multiple file formats (for example, pdf, png, or ppt file types). This type of information sharing interface is ideal for less technical users who may not possess GIS skills or software. In addition, the GCPO LCC Conservation Planning Atlas has the flexibility to add more datasets of interest in the future. An example output image from the GCPO LCC Conservation Planning Atlas is shown in figure 20.

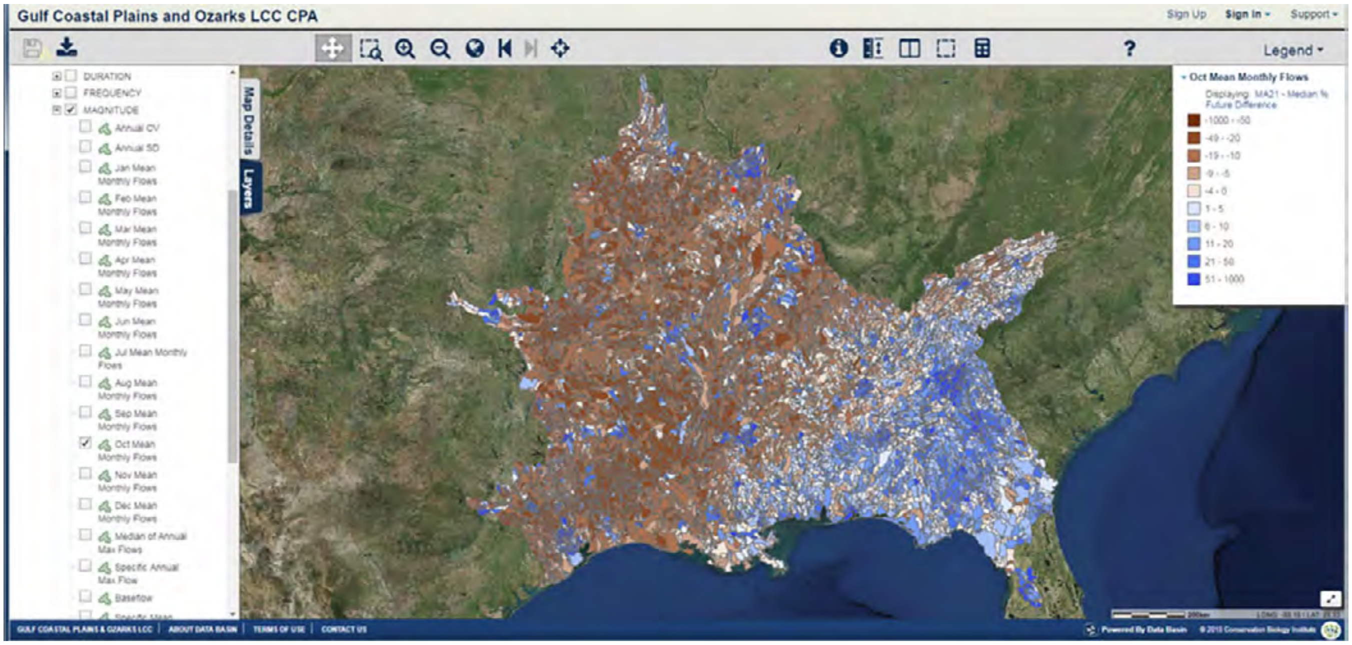

Figure 20. Example screenshot from the Gulf Coastal Plains and Ozarks Landscape Conservation Cooperative Conservation Planning Atlas showing the potential future change, in percent difference, in the MA21 (mean monthly flow for October) statistic for the period 2045–2075 compared to the simulated historical period 1952–2005. The spatial units are the hydrologic response units of the hydrologic model.

Summary

In cooperation with the Gulf Coastal Plains and Ozarks Landscape Conservation Cooperative (GCPO LCC) and the Department of the Interior Southeast Climate Adaptation Science Center, the U.S. Geological Survey (USGS) developed hydrologic simulations for the Southeastern United States to provide resource managers with information that can be used to determine the allocation and potential use of natural resources and how the availability of those resources may change in the future. The estimates of hydrologic response support efforts in the Southeastern United States to define desired environmental conditions for priority habitat types in terms of three primary landscape attributes: (1) amount, (2) configuration, and (3) condition. For aquatic systems, a subset of these landscape attributes can be quantified by streamflow characteristics such as duration, frequency, magnitude, rate of change, and timing. The GCPO Technical Advisory Team for the modeling project identified a suite of 52 streamflow metrics that may be most useful in defining the suitability for each river or stream to support sustaining populations of priority aquatic species across the GCPO LCC. The hydrologic simulations developed as part of this study provide estimates of water availability and hydrologic behavior for historical and potential future effects of climate and land-use change. The Precipitation-Runoff Modeling System (PRMS), a deterministic, distributed-parameter, process-based system that simulates the effects of precipitation, temperature, and land cover on basin hydrology, was used in conjunction with other modeling applications (Monthly Water Balance Model and statistical methods) to simulate hydrologic response for 20,251 hydrologic response units and 10,742 stream segments across the study area. A suite (HRUs) of 52 streamflow statistics were computed from the hydrologic simulations for each modeling unit.

The PRMS model was an extraction from the USGS National Hydrologic Model and simulated streamflow without the effects of water use or flow regulation (for example, dams) at a daily time step for the period 1952–2099. Observed historical climate inputs of air temperature and precipitation (1949–2010) and statistically downscaled general circulation model (GCM) inputs from the Coupled Model Intercomparison Project Phase 5 (CMIP5) that were available for 1951–2099 were used for 13 GCMs and four representative concentration pathways (RCPs; 45 total future simulations). Maps of annual land cover for the period 1949–2099 were used to vary model parameters to incorporate the effects of dynamic land cover across the study area (for example, impervious area, dominant land-cover type, and vegetation canopy interception capacity). The PRMS modeling application was calibrated using historical observations of climate and streamflow and historical simulations of monthly runoff, daily statistically based streamflow, actual evapotranspiration (AET), and snow water equivalent (SWE) in a multistep process. Historical estimates of streamflow were developed in addition to estimates of potential future change in streamflow and other parts of the hydrologic cycle such as precipitation, potential evapotranspiration, and AET.

Maximum and minimum air temperatures were projected to increase by approximately 5 degrees Fahrenheit by the year 2099 according to the median of the 45 future simulations. The seasonal by-HRU distributions of average daily air temperature show the northern and northwestern parts of the study area having the highest increases in maximum air temperature and the southern and southeastern parts of the study area having the lowest increases in air temperature during the four seasonal periods. The increases in average daily air temperature are most pronounced during July to September (summer season). Precipitation accumulations were projected to have a slight increase through 2099, with the full range of GCMs depicting potential change in precipitation accumulation of +20 percent, demonstrating substantial uncertainty in the future precipitation projections. The seasonal by-HRU distributions of precipitation show the northern part of the study area having the highest increases in precipitation during the January to March seasonal period (winter), the southwestern part of the study area having the highest decreases in precipitation during the January to March seasonal period (winter) and the April to June seasonal period (spring). The eastern part of the study area has potential increases in precipitation in the July to September seasonal period (summer). The projected increases in air temperature resulted in projected increases in potential evapotranspiration and a relatively small increase in actual evapotranspiration that remained at the same level into the future, approximately a 5-percent increase. The reason for this relatively flat response is that there are diverging hydrologic responses across the study area that balance each other out when aggregated to the full study area. The northwestern part of the study area is projected to have increases in AET for the January to March and October to December seasonal periods, relatively no change in AET for the April to June seasonal period, and a mix of increases and decreases in AET for the July to September seasonal period. The southern part of the study area is projected to have decreases or relatively no change in AET for all seasons.

In general, streamflow is projected to decrease by approximately 10 percent through the year 2099 based on the median hydrologic response of the 45 future simulations. The western part of the study area has the largest decreases in runoff for the January to March and July to September seasonal periods, with the southern part of the study area having the largest decreases in runoff for the April to June seasonal period. Substantial increases in runoff are projected in areas surrounding large metropolitan areas such as Atlanta, Georgia; Houston, Texas; and St. Louis, Missouri—areas with the most projected urbanization, which includes increases in impervious area and decreases in vegetation land cover. A caveat of these projections of increased runoff is that these simulations do not consider the effects of best management practices such as storm retention and detention structures or specifics of vegetation succession in an urban setting. The modeling structure may need further refinement to accurately represent hydrologic dynamics in urbanizing environments. The magnitude type streamflow statistics show general decreases in the volume-related metrics and increases in the flow-variability and flow-extremes-related metrics. The duration, frequency, rate of change, and timing type statistics are generally split between increasing, decreasing, or no changes in values into the future.

The Kolmogorov-Smirnov statistical test (KS test) was used to compare the historical distributions of streamflow statistics between the observation-based simulations and the downscaled GCM-based simulations. The KS test results showed that many of the streamflow statistic distributions rejected the null hypothesis at the 0.05 level and were therefore considered not from the same distribution. Most of the KS test results that did fail to reject the null hypothesis, and therefore were considered similar between the observation-based and GCM-based simulations, were in the duration and magnitude categories. None of the GCM-based simulations were able to reproduce observation-based statistics for the timing or rate of change categories along with many of the high-flow and flow-variability metrics in the duration, frequency, and magnitude categories. The KS test results also showed that for this particular study area, there were GCMs that were better able to produce historical streamflow statistics than other GCMs. For HRU-based statistics, the bcc-csm1-1, BNU-ESM, GFDL-ESM2G, GFDL-ESM2M, and IPSL-CM5A-LR GCMs matched the most observation-based statistics—at least 26 of the 52 metrics. For the segment-based statistics, the ACCESS1-0, bcc-csm1-1, BNU-ESM, IPSL-CM5A-LR, MIROC-ESM-CHEM, and MIROC-ESM GCMs matched the most observation-based statistics—at least 29 of the 52 metrics. The acceptability results presented in this report characterize general performance of GCM-based hydrologic simulations for the entire study area. For a local area of interest, the KS test results could be evaluated at that location for the acceptability of particular streamflow statistics. Additionally, as new ways are developed to interpret the acceptability of GCM-based hydrologic simulations and the resulting streamflow statistics, these results could be reanalyzed using new criteria. The projected changes in the streamflow statistics and the KS test results are available online through the GCPO LCC Conservation Planning Atlas, an online science-based mapping platform built specifically for land managers and planners.

Several limitations to the results presented in this report were identified and discussed. The hydrologic simulations did not include the effects of water use or flow regulation. These two components of the anthropogenically affected hydrologic cycle could have substantial implications on water management into the future. The PRMS is able to use water-use information in hydrologic simulations, provided the water-use estimates are available for the study area in a convenient format such as the USGS Site-Specific Water Use Data System. Additionally, further refinements to the model calibration procedure through inclusion of additional streamflow information and other hydrologic datasets could further reduce simulation uncertainties in both gaged and ungaged watersheds. Finally, the results of this study show that there is still a substantial range in climate outputs from the available suite of GCMs and the resulting hydrologic response for both historical and future periods using just one type of downscaling method. The use of additional downscaled climate datasets that were developed with other types of downscaling techniques could further characterize the potential future hydrologic response of the study area. Expanding this methodology of hydrologic characterization to other regions could provide nationally consistent metrics for use in environmental assessments and could identify further areas of research for improving hydrologic process representation. Refining the GCM outputs and (or) the downscaling algorithms for use at the watershed scale will further reduce the hydrologic uncertainties with which resource managers currently have to make decisions.

References Cited

Abouali, M., Daneshvar, F., and Nejadhashemi, P.A., 2016, MATLAB Hydrological Index Tool (MHIT)—A high performance library to calculate 171 ecologically relevant hydrological indices: Ecological Informatics, v. 33, p. 17–23, accessed March 5, 2019, at https://doi.org/10.1016/j.ecoinf.2016.03.004.

Andreassian, V., 2004, Waters and forests—From historical controversy to scientific debate: Journal of Hydrology, no. 291, p. 1–27, accessed April 20, 2019, at https://doi.org/10.1016/j.jhydrol.2003.12.015.

Archfield, S.A., Kennen, J.G., Carlisle, D.M., and Wolock, D.M., 2014, An objective and parsimonious approach for classifying natural flow regimes at a continental scale: River Research and Applications, v. 30, no. 9, p. 1166–1183, accessed July 28, 2015, at https://doi.org/10.1002/rra.2710.

Barros, A.P., Duan, Y., Brun, J., and Medina, M.A., Jr., 2014, Flood nonstationarity in the southeast and mid-Atlantic regions of the United States: Journal of Hydrologic Engineering, v. 19, no. 10, 11 p., accessed September 22, 2017, at https://doi.org/10.1061/(ASCE)HE.1943-5584.0000955.

Blodgett, D.L., Booth, N.L., Kunicki, T.C., Walker, J.I., and Viger, R.J., 2011, Description and testing of the Geo Data Portal—A data integration framework and Web processing services for environmental science collaboration: U.S. Geological Survey Open-File Report 2011–1157, 9 p., accessed March 2, 2017, at https://doi.org/10.3133/ofr20111157.

Blöschl, G., 2006, Hydrologic synthesis—Across processes, places, and scales: Water Resources Research, v. 42, no. 3, W03S02, 3 p., accessed November 3, 2017, at https://doi.org/10.1029/2005WR004319.

Blöschl, G., Sivapalan, M., Wagener, T., Viglione, A., and Savenije, H., eds., 2013, Runoff prediction in ungauged basins—Synthesis across processes, places and scales: Cambridge, U.K., Cambridge University Press, 465 p., accessed November 3, 2017, at https://doi.org/10.1017/CBO9781139235761.

Bock, A.R., Hay, L.E., Markstrom, S.L., and Atkinson, R.D., 2016a, Monthly Water Balance Model Hydrology Futures (ver. 3.0, September 2018): U.S. Geological Survey data release, accessed June 24, 2016, at https://doi.org/10.5066/F7VD6WJQ.

Bock, A.R., Hay, L.E., McCabe, G.J., Markstrom, S.L., and Atkinson, R.D., 2016b, Parameter regionalization of a monthly water balance model for the conterminous United States: Hydrology and Earth System Sciences, v. 20, no. 7, p. 2861–2876, accessed June 4, 2018, at https://doi.org/10.5194/hess-20-2861-2016.

Bock, A.R., Hay, L.E., McCabe, G.J., Markstrom, S.L., and Atkinson, R.D., 2018, Do downscaled general circulation models reliably simulate historical climate conditions?: Earth Interactions, v. 22, no. 10, 22 p., accessed June 4, 2018, at https://doi.org/10.1175/EI-D-17-0018.1.

Booth, N.L., Everman, E.J., Kuo, I.-L., Sprague, L., and Murphy, L., 2011, A web-based decision support system for assessing regional water-quality conditions and management actions: Journal of the American Water Resources Association, v. 47, no. 5, p. 1136–1150, accessed September 23, 2017, at https://doi.org/10.1111/j.1752-1688.2011.00573.x.

Bosch, J.M., and Hewlett, J.D., 1982, A review of catchment experiments to determine the effect of vegetation changes on water yield and evapotranspiration: Journal of Hydrology, no. 55, p. 3–23, accessed April 20, 2019, at https://doi.org/10.1016/0022-1694(82)90117-2.

Bosch, D.D., Sullivan, D.G., and Sheridan, J.M., 2006, Hydrologic impacts of land-use changes in Coastal Plain watersheds: Transactions of the American Society of Agricultural and Biological Engineers, v. 49, no. 2, p. 423–432, accessed September 22, 2017, at https://naldc.nal.usda.gov/download/1348/PDF.

Bureau of Reclamation, 2013, Downscaled CMIP3 and CMIP5 climate projections—Release of downscaled CMIP5 climate projections, comparison with preceding information, and summary of user needs: U.S. Department of the Interior, Bureau of Reclamation, Technical Service Center, 116 p., accessed August 23, 2018, at http://gdo-dcp.ucllnl.org/downscaled_cmip_projections/techmemo/downscaled_climate.pdf.

Caldwell, P.V., Kennen, J.G., Sun, G., Kiang, J.E., Butcher, J.B., Eddy, M.C., Hay, L.E., LaFontaine, J.H., Hain, E.F., Nelson, S.A.C., and McNulty, S.G., 2015, A comparison of hydrologic models for ecological flows and water availability: Ecohydrology, v. 8, no. 8, p. 1525–1546, accessed April 15, 2015, at https://doi.org/10.1002/eco.1602.

Caldwell, P.V., Sun, G., McNulty, S.G., Cohen, E.C., and Moore Myers, J.A., 2012, Impacts of impervious cover, water withdrawals, and climate change on river flows in the conterminous US: Hydrology and Earth System Sciences, v. 16, p. 2839–2857, accessed April 20, 2019, at https://doi.org/10.5194/hess-16-2839-2012.

Cruise, J.F., Limaye, A.S., and Al-Abed, N., 1999, Assessment of impacts of climate change on water quality in the southeastern United States: Journal of the American Water Resources Association, v. 35, no. 6, p. 1539–1550, accessed September 22, 2017, at https://doi.org/10.1111/j.1752-1688.1999.tb04236.x.

Driscoll, J.M., Markstrom, S.L., Regan, R.S., Hay, L.E., and Viger, R.J., 2017b, National Hydrologic Model Parameter Database—2017-05-08 Download: U.S. Geological Survey database, accessed September 24, 2017, at https://doi.org/10.5066/F7NS0SCW.

Evenson, E.J., Orndorff, R.C., Blome, C.D., Böhlke, J.K., Hershberger, P.K., Langenheim, V.E., McCabe, G.J., Morlock, S.E., Reeves, H.W., Verdin, J.P., Weyers, H.S., and Wood, T.M., 2013, U.S. Geological Survey water science strategy—Observing, understanding, predicting, and delivering water science to the Nation: U.S. Geological Survey Circular 1383–G, 49 p., accessed September 24, 2017, at https://doi.org/10.3133/cir1383g.

Falcone, J.A., 2011, GAGES II (Geospatial Attributes of Gages for Evaluating Streamflow) summary report: U.S. Geological Survey, 24 p., accessed October 27, 2017, at https://water.usgs.gov/GIS/dsdl/basinchar_and_report_sept_2011.zip.

Farmer, W.H., 2016, Ordinary kriging as a tool to estimate historical daily streamflow records: Hydrology and Earth System Sciences, v. 20, no. 7, p. 2721–2735, accessed September 27, 2017, at https://doi.org/10.5194/hess-20-2721-2016.

Farmer, W.H., Archfield, S.A., Over, T.M., Hay, L.E., LaFontaine, J.H., and Kiang, J.E., 2014, A comparison of methods to predict historical daily streamflow time series in the southeastern United States: U.S. Geological Survey Scientific Investigations Report 2014–5231, 34 p., accessed April 15, 2015, at https://doi.org/10.3133/sir20145231.

Farnsworth, R.K., and Thompson, E.S., 1982, Mean monthly, seasonal, and annual pan evaporation for the United States: National Oceanic and Atmospheric Administration Technical Report NWS 34, 82 p., accessed November 3, 2017, at http://www.nws.noaa.gov/oh/hdsc/Technical_reports/TR34.pdf.

Fowler, H.J., Blenkinsop, S., and Tebaldi, C., 2007, Linking climate change modelling to impacts studies—Recent advances in downscaling techniques for hydrological modelling: International Journal of Climatology, v. 27, no. 12, p. 1547–1578, accessed May 11, 2018, at https://doi.org/10.1002/joc.1556.

Freeman, M.C., Buell, G.R., Hay, L.E., Hughes, W.B., Jacobson, R.B., Jones, J.W., Jones, S.A., LaFontaine, J.H., Odom, K.R., Peterson, J.T., Riley, J.W., Schindler, J.S., Shea, C., and Weaver, J.D., 2013, Linking river management to species conservation using dynamic landscape-scale models: River Research and Applications, v. 29, no. 7, p. 906–918, accessed November 3, 2017, at https://doi.org/10.1002/rra.2575.

Garcia, A.M., Hoos, A.B., and Terziotti, S., 2011, A regional modeling framework of phosphorus sources and transport in streams of the Southeastern United States: Journal of the American Water Resources Association, v. 47, no. 5, p. 991–1010, accessed August 14, 2017, at https://doi.org/10.1111/j.1752-1688.2010.00517.x.

Gao, Y., Vogel, R.M., Kroll, C.N., Poff, N.L., and Olden, J.D., 2009, Development of representative indicators of hydrologic alteration: Journal of Hydrology, v. 374, nos. 1–2, p. 136–147, accessed November 3, 2017, at https://doi.org/10.1016/j.jhydrol.2009.06.009.

Hay, L.E., LaFontaine, J., and Markstrom, S.L., 2014, Evaluation of statistically downscaled GCM output as input for hydrological and stream temperature simulation in the Apalachicola-Chattahoochee-Flint River Basin (1961–99): Earth Interactions, v. 18, no. 9, 32 p., accessed May 15, 2018, at https://doi.org/10.1175/2013EI000554.1.

Hay, L.E., Markstrom, S.L., and Ward-Garrison, C., 2011, Watershed-scale response to climate change through the twenty-first century for selected basins across the United States: Earth Interactions, v. 15, no. 17, 37 p., accessed November 3, 2017, at https://doi.org/10.1175/2010EI370.1.

Henriksen, J.A., Heasley, J., Kennen, J.G., and Niewsand, S. 2006, Users' manual for the hydroecological integrity assessment process software (including the New Jersey Assessment Tools): U.S. Geological Survey, Biological Resources Discipline, Open-File Report 2006–1093, 71 p., accessed November 3, 2017, at https://doi.org/10.3133/ofr20061093.

Hidalgo, H.G., Dettinger, M.D., and Cayan, D.R., 2008, Downscaling with constructed analogues—Daily precipitation and temperature fields over the United States: Sacramento, California Energy Commission, Public Interest Energy Research Program, 62 p., accessed August 23, 2018, at http://meteora.ucsd.edu/cap/pdffiles/analog_pier_report.pdf.

Homer, C., Dewitz, J., Yang, L., Jin, S., Danielson, P., Xian, G., Coulston, J.W., Herold, N., Wickham, J.D., and Megown, K., 2015, Completion of the 2011 National Land Cover Database for the conterminous United States—Representing a decade of land cover change information: Photogrammetric Engineering and Remote Sensing, v. 81, no. 5, p. 346–354, accessed November 3, 2017, at https://www.asprs.org/a/publications/pers/2015journals/PERS_May_2015_Member/HTML/files/assets/basic-html/page8.html.

Hoos, A.B., Moore, R.B., Garcia, A.M., Noe, G.B., Terziotti, S.E., Johnston, C.M., and Dennis, R.L., 2013, Simulating stream transport of nutrients in the Eastern United States, 2002, using a spatially-referenced regression model and 1:100,000-scale hydrography: U.S. Geological Survey Scientific Investigations Report 2013–5102, 33 p., accessed September 23, 2017, at https://doi.org/10.3133/sir20135102.

Hunt, A.M., and García, A.M., 2014, Simulation of natural flows in major river basins in Alabama: U.S. Geological Survey Scientific Investigations Report 2014–5021, 32 p., accessed September 23, 2017, at https://doi.org/10.3133/sir20145021.

Hurrell, J., Visbeck, M., and Pirani, A., 2011, WCRP coupled model intercomparison project—phase 5—CMIP5, Editorial: Exchanges, no. 56, v. 16, no. 2, accessed October 17, 2017, at http://www.clivar.org/sites/default/files/documents/Exchanges56.pdf.

Intergovernmental Panel on Climate Change, 2007, Summary for policymakers, *in* Solomon, S., Qin, D., Manning, M., Chen, Z., Marquis, M., Averyt, K.B., Tignor, M., and Miller, H.L., eds., Climate change 2007—The physical science basis, Contribution of Working Group I to the Fourth Assessment Report of the Intergovernmental Panel on Climate Change: Cambridge, U.K. and New York, Cambridge University Press, 996 p., accessed May 11, 2018, at https://www.ipcc.ch/publications_and_data/publications_ipcc_fourth_assessment_report_wg1_report_the_physical_science_basis.htm.

Kiang, J.E., Stewart, D.W., Archfield, S.A., Osborne, E.B., and Eng, K., 2013, A national streamflow network gap analysis: U.S. Geological Survey Scientific Investigations Report 2013–5013, 79 p., 1 app. as a separate file, accessed September 24, 2917, at https://doi.org/10.3133/sir20135013.

Knight, R.R., Gain, W.S., and Wolfe, W.J., 2012, Modelling ecological flow regime—An example from the Tennessee and Cumberland River Basins: Ecohydrology, v. 5, no. 5, p. 613–627, accessed November 3, 2017, at https://doi.org/10.1002/eco.246.

Knight, R.R., Murphy, J.C., Wolfe, W.J., Saylor, C.F., and Wales, A.K., 2014, Ecological limit functions relating fish community response to hydrologic departures of the ecological flow regime in the Tennessee River Basin, United States: Ecohydrology, v. 7, no. 5, p. 1262–1280, accessed November 3, 2017, at https://doi.org/10.1002/eco.1460.

LaFontaine, J.H., Hay, L.E., Viger, R.J., Markstrom, S.L., Regan, R.S., Elliott, C.M., and Jones, J.W., 2013, Application of the Precipitation-Runoff Modeling System (PRMS) in the Apalachicola-Chattahoochee-Flint River Basin in the Southeastern United States: U.S. Geological Survey Scientific Investigations Report 2013–5162, 118 p., accessed April 30, 2015, at https://doi.org/10.3133/sir20135162.

LaFontaine, J.H., Hay, L.E., Viger, R.J., Regan, R.S., and Markstrom, S.L., 2015, Effects of climate and land cover on hydrology in the Southeastern U.S.—Potential impacts on watershed planning: Journal of the American Water Resources Association, v. 51, no. 5, p. 1235–1261, accessed September 27, 2016, at https://doi.org/10.1111/1752-1688.12304.

LaFontaine, J.H., Jones, L.E., and Painter, J.A., 2017, Simulations of hydrologic response in the Apalachicola-Chattahoochee-Flint River Basin, Southeastern United States: U.S. Geological Survey Scientific Investigations Report 2017–5133, 112 p., accessed May 15, 2018, at https://doi.org/10.3133/sir20175133.

LaFontaine, J.H., Hay, L.E., and Farmer, W.H., 2019, Model Input and Output for Hydrologic Simulations of the Southeastern United States for Historical and Future Conditions: U.S. Geological Survey data release, accessed April 18, 2019, at https://doi.org/10.5066/F74X56PH.

Leasure, D.R., Magoulick, D.D., and Longing, S.D., 2016, Natural flow regimes of the Ozark-Ouachita Interior Highlands region: River Research and Applications, v. 32, no. 1, p. 18–35, accessed May 15, 2018, at https://doi.org/10.1002/rra.2838.

Leavesley, G.H., Lichty, R.W., Troutman, B.M., and Saindon, L.G., 1983, Precipitation-Runoff Modeling System—User's manual: U.S. Geological Survey Water-Resources Investigations Report 83–4238, 207 p., accessed September 24, 2017, at https://pubs.usgs.gov/wri/1983/4238/report.pdf.

Liang, X., Lettenmaier, D.P., Wood, E.F., and Burges, S.J., 1994, A simple hydrologically based model of land surface water and energy fluxes for general circulation models: Journal of Geophysical Research, v. 99, no. D7, p. 14415–14428, accessed November 3, 2017, at https://doi.org/10.1029/94JD00483.

Liang, X., Wood, E.F., and Lettenmaier, D.P., 1996, Surface soil moisture parameterization of the VIC-2L model—Evaluation and modification: Global and Planetary Change, v. 13, nos. 1–4, p. 195–206, accessed November 3, 2017, at https://doi.org/10.1016/0921-8181(95)00046-1.

Liang, X., Wood, E.F., and Lettenmaier, D.P., 1999, Modeling ground heat flux in land surface parameterization schemes: Journal of Geophysical Research, v. 104, no. D8, p. 9581–9600, accessed November 3, 2017, at https://doi.org/10.1029/98JD02307.

Lins, H.F., Hirsch, R.M., and Kiang, J., 2010, Water—the Nation's fundamental climate issue—A White Paper on the U.S. Geological Survey role and capabilities: U.S. Geological Survey Circular 1347, 9 p., accessed November 3, 2017, at https://doi.org/10.3133/cir1347.

Marion, D.A., Sun, G., Caldwell, P.V., Miniat, C.F., Ouyang, Y., Amatya, D.M., Clinton, B.D., Conrads, P.A., Laird, S.G., Dai, Z., Clingenpeel, J.A., Liu, Y., Roehl, E.A., Jr., Moore Meyers, J.A., and Trettin, C., 2014, Managing forest water quantity and quality under climate change, *in* Climate change adaptation and mitigation management options—A guide for natural resource managers in southern forest ecosystems: CRC Press–Taylor and Francis, p. 249–306, accessed September 23, 2017, at https://www.fs.usda.gov/treesearch/pubs/45792.

Markstrom, S.L., Hay, L.E., Ward-Garrison, C.D., Risley, J.C., Battaglin, W.A., Bjerklie, D.M., Chase, K.J., Christiansen, D.E., Dudley, R.W., Hunt, R.J., Koczot, K.M., Mastin, M.C., Regan, R.S., Viger, R.J., Vining, K.C., and Walker, J.F., 2012, Integrated watershed-scale response to climate change for selected basins across the United States: U.S. Geological Survey Scientific Investigations Report 2011–5077, 143 p., accessed November 3, 2017, at https://doi.org/10.3133/sir20115077.

Markstrom, S.L., Regan, R.S., Hay, L.E., Viger, R.J., Webb, R.M.T., Payn, R.A., and LaFontaine, J.H., 2015, PRMS-IV, the Precipitation-Runoff Modeling System, version 4: U.S. Geological Survey Techniques and Methods, book 6, chap. B7, 158 p., accessed February 13, 2017, at https://doi.org/10.3133/tm6B7.

Massey, F.J., Jr., 1951, The Kolmogorov-Smirnov test for goodness of fit: Journal of the American Statistical Association, v. 46, no. 253, p. 68–78, accessed November 7, 2017, at https://r-forge.r-project.org/scm/viewvc.php/*checkout*/pkg/literature/1951-jamsta-massey-kolmsmirntest.pdf?root=glogis.

Maurer, E.P., and Hidalgo, H.G., 2008, Utility of daily vs. monthly large-scale climate data—An intercomparison of two statistical downscaling methods: Hydrology and Earth System Sciences, v. 12, no. 2, p. 551–563, accessed August 23, 2018, at https://doi.org/10.5194/hess-12-551-2008.

Maurer, E.P., Hidalgo, H.G., Das, T., Dettinger, M.D., and Cayan, D.R., 2010, The utility of daily large-scale climate data in the assessment of climate change impacts on daily streamflow in California: Hydrology and Earth System Sciences, v. 14, no. 6, p. 1125–1138, accessed August 23, 2018, at https://doi.org/10.5194/hess-14-1125-2010.

Maurer, E.P., Wood, A.W., Adam, J.C., Lettenmaier, D.P., and Nijssen, B., 2002, A long-term hydrologically based dataset of land surface fluxes and states for the conterminous United States: Journal of Climate, v. 15, no. 22, p. 3237–3251, accessed September 24, 2017, at https://doi.org/10.1175/1520-0442(2002)015%3C3237:ALTHBD%3E2.0.CO;2.

McCabe, G.J., and Markstrom, S.L., 2007, A monthly water-balance model driven by a graphical user interface: U.S. Geological Survey Open-File Report 2007–1088, 6 p., accessed October 27, 2017, at https://pubs.usgs.gov/of/2007/1088/.

McCabe, G.J., Hay, L.E., Bock, A., Markstrom, S.L., and Atkinson, R.D., 2015, Inter-annual and spatial variability of Hamon potential evapotranspiration model coefficients: Journal of Hydrology, v. 521, p. 389–394, accessed November 3, 2017, at https://doi.org/10.1016/j.jhydrol.2014.12.006.

McManamay, R.A., and Frimpong, E.A., 2015, Hydrologic filtering of fish life history strategies across the United States—Implications for stream flow alteration: Ecological Applications, v. 25, no. 1, p. 243–263, accessed November 3, 2017, at https://doi.org/10.1890/14-0247.1.

Meehl, G.A., Goddard, L., Murphy, J., Stouffer, R.J., Boer, G., Danabasoglu, G., Dixon, K., Giorgetta, M.A., Greene, A.M., Hawkins, E., Hegerl, G., Karoly, D., Keenlyside, N., Kimoto, M., Kirtman, B., Navarra, A., Pulwarty, R., Smith, D., Stammer, D., and Stockdale, T., 2009, Decadal prediction—Can it be skillful?: Bulletin of the American Meteorological Society, v. 90, no. 10, p. 1467–1485, accessed October 17, 2017, at https://doi.org/10.1175/2009BAMS2778.1.

Milly, P.C.D., Betancourt, J., Falkenmark, M., Hirsch, R.M., Kundzewicz, Z.W., Lettenmaier, D.P., and Stouffer, R.J., 2008, Stationarity is dead—Whither water management?: Science, v. 319, no. 5863, p. 573–574, accessed October 2, 2014, at https://doi.org/10.1126/science.1151915.

Mulholland, P.J., Best, G.R., Coutant, C.C., Hornberger, G.M., Meyer, J.L., Robinson, P.J., Stenberg, J.R., Turner, R.E., Vera-Herrera, F., and Wetzel, R.G., 1997, Effects of climate change on freshwater ecosystems of the south-eastern United States and the Gulf Coast of Mexico: Hydrological Processes, v. 11, no. 8, p. 949–970, accessed September 22, 2017, at https://doi.org/10.1002/(SICI)1099-1085(19970630)11:8%3C949::AID-HYP513%3E3.0.CO;2-G.

Murphy, J.C., Knight, R.R., Wolfe, W.J., and Gain, W.S., 2013, Predicting ecological flow regime at ungaged sites—A comparison of methods: River Research and Applications, v. 29, no. 5, p. 660–669, accessed November 3, 2017, at https://doi.org/10.1002/rra.2570.

Nash, J.E., and Sutcliffe, J.V., 1970, River flow forecasting through conceptual models part I—A discussion of principles: Journal of Hydrology, v. 10, no. 3, p. 282–290, accessed September 2, 2009, at https://doi.org/10.1016/0022-1694(70)90255-6.

O’Driscoll, M., Clinton, S., Jefferson, A., Manda, A., and McMillan, S., 2010, Urbanization effects on watershed hydrology and in-stream processes in the Southern United States: Water, v. 2, no. 3, p. 605–648, accessed September 22, 2017, at https://doi.org/10.3390/w2030605.

Olden, J.D., and Poff, N.L., 2003, Redundancy and the choice of hydrologic indices for characterizing streamflow regimes: River Research and Applications, v. 19, no. 2, p. 101–121, accessed November 3, 2017, at https://doi.org/10.1002/rra.700.

Omernick, J.M., and Griffith, G.E., 2014, Ecoregions of the conterminous United States—Evolution of a hierarchical spatial framework: Environmental Management, v. 54, no. 6, p. 1249–1266, accessed November 3, 2017, at https://doi.org/10.1007/s00267-014-0364-1.

Paul, M.J., and Meyer, J.L., 2001, Streams in the urban landscape: Annual Review of Ecology and Systematics, v. 32, p. 333–365, accessed November 3, 2017, at https://doi.org/10.1146/annurev.ecolsys.32.081501.114040.

Poff, N.L., 1996, A hydrogeography of unregulated streams in the United States and an examination of scale-dependence in some hydrological descriptors: Freshwater Biology, v. 36, p. 71–91, accessed November 3, 2017, at https://doi.org/10.1046/j.1365-2427.1996.00073.x.

Regan, R.S., and LaFontaine, J.H., 2017, Documentation of the dynamic parameter, water-use, stream and lake flow routing, and two summary output modules and updates to surface-depression storage simulation and initial conditions specification options with the Precipitation-Runoff Modeling System (PRMS): U.S. Geological Survey Techniques and Methods, book 6, chap. B8, 60 p., accessed October 27, 2017, at https://doi.org/10.3133/tm6B8.

Regan, R.S., Markstrom, S.L., Hay, L.E., Viger, R.J., Norton, P.A., Driscoll, J.M., LaFontaine, J.H., 2018, Description of the National Hydrologic Model for use with the Precipitation-Runoff Modeling System (PRMS): U.S. Geological Survey Techniques and Methods, book 6, chap. B9, 38 p., accessed May 16, 2018, at https://doi.org/10.3133/tm6B9.

Richter, B.D., Baumgartner, J.V., Powell, J., and Braun, D.P., 1996, A method for assessing hydrologic alteration within ecosystems: Conservation Biology, v. 10, no. 4, p. 1163–1174, accessed November 3, 2017, at http://ase.tufts.edu/water/pdf/iha_meth.pdf.

Salavati, B., Oudin, L., Furusho, C., and Ribstein, P., 2015, Analysing the impact of urban areas patterns on the mean annual flow of 43 urbanized catchments: Proceedings of the International Association of Hydrological Sciences, no. 370, p. 29–32, accessed April 20, 2019, at https://doi.org/10.5194/piahs-370-29-2015.

Scott, M.C., 2006, Winners and losers among stream fishes in relation to land use legacies and urban development in the southeastern US: Biological Conservation, v. 127, no. 3, p. 301–309, accessed November 3, 2017, at https://doi.org/10.1016/j.biocon.2005.07.020.

Shrestha, S., Bhatta, B., Shrestha, M., and Shrestha, P.K., 2018, Integrated assessment of the climate and landuse change impact on hydrology and water quality in the Songkhram River Basin, Thailand: Science of the Total Environment, no. 643, p. 1610–1622, accessed on April 19, 2019, at https://doi.org/10.1016/j.scitotenv.2018.06.306.

Sun, G., 2013, Impacts of climate change and variability on water resources in the southeast USA, chap. 10 *in* Ingram, K.T., Dow, K., Carter, L., and Anderson, J., eds., Climate of the southeast United States—Variability, change, impacts, and vulnerability: Washington, D.C., Island Press, NCA Regional Input Reports, p. 210–236, accessed September 23, 2017, at https://doi.org/10.5822/978-1-61091-509-0_10.

Sun, G., McNulty, S.G., Moore Myers, J.A., and Cohen, E.C., 2008, Impacts of multiple stresses on water demand and supply across the southeastern United States: Journal of the American Water Resources Association, v. 44, no. 6, p. 1441–1457, accessed September 22, 2017, at https://doi.org/10.1111/j.1752-1688.2008.00250.x.

Suttles, K.M., Singh, N.K., Vose, J.M., Martin, K.L., Emanuel, R.E., Coulston, J.W., Saia, S.M., and Crump, M.T., 2018, Assessment of hydrologic vulnerability to urbanization and climate change in a rapidly changing watershed in the Southeast U.S.: Science of the Total Environment, no. 645, p. 806-816, accessed on April 19, 2019, at https://doi.org/10.1016/j.scitotenv.2018.06.287.

Taylor, K.E., Stouffer, R.J., and Meehl, G.A., 2012, An Overview of CMIP5 and the experiment design: Bulletin of the American Meteorological Society, v. 93, no. 4, p. 485–498, accessed October 17, 2017, at https://doi.org/10.1175/BAMS-D-11-00094.1.

Tebaldi, C., and Knutti, R., 2007, The use of the multi-model ensemble in probabilistic climate projections: Philosophical Transactions of the Royal Society A, v. 365, no. 1857, p. 2053–2075, accessed May 14, 2018, at https://doi.org/10.1098/rsta.2007.2076.

U.S. Environmental Protection Agency [EPA], 2016, Ecoregions of North America: U.S. Environmental Protection Agency website, accessed October 25, 2017, at https://www.epa.gov/eco-research/ecoregions-north-america.

U.S. Geological Survey, 2007, Facing tomorrow's challenges—U.S. Geological Survey science in the decade 2007–2017: U.S. Geological Survey Circular 1309, 67 p., accessed September 24, 2017, at https://pubs.usgs.gov/circ/2007/1309/.

U.S. Geological Survey, 2017, USGS water data for the Nation: U.S. Geological Survey National Water Information System database, accessed May 16, 2018, at https://doi.org/10.5066/F7P55KJN.

Viger, R.J., and Bock, A., 2014, GIS features of the Geospatial Fabric for national hydrologic modeling: U.S. Geological Survey metadata, accessed April 30, 2015, at https://doi.org/10.5066/F7542KMD.

Viger, R.J., Hay, L.E., Markstrom, S.L., Jones, J.W., and Buell, G.R., 2011, Hydrologic effects of urbanization and climate change on the Flint River Basin, Georgia: Earth Interactions, v. 15, no. 20, 25 p., accessed October 17, 2017, at https://doi.org/10.1175/2010EI369.1.

Vuuren, D.P. van, Edmonds, J., Kainuma, M. Riahi, K., Thomson, A., Hibbard, K., Hurtt, G.C., Kram, T., Krey, V., Lamarque, J.-F., Masui, T., Meinshausen, M., Nakicenovic, N., Smith, S.J., and Rose, S.K., 2011, The representative concentration pathways—An overview: Climatic Change, v. 109, no. 5, p. 5–31, accessed August 23, 2018, at https://doi.org/10.1007/s10584-011-0148-z.

Wolock, D.M., 1997, STATSGO soil characteristics for the conterminous United States: U.S. Geological Survey Open-File Report 97–656, accessed November 3, 2017, at https://pubs.er.usgs.gov/publication/ofr97656.

Wolock, D.M. and McCabe, G.J., 1999, Explaining spatial variability in mean annual runoff in the conterminous United States: Climate Research, v. 11, no. 2, p. 149–159, accessed October 27, 2017, at https://doi.org/10.3354/cr011149.

Wood, A.W., Leung, L.R., Sridhar, V., and Lettenmaier, D.P., 2004, Hydrologic implications of dynamical and statistical approaches to downscaling climate model outputs: Climate Change, v. 62, nos. 1–3, p. 189–216, accessed May 11, 2018, at https://doi.org/10.1023/B:CLIM.0000013685.99609.9e.

Wood, A.W., Maurer, E.P., Kumar, A., and Lettenmaier, D.P., 2002, Long-range experimental hydrologic forecasting for the eastern United States: Journal of Geophysical Research, v. 107, no. D20, 15 p., accessed September 22, 2017, at https://doi.org/10.1029/2001JD000659.

Appendix 1. Construction, Calibration, and Evaluation of the Southeastern U.S. Hydrologic Model

Introduction

This appendix describes the construction, calibration, and evaluation of a hydrologic model application for the Gulf Coastal Plains and Ozarks Landscape Conservation Cooperative (GCPO LCC) region and surrounding areas of the Southeastern United States. The U.S. Geological Survey (USGS) Precipitation-Runoff Modeling System (PRMS; Leavesley and others, 1983; Markstrom and others, 2015) was used to provide hydrologic simulations of the study area; this application is referred to as the GCPO-PRMS. The PRMS Model Construction section describes the methodology, which comes from methods described in Viger and Bock (2014) and Regan and others (2018), used for developing model stream segments and hydrologic response units (HRUs). The PRMS Model Calibration section describes the general methodology used for hydrologic model parameter estimation. The PRMS Model Evaluation section describes the methods used to evaluate model performance. Dynamic parameter information for the study area is also summarized in this appendix. Supporting data for the construction, calibration, and evaluation of the hydrologic model are available in LaFontaine and others (2019).

Precipitation-Runoff Modeling System (PRMS) Model Construction

The PRMS watershed hydrology model is a deterministic, distributed-parameter, process-based model used to simulate and evaluate the effects of various combinations of precipitation, climate, and land use on basin response. Response to precipitation and snowmelt can be simulated to evaluate changes in water-balance relations, streamflow regimes, soil-water relations, and groundwater recharge. Each hydrologic component used for generation of streamflow is represented within the PRMS by a process algorithm that is based on a physical law or an empirical relation with measured or calculated characteristics (fig. 5 in main text). The schematic in figure 6 (main text) provides further detail of the various processes conceptualized in the PRMS soil zone. Many internal states (storages) and fluxes (flows) are available as output from the PRMS simulations; see Markstrom and others (2015) for a complete list.

Discretization

Distributed-parameter capabilities of the PRMS are provided by partitioning a basin into HRUs in which a water balance and an energy balance are computed. The PRMS uses daily climate values of measured precipitation and maximum and minimum air temperature distributed to each HRU to compute potential evapotranspiration, actual evapotranspiration, sublimation, snowmelt, streamflow, infiltration, and groundwater recharge in a PRMS simulation. A stream network is used in the PRMS to route HRU-based runoff flow components (surface runoff, shallow subsurface runoff, and groundwater flow) downstream to the study area outlets. For this study, HRUs and stream segments were extracted from the USGS National Hydrologic Model (NHM; Regan and others, 2018) and are based on the GeoSpatial Fabric for National Hydrologic Modeling (Viger and Bock, 2014). A total of 10,742 stream segments and 20,251 HRUs are included in the GCPO-PRMS hydrologic model (fig. 1–1). The GCPO-PRMS stream segments have a mean and median length of 8.8 and 8.4 miles, respectively. The GCPO-PRMS HRUs have a mean and median size of 22.0 and 12.4 square miles, respectively.

Parameterization

PRMS is a distributed-parameter hydrologic model. Many of the model parameters vary spatially on the basis of the surface and subsurface characteristics of the model domain. The PRMS parameters describe processes such as solar radiation, potential evapotranspiration, canopy interception, snow dynamics, surface runoff, soil-zone dynamics, groundwater flow, and streamflow. For this version of PRMS, the soil-zone and groundwater reservoirs have the same spatial delineations (size and shape) as the HRUs. The default set of PRMS parameters used for this application was obtained from the USGS National Hydrologic Model Parameter Database (Driscoll and others, 2017b).

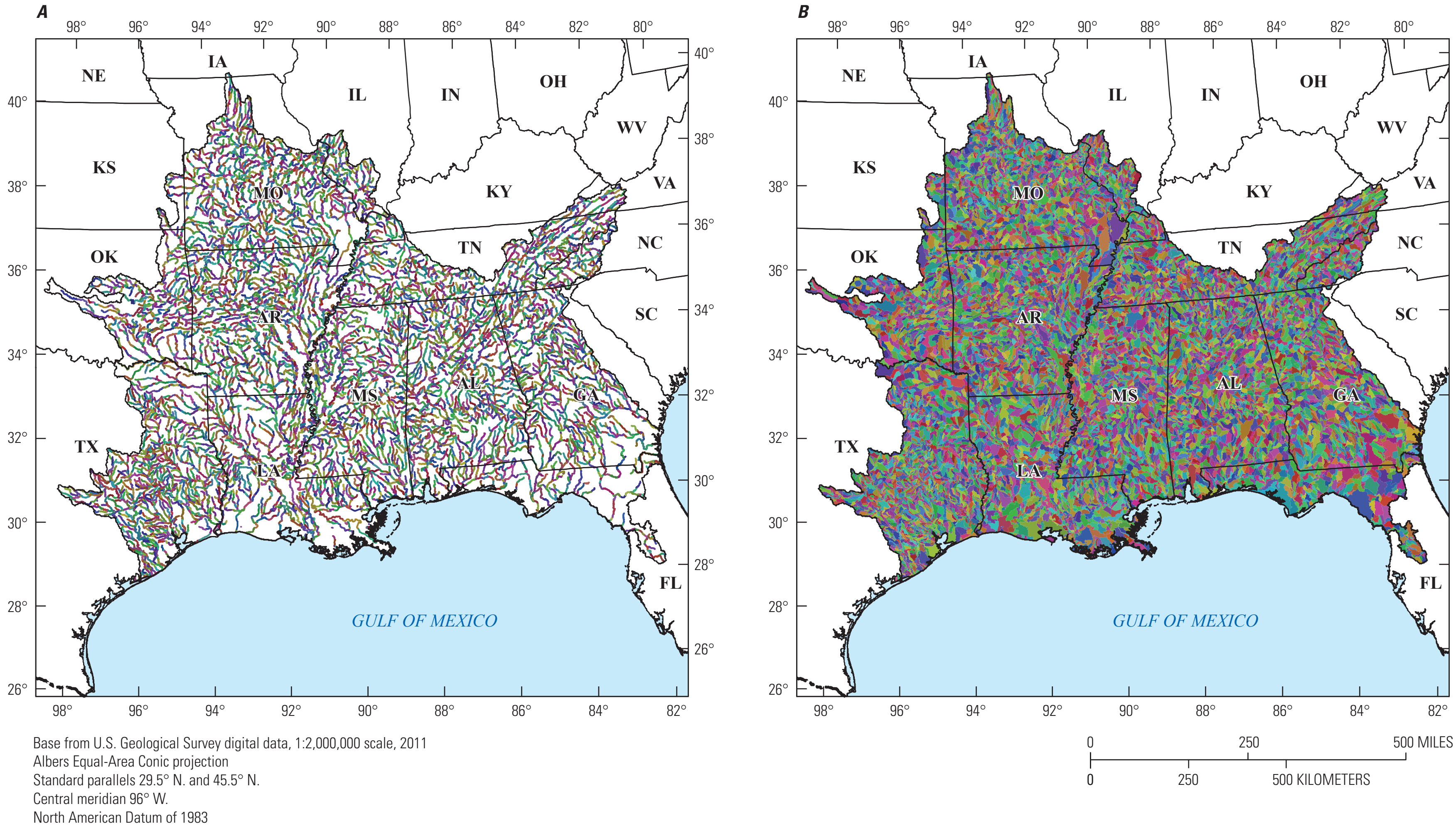

Figure 1–1. Maps showing(*A*) Precipitation-Runoff Modeling System stream segments and (*B*) Precipitation-Runoff Modeling System hydrologic response units. Stream segments and hydrologic response units are differentiated by color.

These default parameter values are based on a combination of (1) long-established defaults assigned on the basis of hydrologic and geographic information gained over 35 years of PRMS operation, (2) estimation methods described by Viger and Leavesley (2007) and Viger (2014) for characterizing topography, land cover, soils, geology, and hydrography, (3) direct solution of PRMS algorithms for unknown variables (such as solar radiation and potential evapotranspiration parameters), (4) long-term simulation-averaged values (such as initialization parameters for water flux and storage), and (5) estimation methods using other hydrologic simulation results (Regan and others, 2018). A static set of default values was used to initialize the PRMS simulations; these parameter values were constant for all simulation periods. Dynamic parameters were derived for five PRMS parameters describing changes in land cover and canopy interception for the period 1950–2099; these parameter values changed on an annual time step for all simulation periods.

Static Model Parameters for the Precipitation-Runoff Modeling System

Default parameter values for the GCPO-PRMS application were computed by Regan and others (2018) using several datasets. Dominant land-cover type and vegetation density parameters were computed by Regan and others (2018) using the National Land Cover Database 2001 (NLCD2001; Homer and others, 2007). Topographic and geographic parameters, including HRU area, latitude, longitude, centroid, altitude, aspect, and slope, were computed by Viger (2014) using the digital elevation model (DEM) included in the National Hydrography Dataset version 1 (NHDPlus). Initial water content parameters for surface-depression storage, capillary reservoir storage, recharge zone storage of the capillary reservoir, gravity reservoir storage, groundwater reservoir storage, and snowpack were computed for each HRU based on the last 20 years of a 35-year simulation for 1980–2014 of the NHM-PRMS (Regan and others, 2018).

Climate-based parameters that partition precipitation into rain and snow fractions were computed by Regan and others (2018) based on estimates of daily air temperature and precipitation from the Daily Surface Weather and Climatological Summaries (DAYMET; Thornton and others, 1997) and snow cover and snow water equivalent estimates from the Snow Data Assimilation System (SNODAS; National Operational Hydrologic Remote Sensing Center, 2004). Solar radiation parameters used to compute daily shortwave radiation were computed by Regan and others (2018) using estimates of mean monthly solar radiation compiled by the National Renewable Energy Laboratory (National Renewable Energy Laboratory, undated). Potential evapotranspiration parameters were computed by Regan and others (2018) using long-term mean monthly estimates of pan evaporation compiled by Farnsworth and others (1982) and Farnsworth and Thompson (1982) and the DAYMET climate data. Precipitation interception parameters were developed by Viger (2014) using the NLCD2001 land cover and vegetation data products. Snow computation parameters were developed by Driscoll and others (2017a) using snow cover and snow water equivalent estimate from SNODAS, precipitation storm type output from the Climate Forecast System Reanalysis model (Saha and others, 2010), and canopy density estimates from the NLCD2001.

Overland runoff parameters describing percent impervious area, maximum contributing area, and runoff fraction were computed using the NLCD2001, the NHDPlus version 1 DEM and waterbodies coverage, and estimates of Topographic Wetness Index (Beven and Kirby, 1979). Surface-depression storage parameters were computed using the NHDPlus version 1 DEM and waterbodies coverage and estimates of monthly runoff from a conterminous U.S. (CONUS)-scale application of the Monthly Water Balance Model (MWBM) by Bock and others (2015). Soil-zone parameters were computed using estimates of near-surface permeability from Gleeson and others (2011), soil information from the Natural Resources Conservation Service Soils Data for the Conterminous United States (STATSGO) dataset (U.S. Department of Agriculture, 1991), and algorithms developed by Viger and Leavesley (2007). Groundwater flow parameters were computed by Regan and others (2018) using a best-fit multiple-linear regression model that used geographic information system (GIS) datasets of geology, drainage density, aquifer type, vegetation type, and base flow index (Rutledge and Mesko, 1996; Sloto and Crause, 1996; Brandes and others, 2005; Falcone, 2011; Berhail and others, 2012). Further details describing the computation of the various PRMS parameters are provided in Regan and others (2018).

Dynamic Model Parameters for the Precipitation-Runoff Modeling System

Deriving hydrologic model parameters from land-cover data is critical to ensuring proper model development and accurate representation of hydrologic processes such as evapotranspiration, runoff, and infiltration (Van Beusekom and others, 2014; LaFontaine and others, 2015). To account for long-term land-cover dynamics (1950–2099), a subset of PRMS model parameters based on historical and potential future land-cover data was developed for each year of hydrologic simulation. Annual representations of land cover developed by Sohl and others (2014, 2016) were obtained from the USGS Earth Resources Observation and Science (EROS) Center (U.S. Geological Survey, undated). These EROS-based data are GIS raster files with 17 land-cover classes for the CONUS for the period 1938–2099. These 17 land-cover classes were redefined to 6 land-cover classes for PRMS parameterization. The conversion from land-cover class to PRMS parameters follows the methods described in Viger and Leavesley (2007).

The PRMS parameters derived using the EROS-based land-cover data for each year of simulation included dominant cover type (**cov_type**), percent impervious area (**hru_percent_imperv**), summer canopy interception (**srain_intcp**), winter canopy interception (**wrain_intcp**), and snow interception (**snow_intcp**). These parameters were developed from the raw land-cover values from the EROS grids and summarized for each HRU. The five hydrologic parameters were derived from both historical and potential future data sources (Sohl and others, 2014, 2016). The historical dataset consisted of (1) annual time step historical land-cover estimates for 1992–2005 from the National Assessment of Ecosystem Carbon and Greenhouse Gas Fluxes project, and (2) annual time step land-cover data for 1938–1992 based on best available tabular and statistical data, including data from the Agriculture Census, Population Census, USGS Land Cover Trends, and other sources (Sohl and others, 2014, 2016). The potential future land-cover estimates for 2006–2050 were simulated by Sohl and others (2014) using the Intergovernmental Panel on Climate Change Special Report on Emissions Scenarios A1B emissions scenario as part of the National Assessment of Ecosystem Carbon and Greenhouse Gas Fluxes project. Decadal changes in the **cov_type** parameter for the period 1950–2070 are shown in table 1–1, and decadal changes in the remaining four parameters (**hru_percent_imperv**, **snow_intcp**, **srain_intcp**, and **wrain_intcp**) for the period 1950–2070 are shown in table 1–2. During the study period, the amount of vegetation type “tree” decreased, the vegetation types “bare” and “grass” increased, and the vegetation type “shrub” remained relatively stable (table 1–1). Fraction of percent impervious area steadily increased through the study period, and the interception parameter values decreased through the study period. The conversion from “tree” vegetation cover to “bare” and “grass” coincides with the decrease in vegetation interception storage capacity. All other land-cover PRMS parameters were held constant for the hydrologic simulations at the values described in the “Static Model Parameters for the Precipitation-Runoff Modeling System” section of this appendix.

Table 1–1. Fraction of the study area classified by the four categories of Precipitation-Runoff Modeling System (PRMS) parameter **cov_type** for decadal time steps from 1950 to 2070.

Year	PRMS parameter cov_type category			
	Bare	Grass	Shrub	Tree
1950	0.009	0.115	0.029	0.847
1960	0.011	0.107	0.030	0.852
1970	0.013	0.115	0.029	0.843
1980	0.015	0.122	0.029	0.834
1990	0.015	0.119	0.031	0.835
2000	0.018	0.118	0.031	0.833
2010	0.024	0.117	0.031	0.828
2020	0.028	0.121	0.031	0.820
2030	0.031	0.125	0.031	0.813
2040	0.033	0.147	0.031	0.789
2050	0.039	0.160	0.031	0.770
2060	0.040	0.168	0.031	0.761
2070	0.042	0.178	0.030	0.750

Table 1–2. Dynamic parameter values for four Precipitation-Runoff Modeling System (PRMS) parameters for decadal time steps from 1950 to 2070.

[Parameter **hru_percent_imperv** describes the fraction of hydrologic response unit (HRU) area that is impervious, parameter **snow_intcp** describes the snow interception storage capacity of the major vegetation type for each HRU, parameter **srain_intcp** describes the summer interception storage capacity of the major vegetation type for each HRU, and parameter **wrain_intcp** describes the winter interception storage capacity of the major vegetation type for each HRU. The **hru_percent_imperv** parameter has units of decimal fraction, and the three interception storage parameters have units of inches]

Year	PRMS parameter			
	hru_percent_imperv	snow_intcp	srain_intcp	wrain_intcp
1950	0.0114	0.0439	0.0363	0.0279
1960	0.0123	0.0441	0.0369	0.0278
1970	0.0134	0.0434	0.0364	0.0274
1980	0.0144	0.0429	0.0360	0.0270
1990	0.0149	0.0430	0.0361	0.0270
2000	0.0164	0.0427	0.0359	0.0266
2010	0.0181	0.0428	0.0357	0.0266
2020	0.0201	0.0424	0.0352	0.0264
2030	0.0220	0.0420	0.0349	0.0261
2040	0.0239	0.0410	0.0340	0.0257
2050	0.0253	0.0403	0.0334	0.0254
2060	0.0263	0.0399	0.0330	0.0251
2070	0.0275	0.0395	0.0325	0.0249

Climate Data and Algorithm

The PRMS requires inputs of daily maximum and minimum air temperature and daily precipitation time-series data. For the GCPO-PRMS model, preprocessed gridded datasets available from the USGS GeoData Portal (GDP; Blodgett and others, 2011; Read and others, 2015) were used. The GDP used a GIS shapefile of the model HRUs to compute the weighted-areal average of the maximum and minimum air temperature and precipitation for each day of the study period for historical and potential future conditions. Climate data from the Maurer and others (2002) climate dataset were used for historical hydrologic simulations based on observed data for 1949–2010. Maurer and others (2002) developed daily precipitation and temperature grids for the CONUS for 1949–2010 using an approximately 12×12-kilometer grid-cell size. Maurer and others (2002) used weather station data from the National Weather Service National Climatic Data Center network to develop the climate forcings (https://www.ncdc.noaa.gov/, accessed May 17, 2016). The daily climate inputs were distributed to the GCPO-PRMS model HRUs using the **climate_hru** module (Markstrom and others, 2015).

PRMS Model Calibration

In the GCPO LCC study area, streamflow measurements do not provide direct observations of water availability at every location of interest. A total of 169 reference-quality streamgages were used in the model calibration and covered approximately 10.9 percent of the 446,600 square miles (1,157,000 square kilometers) of drainage area within the GCPO-PRMS study area (fig. 1–2). The reference-quality streamgages are those classified as relatively unaffected by anthropogenic effects in the GAGES-II dataset developed by Falcone (2011). This limited coverage of reference-quality streamflow information creates the challenge of determining the best method to transfer information from these gaged drainage basins to the data-poor areas within the GCPO LCC study area where results cannot be reliably calibrated or evaluated with measured streamflow (Fernandez and others, 2000). The traditional approach to hydrologic model calibration and evaluation—comparing observed and simulated streamflow—is not sufficient by itself in model calibration and evaluation (Refsgaard, 1997). Intermediate process variables computed by the hydrologic model could be characterized by parameter values that do not replicate those hydrological processes in the physical system (Hay and Umemoto, 2007). To address this issue, intermediate process variables, in addition to streamflow, could be examined when there is an associated observed (simulated or measured) variable that could be used as a calibration dataset. For example, additional calibration datasets such as potential evapotranspiration and solar radiation (Hay and others, 2006), snow-covered area (Hay and others, 2005; Franz and Karsten, 2013; Isenstein and others, 2015), soil moisture (Campo and others, 2006; Santanello and others, 2007; Koren and others, 2008; Wanders and others, 2014; Thorstensen and others, 2016) and evapotranspiration (Cao and others, 2006; Immerzeel and Droogers, 2008; Rientjes and others, 2013) have been used as additional controls or targets within the model calibration process.

For the GCPO-PRMS calibration, in addition to the traditional PRMS calibration using measured daily streamflow, daily values of streamflow with error bounds from ordinary kriging and monthly ranges of runoff, actual evapotranspiration (AET), and snow water equivalent (SWE) derived from other models and remotely sensed data were used in a multiple-objective, step-wise, automated calibration procedure (Hay and Umemoto, 2007) using the Shuffled Complex Evolution (SCE) global search algorithm (Duan and others, 1992, 1993, 1994). Figure 1–3 outlines the three-part procedure used to calibrate the GCPO-PRMS model by (1) HRU, (2) headwater, and (3) streamgage. Figure 1–4 shows where each level of calibration occurs throughout the study area.

Ordinary kriging was used to produce daily time series of streamflow at each of the 1,309 headwater basins with associated error bounds for PRMS calibration (Farmer, 2016). Fifteen headwater basins had GAGES-II reference gages at the headwater outlet. When compared to observed streamflow for the water years 1981 to 2010, the simulated streamflow for those 15 headwater basins had a median Nash-Sutcliffe Efficiency (NSE; Nash and Sutcliffe, 1970) index value of 0.78. The environmental flow components (EFC) algorithm developed by The Nature Conservancy (2009) was used to categorize the daily time step ordinary kriging-based streamflows into high- and low-flow values. For this study, high flows consisted of streamflows categorized by the EFC algorithm as large floods, small floods, or high-flow pulses. Low flows consisted of streamflows categorized by the EFC algorithm as low or extreme low flows. This classification of streamflows as high or low flows was used in steps 2 and 3 of the calibration by the headwaters portion of the calibration process (fig. 1–3) as described in the “Calibration by Headwater” section.

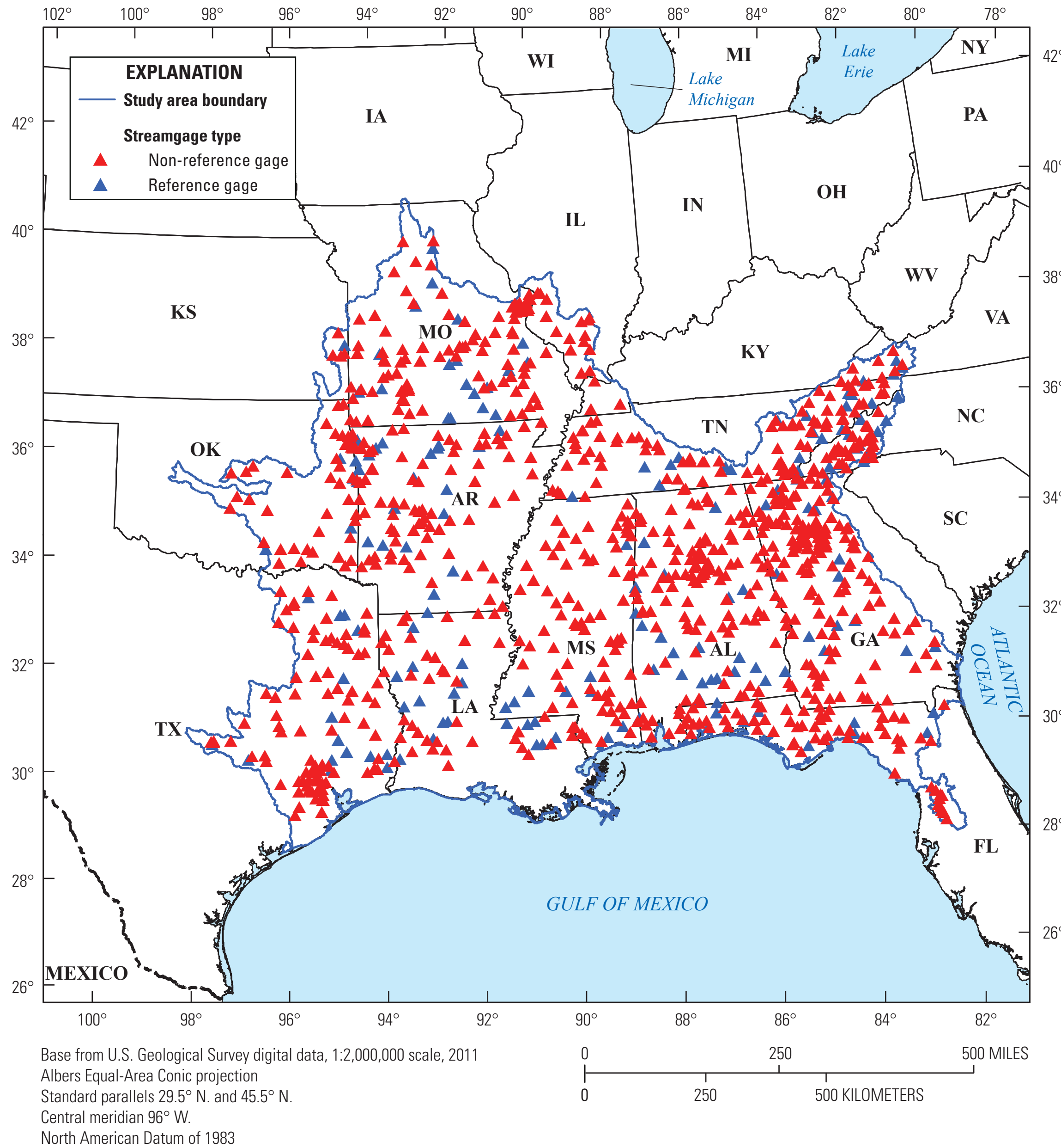

Figure 1–2. Map showing U.S. Geological Survey (USGS) streamgages included for the Precipitation-Runoff Modeling System application. A total of 169 reference-quality and 897 non-reference quality streamgages were used for model evaluation.

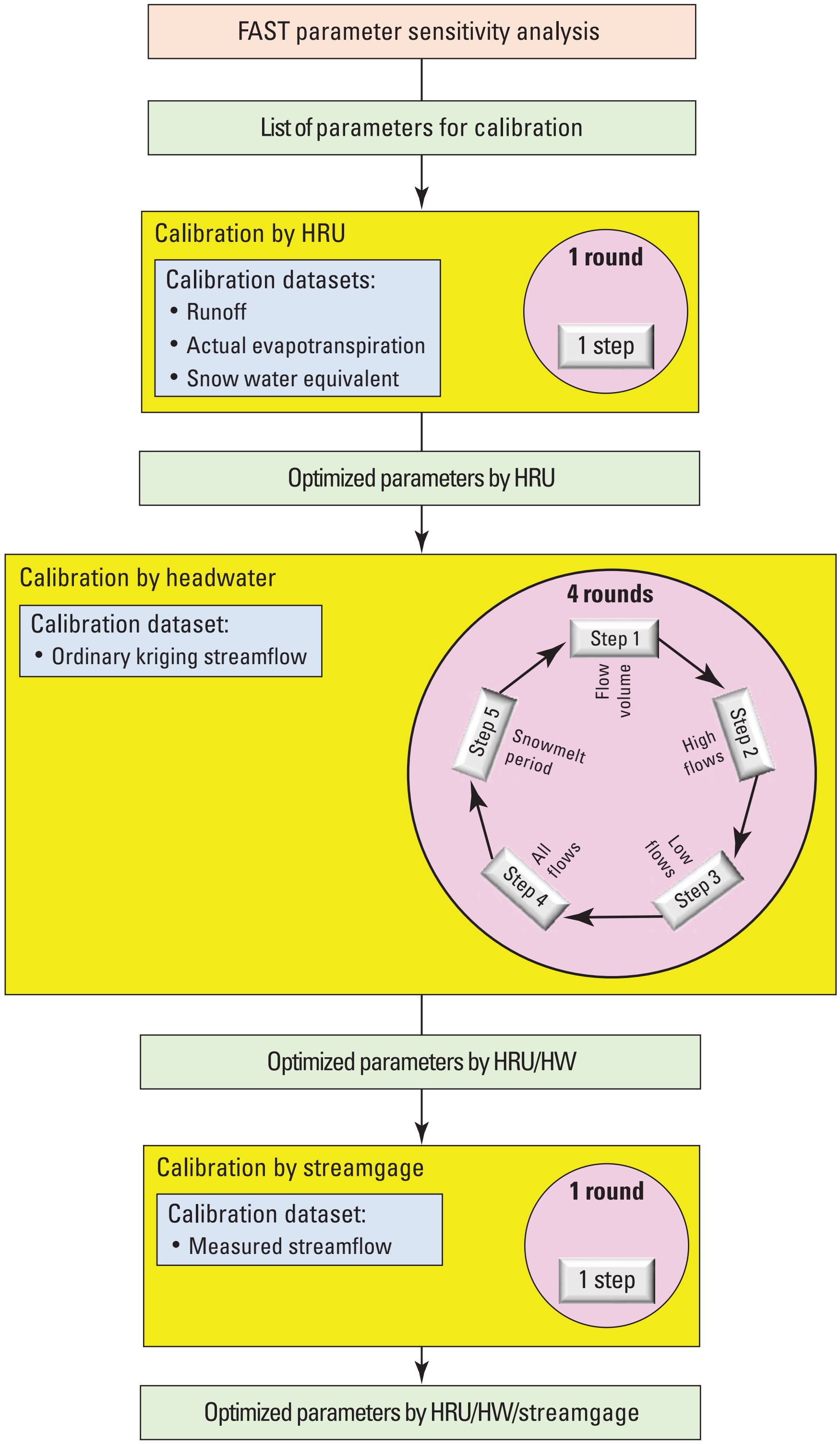

Figure 1–3. Schematic showing the calibration procedure for the application of the Precipitation-Runoff Modeling System in the Southeastern United States (GCPO-PRMS). FAST, Fourier Amplitude Sensitivity Test; HRU, hydrologic response unit; HW, headwater.

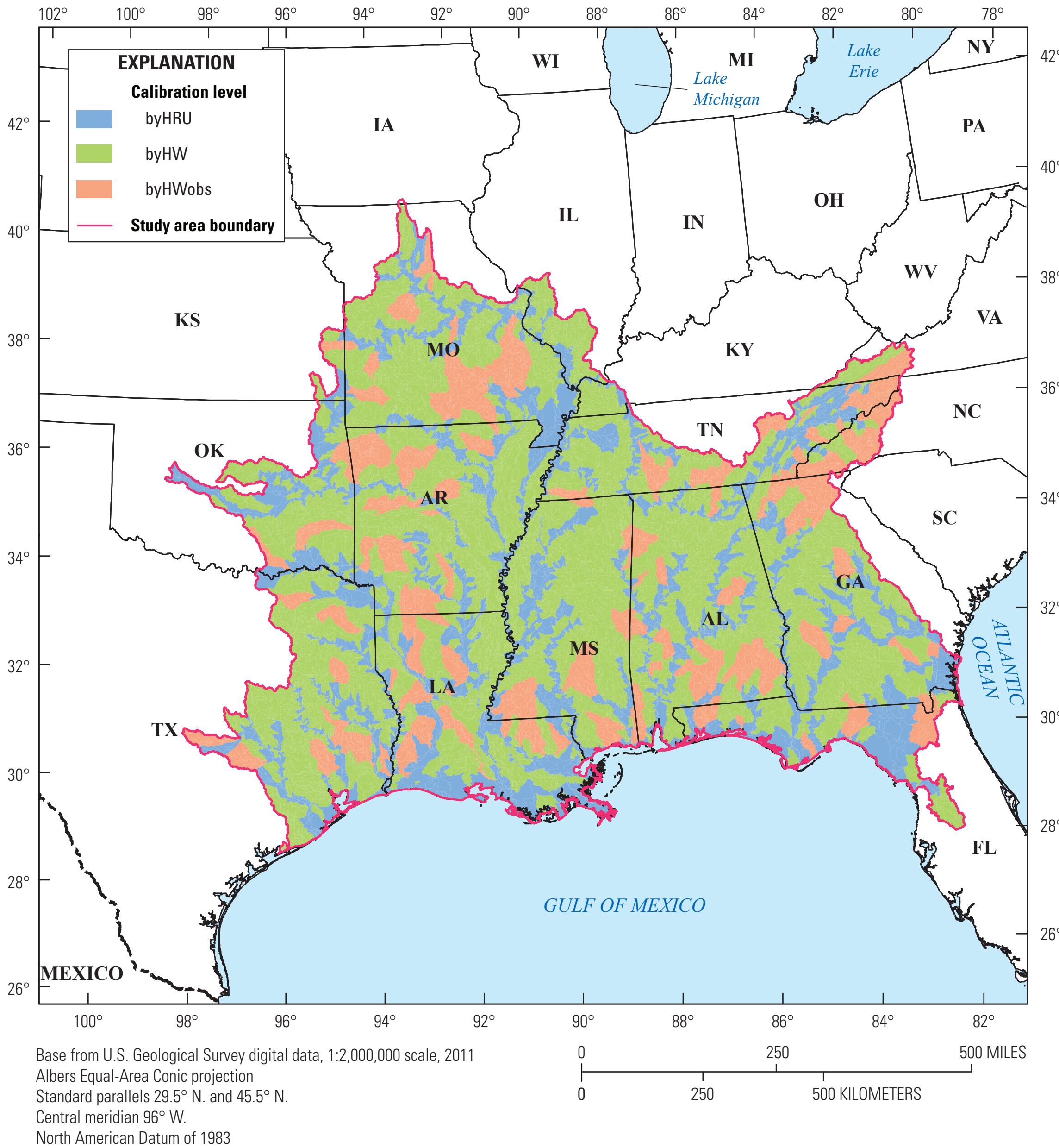

Figure 1–4. Map showing the level of calibration for model hydrologic response units (HRUs). byHRU, by HRU calibration only; byHW, by HRU and by headwater; byHWobs, by HRU and by headwater with measured streamflow.

Calibration by Hydrologic Response Unit

The GCPO-PRMS model contains 20,251 HRUs (fig. 1–1). The hydrologic simulation associated with each HRU was calibrated on a monthly time step to AET, SWE, and runoff monthly calibration datasets derived from existing CONUS-scale modeling applications and remotely sensed datasets that serve as the objective functions for the calibration process. Monthly values of runoff by HRU were derived from the USGS MWBM (Wolock and McCabe, 1999; McCabe and Markstrom, 2007). The CONUS-scale application of the MWBM by Bock and others (2016) used a parameter regionalization procedure that transferred parameter values from gaged to ungaged areas producing simulated runoff for the CONUS on the Geospatial Fabric spatial units with high accuracy in the GCPO LCC study area (see figure 14 of Bock and others, 2016). A plus or minus 10-percent error bound was added to the HRU-runoff values from the MWBM. The MWBM output for the CONUS is available on the USGS Monthly Water Balance Model Futures Portal (Bock and others, 2017). Monthly ranges of AET by HRU were derived using (1) the MWBM (Bock and others, 2017), (2) the MOD16 global evapotranspiration product (National Aeronautics and Space Administration, undated), and (3) the Simplified Surface Energy Balance model (Senay and others, 2013). Based on these three data products, a range of AET was calculated for each HRU on a monthly basis for the period 2000–2010 and used as a target for the PRMS calibration. Monthly values of SWE by HRU were derived from (1) the MWBM (Bock and others, 2017) and (2) the SNODAS dataset (National Operational Hydrologic Remote Sensing Center, 2004). Based on these two data products, a range of SWE was calculated for each HRU on a monthly basis for the period 2003–2010 and used as a target for the PRMS calibration.

Results from the sensitivity analysis performed by Markstrom and others (2016) were used to determine which PRMS parameters should be calibrated in each step of the procedure shown in figure 1–3. Markstrom and others (2016) used the Fourier Amplitude Sensitivity Test (FAST; Cukier and others, 1973; Schaibly and Shuler, 1973; Cukier and others, 1975; Saltelli and others, 2006) to identify dominant hydrologic processes (such as base flow, evapotranspiration, runoff, infiltration, snowmelt, soil moisture, surface runoff, and interflow) based on a CONUS-wide sensitivity analysis of PRMS parameters from the NHM. This same procedure was used with the GCPO-PRMS model to determine the parameters that predominantly influenced runoff, AET, and SWE. The parameters and calibration ranges are shown in table 1–3. The PRMS model parameters were calibrated using either their entire ranges as specified in table 1–3 or were restricted to a range of plus or minus 10 percent of the initial parameter values for each HRU (R or %, respectively, in table 1–3). In general, the percent option was used to preserve the spatial distribution of the parameters as defined by Regan and others (2018).

Table 1–3. Selected parameters, parameter value ranges, and calibration methods for the calibration by hydrologic response unit and calibration by headwater configurations.

[The by-headwater calibration steps optimize model parameters for (1) water budget volumes, (2) high-flow days, (3) low-flow days, (4) timing of all streamflow, and (5) snowpack dynamics parameters. Step 5 of the by-headwater calibration was used only if there was sufficient historical snow accumulation. See Markstrom and others (2015) for parameter descriptions. HRU, hydrologic response unit; R, range used for parameter calibration; %, percent of initial value used for parameter calibration; ET, evapotranspiration]

Parameter name	Parameter description	Minimum allowable parameter value	Maximum allowable parameter value	By-HRU method for parameter range	By-headwater method calibration step
adjmix_rain	Monthly (January to December) factor to adjust rain proportion in a mixed rain/snow event	0.6	1.4	R	5
carea_max	Maximum possible area contributing to surface runoff expressed as a portion of the HRU area	0.2	0.8	R	4
cecn_coef	Monthly (January to December) convection condensation energy coefficient	4.5	5.5	R	3
emis_noppt	Average emissivity of air on days without precipitation	0.757	1	R	5
fastcoef_lin	Linear coefficient in equation to route preferential-flow storage down slope for each HRU	0.01	0.6	R	3
freeh2o_cap	Free-water holding capacity of snowpack expressed as a decimal fraction of the frozen water content of the snowpack (variable pk_ice)	0.01	0.1	R	5
gwflow_coef	Linear coefficient in the equation to compute groundwater discharge for each groundwater reservoir	0	0.1	%	3

Table 1–3. Selected parameters, parameter value ranges, and calibration methods for the calibration by hydrologic response unit and calibration by headwater configurations.—Continued

[The by-headwater calibration steps optimize model parameters for (1) water budget volumes, (2) high-flow days, (3) low-flow days, (4) timing of all streamflow, and (5) snowpack dynamics parameters. Step 5 of the by-headwater calibration was used only if there was sufficient historical snow accumulation. See Markstrom and others (2015) for parameter descriptions. HRU, hydrologic response unit; R, range used for parameter calibration; %, percent of initial value used for parameter calibration; ET, evapotranspiration]

Parameter name	Parameter description	Minimum allowable parameter value	Maximum allowable parameter value	By-HRU method for parameter range	By-headwater method calibration step
K_coef	Travel time of flood wave from one segment to the next downstream segment, called the Muskingum storage coefficient; enter 1.0 for reservoirs, diversions, and segment(s) flowing	0	24	Not used	4
potet_sublim	Fraction of potential ET that is sublimated from snow in the canopy and snowpack	0.4	0.6	R	5
rad_trncf	Transmission coefficient for short-wave radiation through the winter vegetation canopy	0	1	%	5
radmax	Maximum fraction of the potential solar radiation that may reach the ground due to haze, dust, smog, and so forth	0.5	1	R	3
rain_cbh_adj	Monthly (January to December) adjustment factor to measured precipitation on each HRU to account for differences in elevation, and so forth	0.5	1.75	R	1
slowcoef_sq	Non-linear coefficient in equation to route gravity- reservoir storage down slope for each HRU	0	1	R	2
smidx_coef	Coefficient in non-linear contributing area algorithm for each HRU	0.0001	0.8	R	4
snowinfil_max	Maximum snow infiltration per day for each HRU	1	20	R	5
snow_cbh_adj	Monthly (January to December) adjustment factor to measured precipitation on each HRU to account for differences in elevation, and so forth	0.5	1.75	R	5
soil2gw_max	Maximum amount of the capillary reservoir excess that is routed directly to the GWR for each HRU	0	0.5	R	2
soil_moist_max	Maximum available water holding capacity of capillary reservoir from land surface to rooting depth of the major vegetation type of each HRU; affects Hortonian surface runoff, ET, direct recharge, and flow to gravity reservoir	0.001	12	%	3
soil_rechr_max_frac	Maximum storage for soil recharge zone (upper portion of capillary reservoir where losses occur as both evaporation and transpiration); expressed as a fraction of soil_moist_max; affects Hortonian surface runoff and ET	0.1	1	R	1
ssr2gw_exp	Non-linear coefficient in equation used to route water from the gravity reservoirs to the GWR for each HRU	0	3	R	4
ssr2gw_rate	Linear coefficient in equation used to route water from the gravity reservoir to the GWR for each HRU	0.01	0.8	R	2
tmax_allrain_offset	Monthly (January to December) maximum air temperature when precipitation is assumed to be rain; if HRU air temperature is greater than or equal to this value, precipitation is rain; computed as an addition of temperature above tmax_allsnow	0	10	%	5
tmax_allsnow	Monthly (January to December) maximum air temperature when precipitation is assumed to be snow; if HRU air temperature is less than or equal to this value, precipitation is snow	25	40	R	5
tmax_cbh_adj	Adjustment to maximum air temperature for each HRU, estimated based on slope and aspect	-3	3	R	4
tmin_cbh_adj	Adjustment to minimum air temperature for each HRU, estimated based on slope and aspect	-3	3	R	4

The by-HRU calibration procedure converted all the calibration datasets to z scores (distribution with a mean of 0 and a standard deviation of 1) to remove differences in magnitudes between the different datasets. The objective function (OF) for the by-HRU calibration was defined as

$$OF = (OFrun \times 3.0) + (OFaet \times 2.0) + OFswe \quad (1\text{–}1)$$

where

OFrun, *OFaet*, and *OFswe* are the objective functions calculated using the runoff, AET, and SWE datasets, respectively.

Normalized root mean square error (NRMSE) was computed as

$$NRMSE = \sqrt{\frac{\sum_{n=1}^{nstep}\left(SIM_n - MSD_n\right)^2}{\sum_{n=1}^{nstep}\left(MSD_n - MN\right)^2}} \quad (1\text{–}2)$$

where

- n is the time step,
- $nstep$ is the total number of time steps,
- MSD_n are the measured values of the target variable (for example, runoff, AET, SWE),
- SIM_n are the simulated values of the target variable, and
- MN is the mean of all measured values of the target variable for the objective function time period.

The aggregated NRMSE was calculated on a monthly and mean monthly basis where

$$OFrun = NRMSEmonth + (NRMSEmeanmonth \times 3.0), \quad (1\text{–}3)$$

$$OFaet = NRMSEmonth + (NRMSEmeanmonth \times 2.0), \quad (1\text{–}4)$$

and

$$OFswe = NRMSEmonth. \quad (1\text{–}5)$$

The weighting of the objective functions was determined through trial and error. The NRMSE statistic was assessed when the simulated value fell outside of the range of the calibrations dataset. The by-HRU calibration period was for odd years of the period 1981–2010 (such as 1981, 1983, 1985, and so forth).

Calibration by Headwater Basins

To provide additional calibration refinement, headwater basins with drainage areas less than 1,158 square miles (3,000 square kilometers) (an upper limit for an approximate instream travel time of 1 day) were identified in the GCPO-PRMS study area (fig. 1–5). This headwater selection included all headwater subbasins less than the size threshold, not just those with reference-quality streamgages. These headwater subbasins were used in a five-step calibration procedure that included the results from the by-HRU calibration to optimize the match between PRMS-based streamflows at the headwater outlets and the statistically based streamflow simulations developed using ordinary kriging (fig. 1–3). The five-step by-headwater calibration procedure adjusted parameters to optimize the match between PRMS-based and statistically based streamflow by comparing (1) streamflow volume, (2) timing and magnitude of high-flow days, (3) timing and magnitude of low-flow days, (4) timing and magnitude of all days, and (5) streamflow during snowmelt period (when applicable). The FAST-based parameter sensitivity analysis was used to determine the appropriate calibration step for each PRMS parameter (table 1–3).

The by-HRU calibration produced spatially distributed parameter values that could then be calibrated by headwater basin. The by-headwater calibration configuration is shown in table 1-3. The PRMS parameters were calibrated by the mean parameter value across all HRUs within a given headwater subbasin (instead of each individual HRU parameter value). Each execution of the SCE algorithm produced a new mean parameter value. The new mean parameter value was then redistributed to the individual HRUs based on the previous distribution of the HRU parameter values. For each calibration step, parameters identified for that step were calibrated using the parameter range listed in table 1–3. Parameters not associated with a given step are still adjusted but are allowed to vary by only plus or minus 10 percent of their initial value (PCNT in equations 1-7 and 1-8) of their initial mean parameter value (Pmean). These ranges are calculated as follows:

$$BNDi = maxi - mini \quad (1\text{–}6)$$

$$BNDlowi = Pmeani - (PCNT \times BNDi) \quad (1\text{–}7)$$

$$BNDuppi = Pmeani + (PCNT \times BNDi) \quad (1\text{–}8)$$

where

- i is the parameter index,
- BND is the range between the maximum and minimum parameter values,
- max is the maximum value of parameter range from table 1–3,
- min is the minimum value of parameter range from table 1–3,
- $BNDlow$ is the lower value of the allowable calibration range, and
- $BNDupp$ is the upper value of the allowable calibration range.

For each headwater subbasin, the snow dynamics parameters (parameters with a "5" in the last column of table 1–3) were calibrated in step 5 of the by-headwater calibration if there was sufficient snow in the headwater subbasin (fig. 1–5). A threshold of 7 months with non-zero SWE during the period 1980–2010 was used to classify HRUs as sufficient for inclusion of SWE in the model calibration. If there was not sufficient SWE in a headwater, four rounds of the five-step calibration procedure were executed for each headwater subbasin, with the results from the previous step determining the initial parameter values for the current step (fig. 1–3).

The objective function for each calibration step (OFstep) was calculated using equation 1–9 and is further described in table 1–4. Objective functions are computed as weighted sums of NRMSE calculated on monthly and mean monthly time steps (OF1–OF4) or daily time steps (OF5) with subsets of high- (OF6) and low-flow days (OF7) as listed in table 1–4. The NRMSE was calculated two ways: computing error if (1) the simulated value fell inside or outside of the target range or (2) using the median value of the range of values in the calibration dataset for each time step. For the first option, if the simulated value for a time step was between the upper and lower bounds of the calibration dataset, the difference between simulated and observed was assumed to be zero. For the second option, a single value was computed for each time step in the calibration dataset that was then compared to the simulated values.

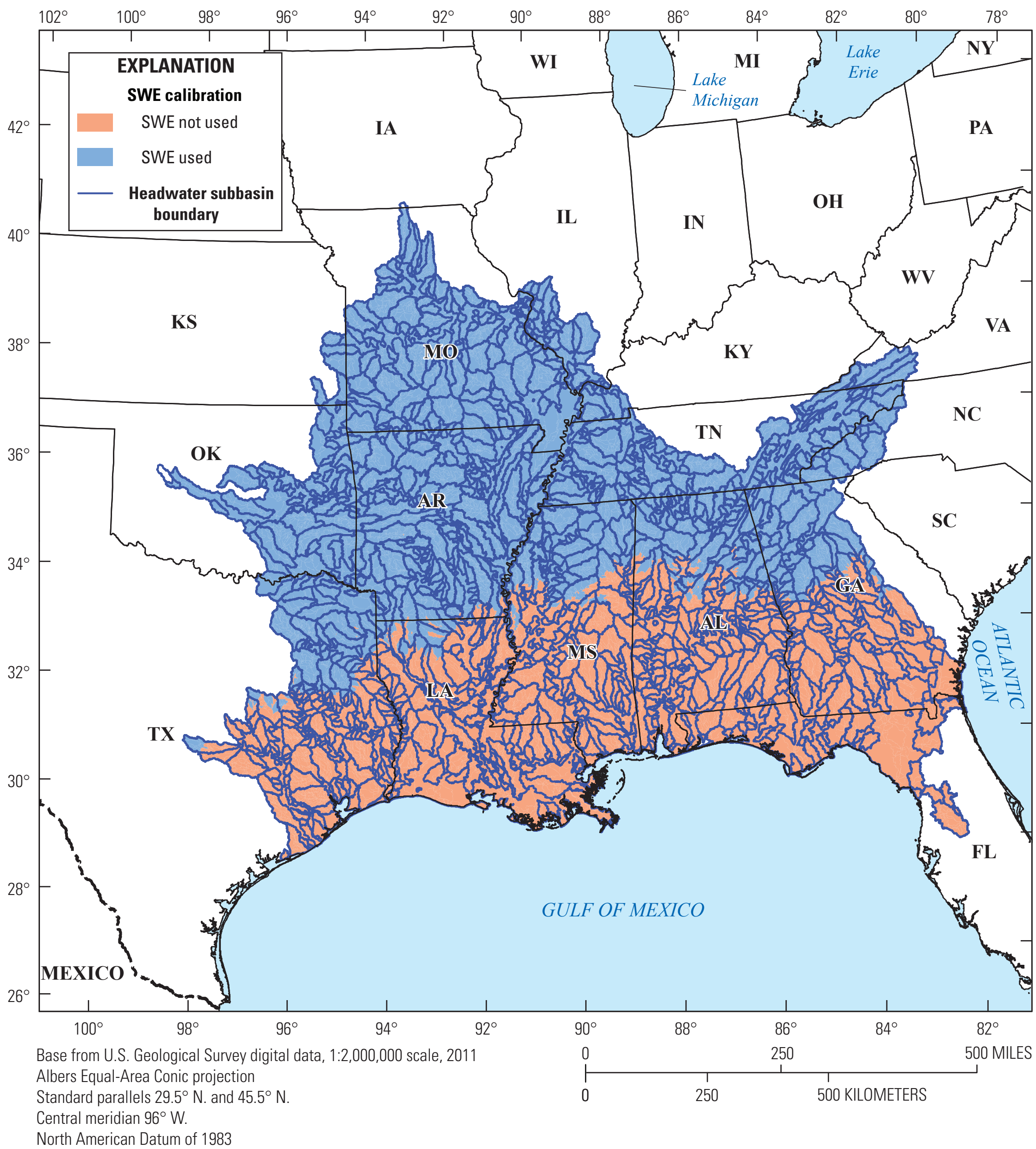

Figure 1–5. Map showing headwater subbasins used for model calibration and classification of hydrologic response units with and without sufficient snow water equivalent (SWE) to include the fifth step of the by-headwater calibration scheme (table 1–3).

$$OFstep = OF1 \times w + OF2 \times w + OF3 \times w + OF4 \times w + OF5 \times w + OF6 \times w + OF7 \times w \quad (1\text{–}9)$$

where

- $OFstep$ is the aggregated objective function value,
- $OF1$ is the objective function for monthly streamflow range of the ordinary kriging-based streamflow time series,
- $OF2$ is the objective function for mean monthly streamflow range of the ordinary kriging-based streamflow time series,
- $OF3$ is the objective function for monthly streamflow median of the ordinary kriging-based streamflow time series,
- $OF4$ is the objective function for mean monthly streamflow median of the ordinary kriging-based streamflow time series,
- $OF5$ is the objective function for daily streamflow using the range of the ordinary kriging-based streamflow time series,
- $OF6$ is the objective function for daily streamflow high-flow days using the median of the ordinary kriging-based streamflow time series,
- $OF7$ is the objective function for daily streamflow low-flow days using the median of the ordinary kriging-based streamflow time series, and
- w is the weight for each objective function.

The weighting of the by-headwater objective functions was determined through trial and error. The by-headwater calibration period was for odd years of the period 1981–2010 (such as 1981, 1983, 1985, and so forth).

Calibration by Streamgage

No measured streamflow was used in the first two steps in the calibration procedure (by-HRU and by-headwater; fig. 1–3). The NHM-PRMS includes 297 GAGES-II reference-quality streamflow gages in the GCPO-PRMS study area; however, only 169 of the 297 streamgages had sufficient streamflow data for the simulation period of 1951–2010. The by-streamgage calibration started with the final by-headwater calibration parameter values for those headwaters that contained measured streamflow. A one-step, one-round procedure was used to adjust the final parameter values from the by-headwater calibration on the basis of available measured streamflow in each headwater subbasin (fig. 1–3). All parameters in table 1–3 (excluding snow parameters when not applicable, see fig. 1–5) were calibrated using ranges calculated from equations 1–6, 1–7, and 1–8, with a PCNT of 0.20. A list of the streamgages used for calibration is provided in LaFontaine and others (2019).

The objective function for the by-streamgage calibration (OFgage) was calculated as follows:

$$OFgage = (NSE \times 2.0) + NSElog + CVdiff \quad (1\text{–}10)$$

where

- NSE is the Nash-Sutcliffe model efficiency index,
- $NSElog$ is the Nash-Sutcliffe model efficiency index with logarithmic values, and
- $CVdiff$ is the summed difference between observed and simulated annual values of the coefficient of variation.

The by-streamgage calibration period was for odd years of the period 1981–2010 (such as 1981, 1983, 1985, and so forth).

Table 1–4. Objective function descriptions and weights for each calibration step in the calibration by headwater procedure.

[NRMSE, normalized root mean square error]

Objective function (OF)			Objective function weights (w) by calibration step				
OF	Description		1 (Volume)	2 (High)	3 (Low)	4 (All)	5 (Snow)
	Time step	NRMSE used					
OF1	monthly	range	3	1	1	1	1
OF2	mean monthly	range	3	1	1	1	1
OF3	monthly	median	3	1	1	1	1
OF4	mean monthly	median	3	1	1	1	1
OF5	daily	range	1	1	1	3	1
OF6	daily, high flows	median	1	3	3	3	1
OF7	daily, low flows	median	1	1	1	3	1

PRMS Model Evaluation

A total of 1,235 streamgages were available in the GCPO-PRMS model application based on those included in the Geospatial Fabric for National Hydrologic Modeling (Viger and Bock, 2014). Of those 1,235 streamgages, 1,065 streamgages had available streamflow during the simulation period 1951–2010 and had a modeled drainage area within 15 percent of the USGS published drainage area. A subset of 169 streamgages was used to calibrate the GCPO-PRMS; these streamgages had available data for the study period and were classified as reference-quality streamgages in the GAGES-II dataset (Falcone, 2011). The hydrologic simulation results were evaluated using three statistics based on the analysis by Moriasi and others (2007): *NSE* (Nash and Sutcliffe, 1970; eq. 1–11), percent bias (P_{bias}; eq. 1–12), and the ratio of the root mean square error to the standard deviation of the measured streamflow, previously described as NRMSE (eq. 1–2). The NSE metric was calculated using the following equation:

$$NSE = 1.0 - \left[\frac{\sum_{n=1}^{nstep} \left(SIM_n - MSD_n \right)^2}{\sum_{n=1}^{nstep} \left(MSD_n - MN \right)^2} \right] \qquad (1–11)$$

An *NSE* value of 1.0 indicated a perfect fit between the simulated and measured values, an *NSE* value of zero indicated the simulated values represented the hydrologic response as well as the mean of the measured values, and a negative *NSE* value indicated that the mean of the measured values provided a better fit than the simulated values.

The P_{bias} metric was calculated as follows:

$$P_{bias} = \frac{\left(SIM_{avg} - MSD_{avg} \right)}{MSD_{avg}} \times 100 \qquad (1–12)$$

where

SIMavg is the mean of all simulated values for the evaluation period, and

MSDavg is the mean of all observed values for the evaluation period.

A negative or positive P_{bias} value indicated an underestimation or overestimation of streamflow, respectively.

Spatial distributions of model performance using the NSE metric are shown for the reference-quality streamgage locations (169) and non-reference streamgage locations (896) in figure 1–6. In general, the GCPO-PRMS model performs better in the eastern part of the study area than in the western part. Spatial distributions of model performance using the percent bias metric are shown for the reference-quality streamgage locations (169) and non-reference streamgage locations (896) in figure 1–7. Streamflow simulations have a generally negative bias (simulated less than measured) for streamflow volume. Cumulative distributions of streamgage NSE for both the reference-quality streamgage locations (169) and non-reference streamgage locations (896) are shown in figure 1–8. Approximately 75 percent of the reference-quality streamgages and 35 percent of the non-reference streamgages have an NSE greater than the acceptable criteria of 0.5. Because the non-reference streamgages tend to be affected by water use, flow regulation, or substantial urbanization, these streamgages are expected to have poorer performance compared to the reference-quality streamgages.

The performance metrics of NSE, NRMSE, and P_{bias} for each calibration and evaluation streamgage are summarized in table 1–5. An NSE value of 0.5 or greater was defined as the passing performance threshold. The passing performance thresholds for the NRMSE and P_{bias} metrics were less than 0.7 and between plus or minus 25 percent, respectively. Simulations at each of the 1,065 streamgage locations were evaluated on the basis of how many performance metrics were within the acceptable criteria. Streamgage locations that passed all three performance metrics were rated “good,” streamgage locations that passed only two performance metrics were rated “fair,” and streamgage locations that passed less than two performance metrics were rated “poor.” A summary of simulation performance for all streamgage locations and reference-quality streamgage locations is shown in table 1–5. The evaluation results show that 130 of the 169 reference-quality streamgage locations (75.7 percent) were rated at least “fair” while 324 of the 896 non-reference streamgage locations (35.5 percent) were rated at least “fair.” Figure 1–9 shows the spatial distribution of the simulation performance results given in table 1–5. The distribution of simulation performance at the reference-quality streamgage locations is relatively even across the study area. The distribution of simulation performance at the non-reference-quality streamgage locations is weighted toward the eastern part of the study area for “good” ratings, with the western part of the study area having more “fair” and “poor” ratings than “good.” These results are in line with past hydrologic studies that have shown that hydrologic models tend to perform better in the wetter eastern United States than the drier part of the country (Bock and others, 2015).

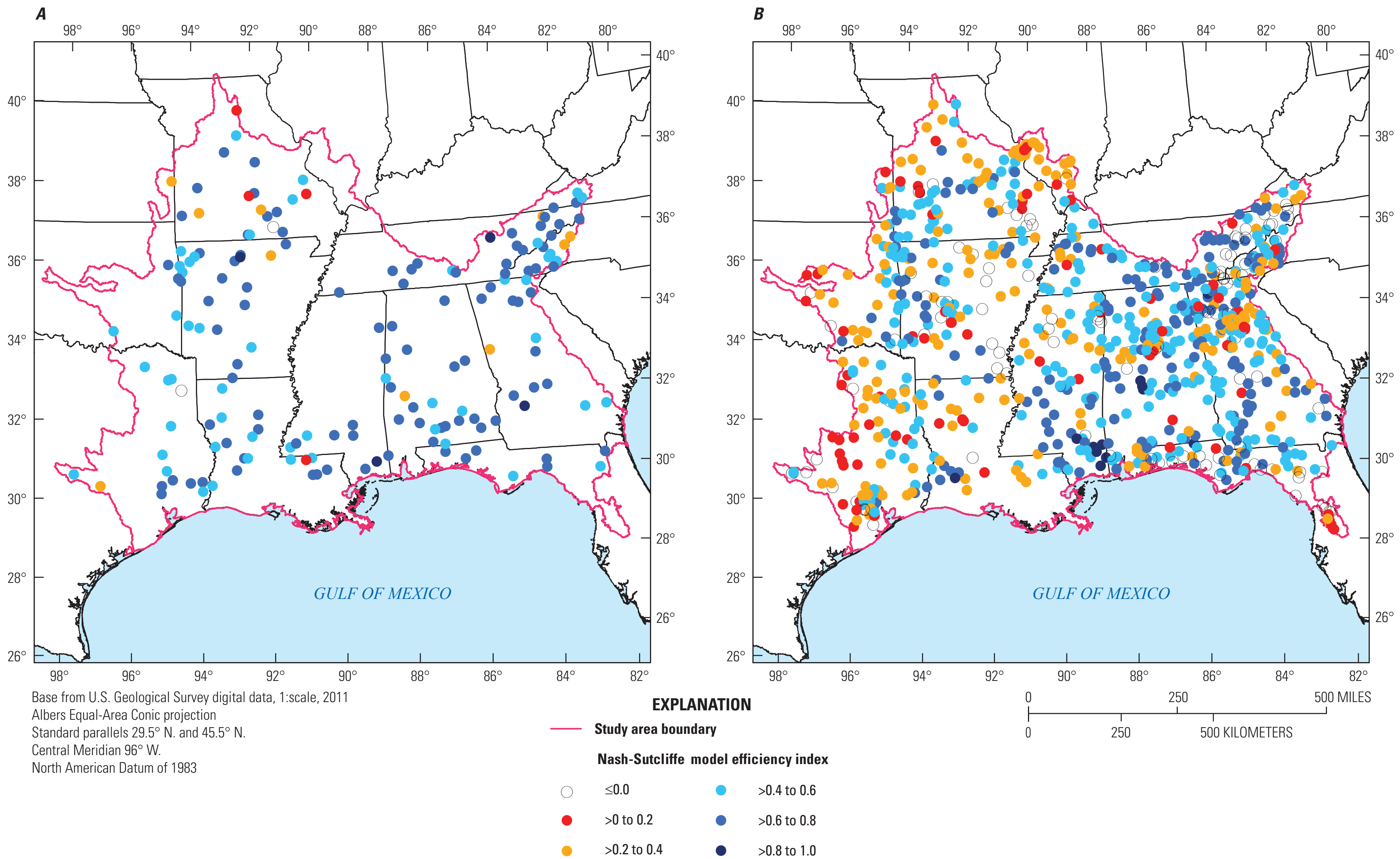

Figure 1–6. Maps showing the Nash-Sutcliffe model efficiency index (Nash and Sutcliffe, 1970) for the (*A*) 169 reference-quality streamgages and (*B*) 896 non-reference streamgages within the study area that have available data for the study period and a modeled drainage area within 15 percent of the published U.S. Geological Survey drainage area. Period of evaluation was 1951–2009.

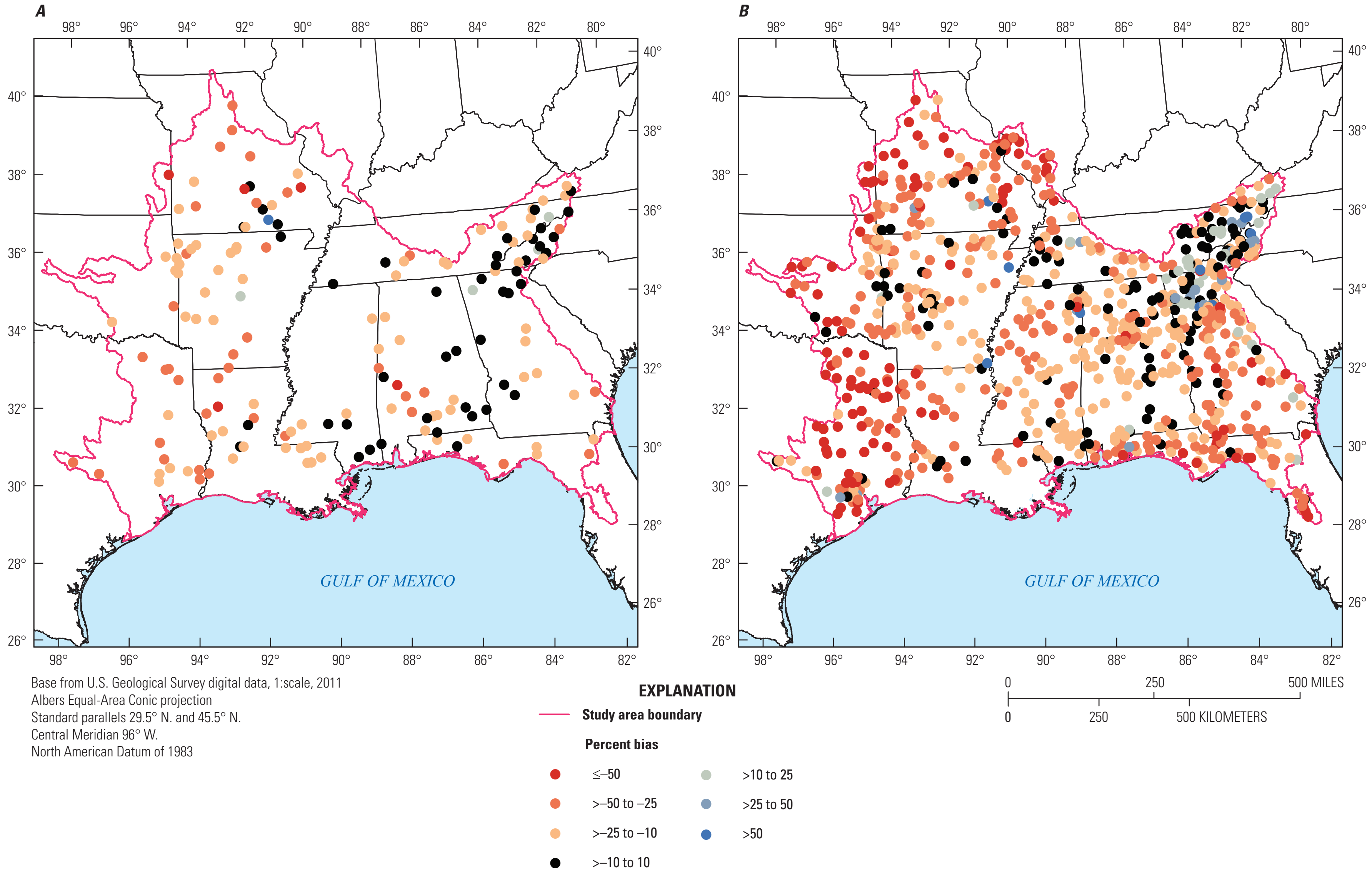

Figure 1–7. Maps showing the percent bias in streamflow volume for the (*A*) 169 reference-quality streamgages and (*B*) 896 non-reference streamgages within the study area that have available data for the study period and a modeled drainage area within 15 percent of the published U.S. Geological Survey drainage area. Period of evaluation was 1951–2009.

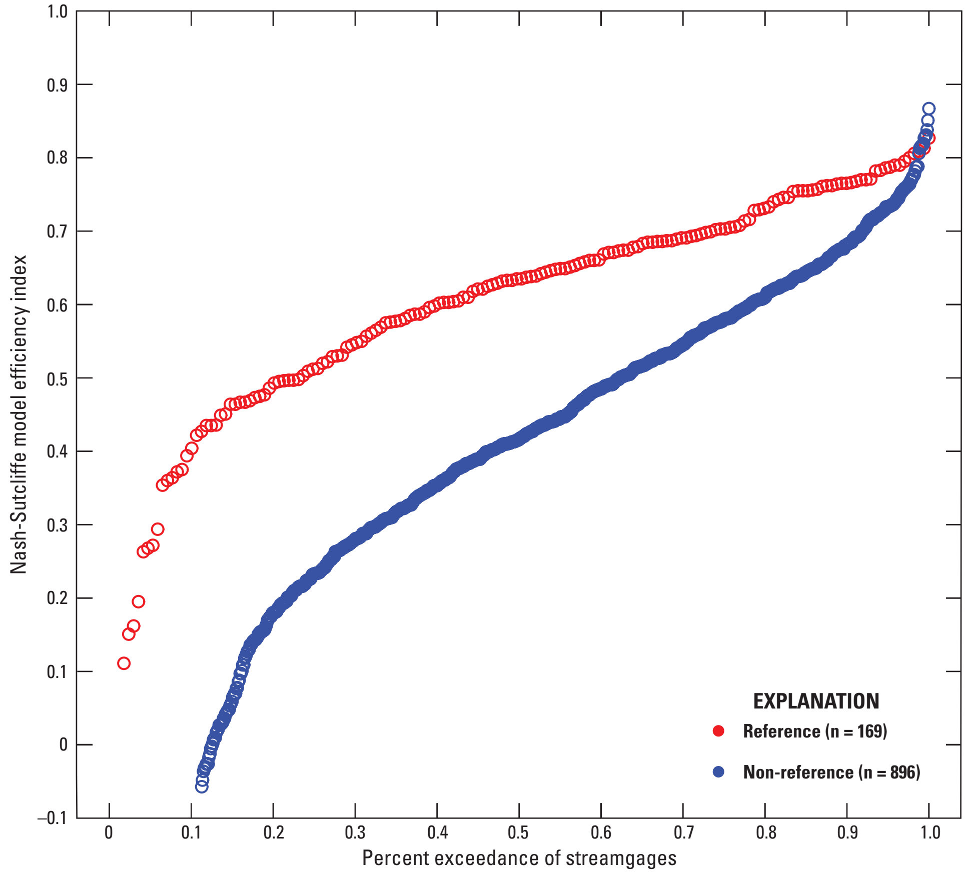

Figure 1–8. Graph showing the cumulative distribution of the Nash-Sutcliffe model efficiency index (Nash and Sutcliffe, 1970) for the 169 reference-quality streamgages and 896 non-reference streamgages with available data for the study period and a modeled drainage area within 15 percent of the published U.S. Geological Survey drainage area. Period of evaluation was 1951–2009.

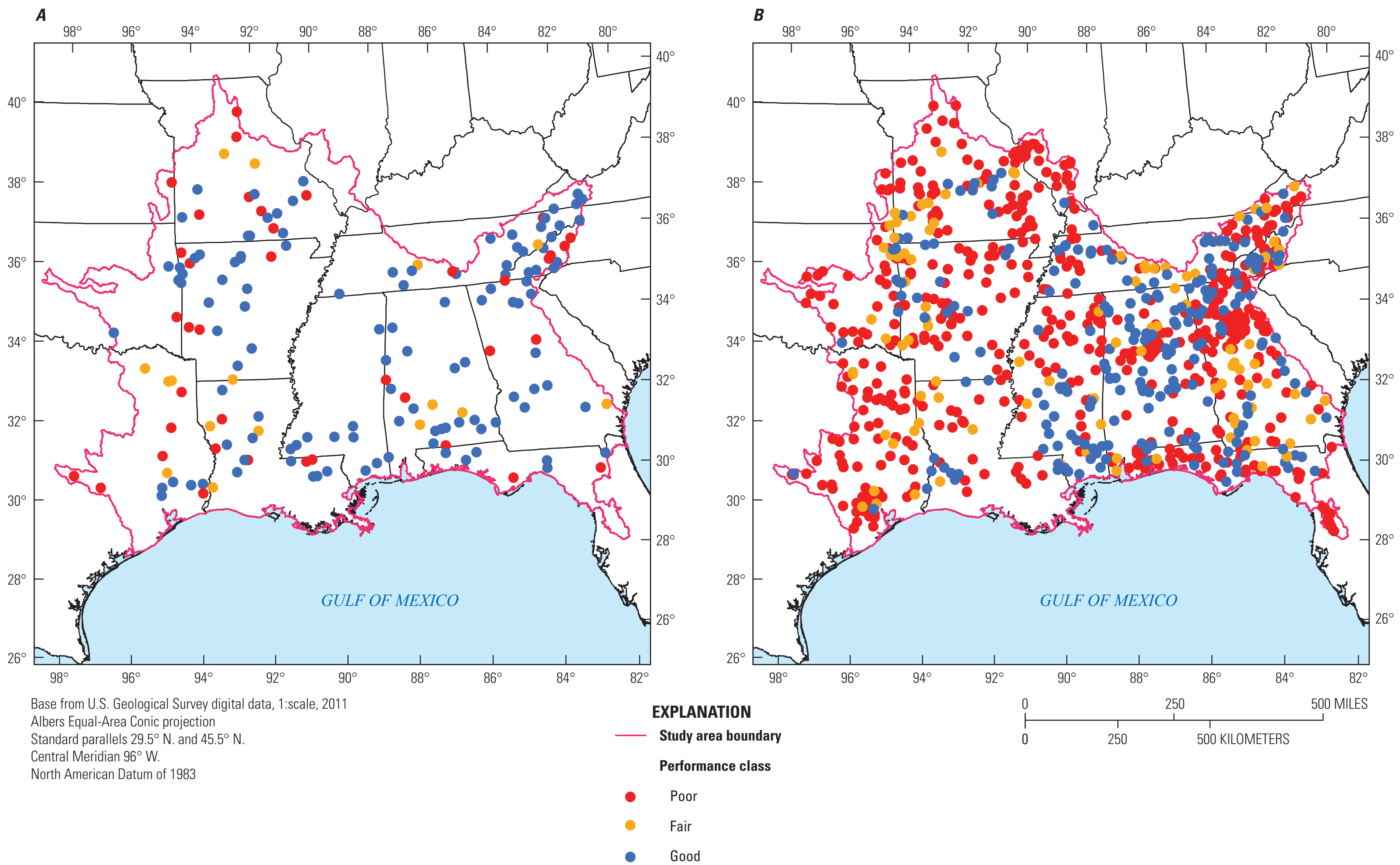

Figure 1–9. Maps showing the evaluation results for the (*A*) 169 reference-quality streamgages and (*B*) 896 non-reference streamgages with available data for the study period and a modeled drainage area within 15 percent of the U.S. Geological Survey drainage area. Period of evaluation was 1951–2009. This map shows the spatial distribution of the results presented in table 1–5.

Table 1–5. Summary of daily time step performance statistics for the Precipitation-Runoff Modeling System hydrologic simulations.

[Overall performance is based on how many of the three metrics (NSE, P_{bias}, and NRMSE) were considered satisfactory, with all three metrics considered "good," two metrics considered "fair," and one or no metrics considered "poor." NSE, Nash-Sutcliffe Index; P_{bias}, percent bias; NRMSE, normalized root mean square error]

Overall performance	All	Reference	Non-reference
Total	1,065	169	896
Good	335	114	221
Fair	119	16	103
Poor	611	39	572
NSE			
Total	1,065	169	896
Satisfactory	462	130	332
Unsatisfactory	603	39	564
P_{bias}			
Total	1,065	169	896
Satisfactory	586	133	453
Unsatisfactory	479	36	443
NRMSE			
Total	1,065	169	896
Satisfactory	444	128	316
Unsatisfactory	621	41	580

References Cited

Berhail, S., Ouerdachi, L., and Boutaghane, H., 2012, The use of the recession index as indicator for components of flow: Energy Procedia, v. 18, p. 741–750, accessed November 3, 2017, at https://doi.org/10.1016/j.egypro.2012.05.090.

Beven, K.J., and Kirby, M.J., 1979, A physically based, variable contributing area model of basin hydrology: Hydrological Sciences Bulletin, v. 24, no. 1, p. 43–69, accessed October 27, 2017, at https://doi.org/10.1080/02626667909491834.

Blodgett, D.L., Booth, N.L., Kunicki, T.C., Walker, J.I., and Viger, R.J., 2011, Description and testing of the Geo Data Portal—A data integration framework and web processing services for environmental science collaboration: U.S. Geological Survey Open-File Report 2011–1157, 9 p., accessed March 2, 2017, at https://doi.org/10.3133/ofr20111157.

Bock, A.R., Hay, L.E., Markstrom, S.L., Emmerich, C., and Talbert, M., 2017, The U.S. Geological Survey Monthly Water Balance Model Futures Portal: U.S. Geological Survey Open-File Report 2016–1212, 21 p., accessed November 3, 2017, at https://doi.org/10.3133/ofr20161212.

Bock, A.R., Hay, L.E., McCabe, G.J., Markstrom, S.L., and Atkinson, R.D., 2016, Parameter regionalization of a monthly water balance model for the conterminous United States: Hydrology and Earth System Sciences, v. 20, no. 7, p. 2861–2876, accessed June 4, 2018, at https://doi.org/10.5194/hess-20-2861-2016.

Brandes, D., Hoffmann, J.G., and Mangarillo, J.T., 2005, Base flow recession rates, low flows, and hydrologic features of small watersheds in Pennsylvania, USA: Journal of the American Water Resources Association, v. 41, no. 5, p. 1177–1186, accessed November 3, 2017, at https://doi.org/10.1111/j.1752-1688.2005.tb03792.x.

Campo, L., Caparrini, F., and Castelli, F., 2006, Use of multi-platform, multi-temporal remote-sensing data for calibration of a distributed hydrological model—An application in the Arno basin, Italy: Hydrological Processes, v. 20, no. 13, p. 2693–2712. [Also available at https://doi.org/10.1002/hyp.6061.]

Cao, W., Sun, G., McNulty, S.G., Chen, J., Noormets, A., Skaggs, R.W., and Amatya, D.M., 2006, Evapotranspiration of a mid-rotation loblolly pine plantation and a recently harvested stands on the coastal plain of North Carolina, U.S.A., *in* Williams, T., ed., Hydrology and management of forested wetlands: American Society of Agricultural and Biological Engineers, Proceedings of the International Conference, St. Joseph, Mich., p. 27–33, accessed January 30, 2017, at https://www.treesearch.fs.fed.us/pubs/22421.

Cukier, R.I., Fortuin, C.M., and Shuler, K.E., 1973, Study of the sensitivity of coupled reaction systems to uncertainties in rate coefficients, I. Theory: The Journal of Chemical Physics, v. 59, no. 8, p. 3873–3878, accessed October 27, 2017, at https://doi.org/10.1063/1.1680571.

Cukier, R.I., Schaibly, J.H., and Shuler, K.E., 1975, Study of the sensitivity of coupled reaction systems to uncertainties in rate coefficients, III. Analysis of the approximations: The Journal of Chemical Physics, v. 63, no. 3, p. 1140–1149, accessed October 27, 2017, at https://doi.org/10.1063/1.431440.

Driscoll, J.M., Hay, L.E., and Bock, A.R., 2017b, Spatiotemporal variability of snow depletion curves derived from SNODAS for the conterminous United States, 2004–2013: Journal of the American Water Resources Association, v. 53, no. 3, p.655–666, accessed September 22, 2017, at https://doi.org/10.1111/1752-1688.12520.

Driscoll, J.M., Markstrom, S.L., Regan, R.S., Hay, L.E., and Viger, R.J., 2017b, National Hydrologic Model Parameter Database—2017-05-08 download: U.S. Geological Survey database, accessed September 24, 2017, at https://doi.org/10.5066/F7NS0SCW.

Duan, Q.Y., Gupta, V.K., and Sorooshian, S., 1993, Shuffled complex evolution approach for effective and efficient global minimization: Journal of Optimization Theory and Applications, v. 76, no. 3, p. 501–521, accessed November 3, 2017, at https://link.springer.com/article/10.1007/BF00939380.

Duan, Q., Sorooshian, S., and Gupta, V., 1992, Effective and efficient global optimization for conceptual rainfall-runoff models: Water Resources Research, v. 28, no. 4, p. 1015–1031, accessed September 2, 2009, at https://doi.org/10.1029/91WR02985.

Duan, Q., Sorooshian, S., and Gupta, V.K., 1994, Optimal use of the SCE-UA global optimization method for calibrating watershed models: Journal of Hydrology, v. 158, nos. 3–4, p. 265–284, accessed September 2, 2009, at https://doi.org/10.1016/0022-1694(94)90057-4.

Falcone, J.A., 2011, GAGES II (Geospatial Attributes of Gages for Evaluating Streamflow) summary report: U.S. Geological Survey publication, accessed October 27, 2017, at https://water.usgs.gov/GIS/dsdl/basinchar_and_report_sept_2011.zip.

Farmer, W.H., 2016, Ordinary kriging as a tool to estimate historical daily streamflow records: Hydrology and Earth System Sciences, v. 20, no. 7, p. 2721–2735, accessed September 26, 2017, at https://doi.org/10.5194/hess-20-2721-2016.

Farnsworth, R.K., and Thompson, E.S., 1982, Mean monthly, seasonal, and annual pan evaporation for the United States: National Oceanic and Atmospheric Administration Technical Report NWS 34, 82 p., accessed November 3, 2017, at http://www.nws.noaa.gov/oh/hdsc/Technical_reports/TR34.pdf.

Farnsworth, R.K., Thompson, E.S., and Peck, E.L., 1982, Evaporation atlas for the contiguous 48 States: National Oceanic and Atmospheric Administration, NOAA Technical Report NWS 33, 26 p., 4 maps, accessed November 3, 2017, at http://www.nws.noaa.gov/oh/hdsc/Technical_reports/TR33.pdf.

Fernandez, W., Vogel, R.M., and Sankarasubramanian, A., 2000, Regional calibration of a watershed model: Hydrological Sciences Journal, v. 45, no. 5, p. 689–707, accessed October 27, 2017, at https://doi.org/10.1080/02626660009492371.

Franz, K.J., and Karsten, L.R., 2013, Calibration of a distributed snow model using MODIS snow covered area data: Journal of Hydrology, v. 494, p. 160–175, accessed January 27, 2017, at https://doi.org/10.1016/j.jhydrol.2013.04.026.

Gleeson, T., Smith, L., Moosdorf, N., Hartmann, J., Durr, H.H., Manning, A.H., van Beek, L.P.H., and Jellinek, A.M., 2011, Mapping permeability over the surface of the Earth: Geophysical Research Letters, v. 38, no. 2, 6 p., accessed October 27, 2017, at https://doi.org/10.1029/2010GL045565.

Hay, L.E., Leavesley, G.H., and Clark, M.P., 2005, Use of remotely sensed snow covered area in watershed model calibration for the Sprague River, Oregon: Proceedings of the 2005 American Geophysical Union Fall Meeting, December 5–9, 2005, San Francisco, Calif., 8 p., accessed October 27, 2017, at https://acwi.gov/hydrology/mtsconfwkshops/conf_proceedings/3rdFIHMC/7D_Hay.pdf.

Hay, L.E., Leavesley, G.H., Clark, M.P., Markstrom, S.L., Viger, R.J., and Umemoto, M., 2006, Step wise multiple objective calibration of a hydrologic model for a snowmelt dominated basin: Journal of the American Water Resources Association, v. 42, no. 4, p. 877–890. [Also available at https://doi.org/10.1111/j.1752-1688.2006.tb04501.x.]

Hay, L.E., and Umemoto, M., 2007, Multiple-objective stepwise calibration using Luca: U.S. Geological Survey Open-File Report 2006–1323, 25 p. [Also available at https://doi.org/10.3133/ofr20061323.]

Homer, C., Dewitz, J., Fry, J., Coan, M.J., Hossain, N., Larson, C., Herold, N., McKerrow, A., VanDriel, J.N., and Wickham, J.D., 2007, Completion of the 2001 National Land Cover Database for the conterminous United States: Photogrammetric Engineering & Remote Sensing, v. 73, no. 4, p. 337–341, accessed September 15, 2016, at https://www.researchgate.net/publication/237239863.

Immerzeel, W.W., and Droogers, P., 2008, Calibration of a distributed hydrological model based on satellite evapotranspiration: Journal of Hydrology, v. 349, nos. 3–4, p. 411–424, accessed January 30, 2017, at https://doi.org/10.1016/j.jhydrol.2007.11.017.

Isenstein, E.M., Wi, S., and Yang, Y.C.E., 2015, Calibration of a distributed hydrologic model using streamflow and remote sensing snow data: American Society of Civil Engineers, World Environmental and Water Resources Congress 2015, Austin, Tex., May 17–21, 2015, p. 973–982, accessed October 27, 2017, at https://doi.org/10.1061/9780784479162.093.

Koren, V., Moreda, F., and Smith, M., 2008, Use of soil moisture observations to improve parameter consistency in watershed calibration: Physics and Chemistry of the Earth, v. 33, nos. 17–18, p. 1068–1080, accessed January 27, 2017, at https://doi.org/10.1016/j.pce.2008.01.003.

LaFontaine, J.H., Hay, L.E., Viger, R.J., Regan, R.S., and Markstrom, S.L., 2015, Effects of climate and land cover on hydrology in the Southeastern U.S.—Potential impacts on watershed planning: Journal of the American Water Resources Association, v. 51, no. 5, p. 1235–1261, accessed September 27, 2016, at https://doi.org/10.1111/1752-1688.12304.

LaFontaine, J.H., Hay, L.E., and Farmer, W.H., 2019, Model Input and Output for Hydrologic Simulations of the Southeastern United States for Historical and Future Conditions: U.S. Geological Survey data release, accessed April 18, 2019, at https://doi.org/10.5066/F74X56PH.

Leavesley, G.H., Lichty, R.W., Troutman, B.M., and Saindon, L.G., 1983, Precipitation-Runoff Modeling System—User's manual: U.S. Geological Survey Water-Resources Investigations Report 83–4238, 207 p., accessed April 26, 2017, at https://pubs.usgs.gov/wri/1983/4238/report.pdf.

Markstrom, S.L., Hay, L.E., and Clark, M.P., 2016, Towards simplification of hydrologic modeling: identification of dominant processes: Hydrology and Earth System Sciences, v. 20, p. 4655–4671, accessed February 9, 2017, at https://doi.org/10.5194/hess-20-4655-2016.

Markstrom, S.L., Regan, R.S., Hay, L.E., Viger, R.J., Webb, R.M.T., Payn, R.A., and LaFontaine, J.H., 2015, PRMS-IV, the Precipitation-Runoff Modeling System, version 4: U.S. Geological Survey Techniques and Methods, book 6, chap. B7, 158 p., accessed February 13, 2017, at https://doi.org/10.3133/tm6B7.

Maurer, E.P., Wood, A.W., Adam, J.C., Lettenmaier, D.P., and Nijssen, B., 2002, A long-term hydrologically based dataset of land surface fluxes and states for the conterminous United States: Journal of Climate, v. 15, no. 22, p. 3237–3251, accessed September 24, 2017, at https://doi.org/10.1175/1520-0442(2002)015%3C3237:ALTHBD%3E2.0.CO;2.

McCabe, G.J., and Markstrom, S.L., 2007, A monthly water-balance model driven by a graphical user interface: U.S. Geological Survey Open-File Report 2007–1088, 6 p., accessed October 27, 2017, at https://pubs.usgs.gov/of/2007/1088/.

Moriasi, D.N., Arnold, J.G., Van Liew, M.W., Bingner, R.L., Harmel, R.D., and Veith, T.L., 2007, Model evaluation guidelines for systematic quantification of accuracy in watershed simulations: Transactions of the American Society of Agricultural and Biological Engineers, v. 50, no. 3, p. 885–900, accessed January 5, 2017, at http://ssl.tamu.edu/media/1312/MoriasiModelEval.pdf.

Nash, J.E., and Sutcliffe, J.V., 1970, River flow forecasting through conceptual models part I—A discussion of principles: Journal of Hydrology, v. 10, no. 3, p. 282–290, accessed September 2, 2009, at https://doi.org/10.1016/0022-1694(70)90255-6.

National Aeronautics and Space Administration, undated, MODIS evapotranspiration: Moderate Resolution Imaging Spectroradiometer [MODIS] web page, accessed May 18, 2015, at https://modis.gsfc.nasa.gov/data/dataprod/mod16.php.

National Operational Hydrologic Remote Sensing Center, 2004, Snow Data Assimilation System (SNODAS) Data Products at NSIDC, Version 1: National Snow & Ice Data Center web page, accessed October 27, 2017 at https://doi.org/10.7265/N5TB14TC.

National Renewable Energy Laboratory, undated, National Solar Radiation Data Base: National Renewable Energy Laboratory website, accessed December 2016, at https://rredc.nrel.gov/solar/old_data/nsrdb/.

Read, J.S., Walker, J.I., Appling, A.P., Blodgett, D.L., Read, E.K., and Winslow, L.A., 2015, Geoknife—Reproducible web-processing of large gridded datasets: Ecography, v. 39, no. 4, p. 354–360, accessed October 27, 2017, at https://doi.org/10.1111/ecog.01880.

Refsgaard, J.C., 1997, Parameterization, calibration and validation of distributed hydrological models: Journal of Hydrology, v. 198, nos. 1–4, p. 69–97, accessed February 9, 2017, at https://doi.org/10.1016/S0022-1694(96)03329-X.

Regan, R.S., and LaFontaine, J.H., 2017, Documentation of the dynamic parameter, water-use, stream and lake flow routing, and two summary output modules and updates to surface-depression storage simulation and initial conditions specification options with the Precipitation-Runoff Modeling System (PRMS): U.S. Geological Survey Techniques and Methods, book 6, chap. B8, 60 p., accessed October 27, 2017, at https://doi.org/10.3133/tm6B8.

Regan, R.S., Markstrom, S.L., Hay, L.E., Viger, R.J., Norton, P.A., Driscoll, J.M., and LaFontaine, J.H., 2018, Description of the National Hydrologic Model for use with the Precipitation-Runoff Modeling System (PRMS): U.S. Geological Survey Techniques and Methods, book 6, chap B9, 38 p., accessed on May 16, 2018, at https://doi.org/10.3133/tm6B9.

Rientjes, T.H.M., Muthuwatta, L.P., Bos, M.G., Booij, M.J., and Bhatti, H.A., 2013, Multi-variable calibration of a semi-distributed hydrological model using streamflow data and satellite-based evapotranspiration: Journal of Hydrology, v. 505, p. 276–290, accessed January 30, 2017, at https://doi.org/10.1016/j.jhydrol.2013.10.006.

Rutledge, A.T., and Mesko, T.O., 1996, Estimated hydrologic characteristics of shallow aquifer systems in the Valley and Ridge, the Blue Ridge, and the Piedmont Physiographic Provinces based on analysis of streamflow recession and base flow: U.S. Geological Survey Professional Paper 1422–B, 68 p., accessed November 3, 2017, at https://doi.org/10.3133/pp1422b.

Saha, S., Moorthi, S., Pan, H.-L., Wu, X., Wang, J., Nadiga, S., Tripp, P., Kistler, R., Woollen, J., Behringer, D., Liu, H., Stokes, D., Grumbine, R., Gayno, G., Wang, J., Hou, Y.-T., Chuang, H.-Y., Juang, H.-M.H., Sela, J., Iredell, M., Treadon, R., Kleist, D., Van Delst, P., Keyser, D., Derber, J., Ek, M., Meng, J., Wei, H., Yang, R., Lord, S., Van Den Dool, H., Kumar, A., Wang, W., Long, C., Chelliah, M., Xue, Y., Huang, B., Schemm, J.-K., Ebisuzaki, W., Lin, R., Xie, P., Chen, M., Zhou, S., Higgins, W., Zou, C.-Z., Liu, Q., Chen, Y., Han, Y., Cucurull, L., Reynolds, R.W., Rutledge, G., and Goldberg, M., 2010, The NCEP climate forecast system reanalysis: Bulletin of the American Meteorological Society, v. 91, p. 1015–1057, accessed November 3, 2017, at https://doi.org/10.1175/2010BAMS3001.1.

Saltelli A., Ratto, M., Tarantola, S., Campolongo, F., and European Commission, Joint Research Centre of Ispra, 2006, Sensitivity analysis practices—Strategies for model-based inference: Reliability Engineering & System Safety, v. 91, nos. 10–11, p. 1109–1125. [Also available at https://doi.org/10.1016/j.ress.2005.11.014.]

Santanello, J.A., Peters-Lidard, C.D., Garcia, M.E., Mocko, D.M., Tischler, M.A., Moran, M.S., and Thoma, D.P., 2007, Using remotely-sensed estimates of soil moisture to infer soil texture and hydraulic properties across a semi-arid watershed: Remote Sensing of Environment, v. 110, no. 1, p. 79–97, accessed January 27, 2017, at https://doi.org/10.1016/j.rse.2007.02.007.

Schaibly, J.H., and Shuler, K.E., 1973, Study of the sensitivity of coupled reaction systems to uncertainties in rate coefficients, II. Applications: The Journal of Chemical Physics, v. 59, no. 8, p. 3879–3888, accessed October 27, 2017, at https://doi.org/10.1063/1.1680572.

Senay, G.B., Bohms, S., Singh, R.K., Gowda, P.H., Velpuri, N.M., Alemu, H., and Verdin, J.P., 2013, Operational evapotranspiration mapping using remote sensing and weather datasets—A new parameterization for the SSEB approach: Journal of the American Water Resources Association, v. 49, no. 3, p. 577–591, accessed October 27, 2017, at https://doi.org/10.1111/jawr.12057.

Sloto, R.A., and Crouse, M.Y., 1996, HYSEP—A computer program for streamflow hydrograph separation and analysis: U.S. Geological Survey Water-Resources Investigations Report 96–4040, 46 p., accessed November 3, 2017, at https://pubs.er.usgs.gov/publication/wri964040.

Sohl, T., Reker, R., Bouchard, M., Sayler, K., Dombierer, J., Wika, S., Quenzer, R., and Friesz, A., 2016, Modeling historical land use and land cover for the conterminous United States: Journal of Land Use Science, v. 11, no. 4, p. 476–499, accessed May 24, 2016, at https://doi.org/10.1080/1747423X.2016.1147619.

Sohl, T.L., Sayler, K.L., Bouchard, M.A., Reker, R.R., Friesz, A.M., Bennett, S.L., Sleeter, B.M., Sleeter, R.R., Wilson, T., Soulard, C., Knuppe, M., and Van Hofwegen, T., 2014, Spatially explicit modeling of 1992–2100 land cover and forest stand age for the conterminous United States: Ecological Applications, v. 24, no. 5, p. 1015–1036, accessed July 26, 2016, at https://doi.org/10.1890/13-1245.1.

The Nature Conservancy, 2009, Indicators of hydrologic alteration, version 7.1, user's manual: The Nature Conservancy, accessed November 3, 2017, at https://www.conservationgateway.org/ConservationPractices/Freshwater/EnvironmentalFlows/MethodsandTools/IndicatorsofHydrologicAlteration/Documents/IHAV7.pdf.

Thornton, P.E., Running, S.W., and White, M.A., 1997, Generating surfaces of daily meteorological variables over large regions of complex terrain: Journal of Hydrology, v. 190, nos. 3–4, p. 214–251, accessed March 30, 2015, at https://doi.org/10.1016/S0022-1694(96)03128-9.

Thorstensen, A., Nguyen, P., Hsu, K., and Sorooshian, S., 2016: Journal of Hydrometeorology, v. 17, p. 571–590, accessed February 9, 2017, at https://doi.org/10.1175/JHM-D-15-0071.1.

U.S. Department of Agriculture, Natural Resources Conservation Service, 1991, U.S. General Soil Map (STATSGO2) database: U.S. Department of Agriculture, Natural Resources Conservation Service database, accessed November 3, 2017, at https://sdmdataaccess.sc.egov.usda.gov/.

U.S. Geological Survey, undated, Land-cover modeling at USGS Earth Resources Observation and Science (EROS) Center: U.S. Geological Survey website, accessed May 15, 2017, at https://landcover-modeling.cr.usgs.gov/.

Van Beusekom, A.E., Hay, L.E., Viger, R.J., Gould, W.A., Collazo, J.A., and Khalyani, A.H., 2014, The effects of changing land cover on streamflow simulation in Puerto Rico: Journal of the American Water Resources Association, v. 50, no. 6, p. 1575–1593, accessed October 17, 2017, at https://doi.org/10.1111/jawr.12227.

Viger, R.J., 2014, Preliminary spatial parameters for PRMS based on the Geospatial Fabric, NLCD2001 and SSURGO: U.S. Geological Survey metadata, accessed April 30, 2015, at https://doi.org/10.5066/F7WM1BF7.

Viger, R.J., and Bock, A., 2014, GIS features of the Geospatial Fabric for national hydrologic modeling: U.S. Geological Survey metadata, accessed April 30, 2015, at https://doi.org/10.5066/F7542KMD.

Viger, R.J., and Leavesley, G.H., 2007, The GIS Weasel user's manual: U.S. Geological Survey Techniques and Methods, book 6, chap. B4, 201 p., accessed September 24, 2017, at https://pubs.usgs.gov/tm/2007/06B04/.

Wanders, N., Karssenberg, D., de Roo, A., de Jong, S.M., and Bierkens, M.F.P., 2014, The suitability of remotely sensed soil moisture for improving operational flood forecasting: Hydrology and Earth System Sciences, v. 18, p. 2343–2357, accessed January 27, 2017, at https://doi.org/10.5194/hess-18-2343-2014.

Wolock, D.M., and McCabe, G.J., 1999, Explaining spatial variability in mean annual runoff in the conterminous United States: Climate Research, v. 11, no. 2, p. 149–159, accessed October 27, 2017, at https://doi.org/10.3354/cr011149.

For more information about this report, contact
Director, South Atlantic Water Science Center
U.S. Geological Survey
720 Gracern Road,
Stephenson Center, Suite 129
Columbia, SC 29210

Or visit the South Atlantic Water Science Center website at
https://www.usgs.gov/centers/sa-water/

Publishing support provided by the U.S. Geological Survey
Science Publishing Network, Reston and Sacramento
Publishing Service Centers

ISSN 2328-0328 (online)
https://doi.org/10.3133/sir20195039

LaFontaine and others—**Simulation of Water Availability in the Southeastern United States for Historical and Potential Future Climate and Land-Cover Conditions**—SIR 2019–5039